Mechanism Analysis by Using a Large Flume Experiment and Physical-based Model for Shallow Landslide Study

May 2015

Minseok KIM

Mechanism Analysis by Using a Large Flume Experiment and Physical-based Model for Shallow Landslide Study

A Dissertation Submitted to
the Graduate School of Life and Environmental Sciences,
the University of Tsukuba
in Partial Fulfillment of the Requirements
for the Degree of Doctor of Philosophy in Science
(Doctoral Program in Integrative Environmental Science)

Minseok KIM

Contents

Abstract

Shallow landslides pose a significant hazard to mountain communities because they are frequent, difficult to predict. It also can be developed into debris flow, which is potentially destructive due to their velocity and their bulking capability during propagation. Therefore, the interpretation on mechanisms of rainfall-induced shallow landslide can make improvement for the prediction and mitigation for sediment disasters due to shallow landslide.

In the chapter II, the physically based H-slider (hillslope-scale shallow landslide-induced debris flow risk evaluation) model was used to evaluate the effects of topography and soil parameterization reflecting soil depth on shallow landslide prediction accuracy. Two digital elevation models (DEMs; i.e. ground surface and bedrock surface) and three soil thicknesses (average soil thickness, soil thickness to weathered rock and soil thickness to bedrock) and physical soil parameters (cohesion and internal friction angle) at a small hillslope site in Jinbu, Kangwon Prefecture, eastern part of the Korean Peninsula, were considered. Each prediction result simulated with the H-slider model was evaluated by receiver operating characteristic (ROC) analysis for modelling accuracy. The results of the ROC analysis for shallow landslide prediction using the ground surface DEM (GSTO) and the bedrock surface DEM (BSTO) indicated that the prediction accuracy was higher using the GSTO compared to the BSTO. Moreover, the prediction accuracy based on soil parameterization reflecting soil thickness was highest in all cases. These results imply that the effect of soil parameters on shallow landslide prediction could be larger than the effects of topography and soil thickness.

In chapter III, SHALSTAB model applied to shallow landslides induced by rainfall to evaluate soil properties related with the effect of soil depth for a granite area in Jinbu region, Republic of Korea. Soil depth measured by a knocking pole test and two soil parameters from direct shear test (a and b) as well as one soil parameters from a tri-axial compression test (c) were collected to determine the input parameters for the model. Experimental soil data were used for the first simulation (Case I) and, soil data represented the effect of measured soil depth and average soil depth from soil data of Case I were used in the second (Case II) and third simulations (Case III), respectively. All simulations were analysed using receiver operating characteristic (ROC) analysis to determine the accuracy of prediction. ROC analysis results for first simulation showed the low ROC values under 0.75 may be due to the internal friction angle and particularly the cohesion value. Soil parameters calculated from a stochastic hydro-geomorphological model were applied to the SHALSTAB model. The accuracy of Case II and Case III using ROC analy-

sis showed higher accuracy values rather than first simulation.

In Chapter IV, to evaluate the initiation process of rainfall-induced landslide and artificial seepage-induced landslide, laboratory slope failure experiments and the artificial rainfall simulators have been conducted. And numerical modeling and factor of safety were accomplished to analysis the effect of seepage according to change of subsurface flow using two experiment data for landslide initiation evaluation. During entire experiment performance, surface runoff did not observe and the seepage outflow only observed from toe of flume to middle part of flume by interflow along the soil–bedrock interface according to rising of groundwater.

In rainfall-induced landslide experiment, undercutting by seepage erosion and seeping water were main factors caused to failure. Numerical modeling indicated that seepage direction was effected to rising of ground water table and especially change of topography (near the failure surface plane). In artificial seepage-induced landslide experiment considered seepage force, multi-failures were occurred and rapidly accelerated to downward direction during water injection. Numerical modeling indicated seepage direction and force were effected to landslide initiation according to abrupt increasing of pore water pressure and groundwater level at near failures plan. And changing of seepage direction was calculated at near failures plan while failure move to downward direction.

In rainfall induced-landslide experiment, FS was reduced due to change of seepage direction and, from slope parallel seepage flow ($\lambda = 90^{\circ}$) showed under FS value 1 indicated unstable. In artificial seepage-induced landslide experiment, FS was reduced due to change of seepage direction and especially seepage force. However, when λ that have 5.6 (i.e. hydraulic gradient) was changed from vertically downward direction to slope parallel, FS value showed under 1 indicated unstable by comparing with rainfall-induced landslide experiment. In this study, these monitoring and modeling results indicated that seepage force by subsurface can be more affected to landslide initiation rather than effect of seepage direction.

Keywords: Shallow landslide, physically based model, a large flume experiment, bedrock flow, piping, seepage direction, seepage force, subsurface flow, topography, soil thickness

List of Tables

Chapter 2

Chapter 3

Chapter 4

List of Figures

Chapter 1

Chapter 2

Chapter 3

Chapter 4

Chapter 1. General Introduction

1.1 Previous studies on rainfall-induced shallow landslide model

Shallow landslides are a major landform-shaping process in many mountain areas (Acharya et al., 2006). Landslides can transform into debris flows or hyper-concentrated flows under specific conditions (Iverson et al., 1997). Flows with sediments induced by shallow landslides are much more dangerous than those resulting from continuous erosive processes due to their high density and mobility. These shallow landslide initiation is frequently related to rainfall intensity and duration (Caine, 1980; Aleotti, 2004; Giannecchini, 2006; Guzzetti et al., 2007, 2008; Cannon et al., 2008; Coe et al., 2008; Dahal and Hasegawa, 2008). It commonly has been observed that a significant fraction of hillslope failure such as shallow landslide is often related to short (<1 hour) and intense rainfall rather than daily-averaged precipitation(Reid et al., 1997; Montromery et al., 1997; Torres et al., 1998; Caine, 1980; Casadei et al., 2003).

Researchers have attributed the occurrence of landslides to spatial variation in topography, soil depth, cohesion, hydraulic conductivity, seepage response by subsurface flow, and the internal friction angle (e.g., Shimokawa et al., 1989; Yoshinaga and Saijo,1989; Dietrich et al. 1995; Wu and Sidle, 1995; Casasei et al., 2003; Roering et al., 2003; Onda et al., 2004). Shallow landslide often occurs in areas of convergent topography, where subsurface soil water flow paths increase the excess pore water pressure downslope (e.g. Anderson et al., 1991; Wilkinson et al., 2002; Talebi et al., 2008). Topography influences the initiation of shallow landslides through both the concentration of subsurface flow and the effects of slope (e.g. Montgomery and Dietrich, 1994; Talebi et al., 2008).

To analysis shallow landsliding, one of the simplest approaches combines an infinite

slope stability analysis with a steady-state shallow subsurface flow model (e.g., Okimura et al, 1985; Montgomery and Dietrich, 1994; Pack et al, 1998). Recently, more complex processes of shallow landslide occurrence have been incorporated into physically based models predicting the spatial patterns of shallow landslide susceptibility (e.g., Hiramatsu et al, 1990; Wu and Sidle, 1995; Rosso et al, 2006; Talebi et al, 2008; Uchida et al., 2011). The use of spatially distributed and physically based models poses a versatile and alternative approach that can be used in determining which areas are prone to shallow landslides, and consequently in helping planners and decision makers to choose strategies that minimize hazards associated to this process.

Many of these models and methodological approaches are based on the physically-based model developed by Montgomery and Dietrich (1994) in which a slope stability method and a topographically based groundwater flow model are coupled. The slope stability approach is based on an infinite slope form of the Mohr–Coulomb failure law. Concerning the hydrologic model, a steady state shallow subsurface flow based on the work by O'Loughlin (1986) has been usually considered. This is only valid if recharge to a perched water table occurs at every point along the hillslope, reaching subsurface drainage equilibrium and experiencing drainage from its entire upslope contributing area (Barling et al., 1994).

For examples, SHALSTAB (Dietrich and Montgomery, 1998) is a physically based model including the infinite slope equation and a steady-state shallow subsurface flow (O'Loughlin, 1986) to evaluate landslide susceptibility at a regional scale. Claessens et al. (2005) proposed a model to assess the location of shallow landslide and their impact on landscape development within a time frame of decades, based on the dynamic landscape evolution model LAPSUS. TRIGRS (Transient Rainfall Infiltration and Grid based Regional Slope-stability analysis) which was developed to account for the transient effects of rainfall on shallow landslide initiation and combines an analytical solution for groundwater flow in one vertical dimension with an infinite-slope stability calculation (Baum et al., 2002; Savage et al., 2003). And STARWARS+ and

PROBSTAB (van Beek, 2002) and GEOtop-FS (Simoni et al., 2008) applied to prediction of shallow landslide.

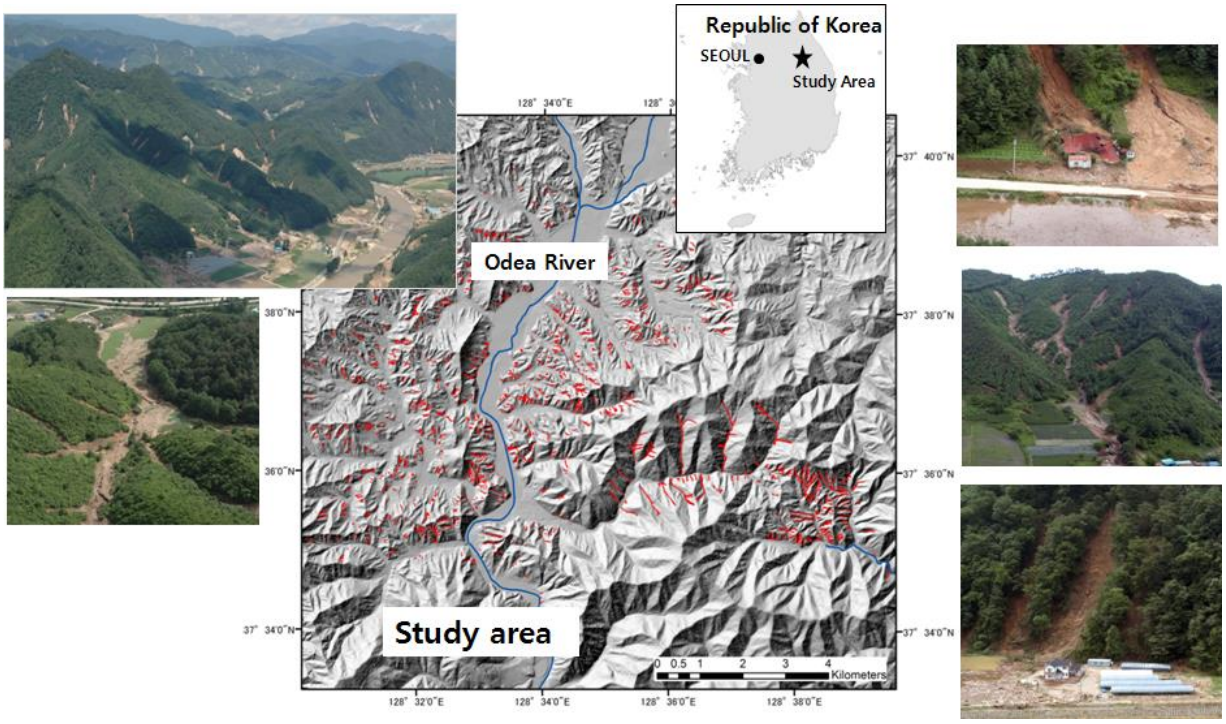

Fig. 1.1 Rainfall induced shallow landslides in Republic of Korea

Some issues, however, remain unsolved regarding steady state models. For examples, one is a time scale discrepancy in the supposed hydrological process. The concept of steady groundwater flow parallel to the slope above an impermeable bed can predict only the long-term distribution of groundwater pressure, which should be identified as a predisposition to landsliding. The second concern is that the model cannot apply to hill slopes underlain by highly permeable bedrocks, where the near surface lateral water movement becomes an unfeasible proposition. And these mostly physically based models have been used by factor of safety concept combined a simple hydrology model related with ground water increasing within soil layer by hydraulic conductivity and, they have expressed the output to stable or/and unstable using values of FS

where the shallow landslide area is sensitive. So, to perform the shallow landslide prediction, weakness on steady state shallow landslide models have to be considered and the timing caused shallow landslide by rainfall also was needed to be considered.

These physically based models only allow the complete parameterization, especially considering rainfall induced landslides where the definition of components, such as hydrological response of the soil and its geotechnical properties, is needed (Duan and Grant, 2000; Schmidt et al., 2001; Giannecchini et al., 2007; Minder et al., 2009; Uchida et al., 2011; Lanni et al., 2013). Unfortunately, few studies have attempted to measure their spatial variation at the scale that influences slope stability but these variables are exceedingly difficult to measure. Only few contain a dynamic hydrology component and still fewer allow the user to change the parameterization.

Many researchers have variously attributed the seemingly random occurrence of landslides to spatial variation in topography, soil depth, cohesion of the soil and roots, hydraulic conductivity, groundwater response, and the angle of internal friction (e.g., Dietrich et al. 1995; Wu and Sidle, 1995; Montgomery et al., 1997). This physical parameters, however, can be changed by topography and distribution of soil depth due to local conditions and affect shallow landslide modeling by one of the important factors (Dietrich et al., 1995; Claessens et al., 2005; Rosso et al., 2006; Uchida et al., 2011). Recently, hillslope hydrology studies have shown that not the ground surface topography but the bedrock surface may be the most important controlling factor in the routing of subsurface flow on steep, wet and soil-mantled hillslopes (e.g., Freer et al, 2002; Uchida et al., 2011) because the landslide slip surface can be also strongly affected by bedrock surface topography. To better predict the shallow landslide, therefore, shallow landslide modeling has to be considered on the topography and detailed information of soil thickness.

1.2 Interpretation of rainfall-induced shallow landslides using flume experiment and artificial rainfall

Rainfall-induced shallow landslides have been studied for practical and scientific reasons (Anderson and sitar, 1995; Iverson et al., 1997; Gabet and Muss, 2006). In spite of their size, shallow landslides pose a significant hazard to mountain communities because they are frequent, difficult to predict, and they can develop into debris flow, which are potentially destructive due to their velocity and their bulking capability during propagation (Campbell, 1975; Rickenmann and Zimmermann, 1993; Iverson et al., 1997; Reid et al., 2000; Crosta and Dal Negro, 2003; Crosta et al., 2003).

Recently, quantitative studies addressed shallow groundwater strongly influences the effective stress state in earth materials and can therefore precipitate hill-slope instability (Terzaghi 1923, 1943, 1950; Iverson and Major, 1987). A variety of theoretical studies have clarified the destabilizing role of steady, Darcian groundwater flow in slopes (Patton and Hendron, 1974; Hodge and Freeze, 1977; Iverson and Major, 1987). The slope stability approach is based on an infinite slope form of the Mohr–Coulomb failure law. Concerning the hydrologic model, a steady state shallow subsurface flow based on the work by O'Loughlin (1986) has been usually considered. This is only valid if recharge to a perched water table occurs at every point along the hillslope, reaching subsurface drainage equilibrium and experiencing drainage from its entire upslope contributing area

However, bedrockflow by piping may recently contribute to landslide initiation and/or slope stability, since the spatial variation in hydrologic response is attributed to the influence of pipeflow (e.g. Pierson, 1980; Brand et al., 1986; Jenkins et al., 1988; Sidle, 1995a; Fannin et al., 2000). Proofs that occurred increasing groundwater like bedrock flow are often found in

scars of shallow landslides (e.g. Ohta et al. 1981 ; Brand et al., 1986; Jenkins et al., 1988; Selby, 1993). Several field investigations have attempted to record the shallow groundwater conditions that initiate debris flows by landslide (e.g. Harp et al.,1990; Johnson and Sitar 1990; Montgomery et al. 1990; Iverson et al., 1997). Ohta et al. (1981) and Pierson (1983) reported that 50–90% of landslide scars had soil pipes in head scarps (Uchida et al., 2001). Since soil pipes have significant impact on the effective hydraulic conductivity (e.g. Montgomery and Dietrich, 1995) and the storm runoff generation processes (e.g. Kitahara, 1994), it has been considered that pipeflow may contribute to landslide initiation (e.g. Wieczorek, 1993; Sidle, 1994; Onda et al., 1996; Iverson et al., 1997).

Numerical simulation showed that relatively slight hydraulic conductivity contrasts of less than one order of magnitude markedly affect the slope failure potential (Reid and Iverson, 1992). Indeed, soil pipe outlets are often found in scars of shallow landslides (e.g. Brand et al., 1986; Jenkins et al., 1988; Selby, 1993). Since the 1980s, a variety of processes have been suggested to explain the effects of pipeflow on the slope stability (e.g. Pierson, 1983; Sidle et al., 1985; Shindo, 1993; Uchida et al., 1996; Onda et al., 1996).

Theoretical analyses and observations of the movement of soil particles within slopes that have an emerging subsurface flow have been presented (e.g. Iverson and Major, 1986; Kohno et al., 1987; Selby, 1993; Terajima and Sakura, 1993) The importance of seepage flow convergence in hillslope hollows with respect to shallow landslide initiation has also been discussed in many studies (e.g. Anderson and Burt, 1978; Pierson, 1980; Sidle, 1984; Montgomery and Dietrich, 1994; Tsuboyama et al.,1994; Terajima et al., 2014)

However, the effects of piping on shallow landslide initiation have not been fully understood, because of insufficient information about the runoff generation processes of pipeflow. For instance, in infinite slope stability analyses, it is commonly assumed that the groundwater

flow, and hence, the seepage force vector, is parallel to the topographical surface. Common theory in soil mechanics will show, however, that when the seepage force turns more and more in a direction opposite to gravity, effective stress progressively decreases, may become null and causes liquefaction of the sliding block (Nieuwenhuis, 1989; Iverson et al., 1997).

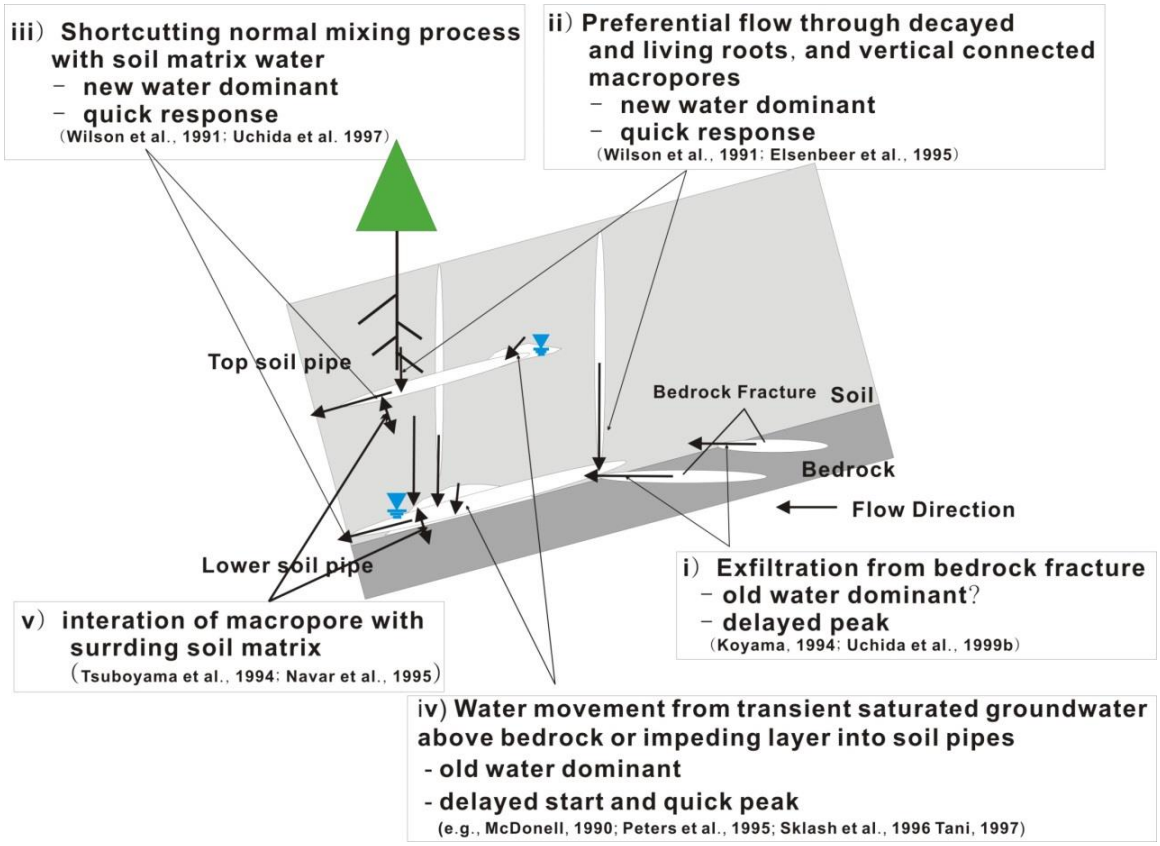

Fig. 1.2 Conceptual model of an expansion of hydrologically active area at soil matrix–pipe interface, the expansion of surrounding soil that interacts with water in macropores and the extension of macropore network upslope. Based on Tsuboyama et al. (1994) (Tsuboyama Y, Sidle RC, Noguchi S, Hosoda I, Water Resources Research, 30: 879–890, 1994 (Modified from Uchida et al., 2001)

1.3 Objectives of this study

Prediction of shallow landslide performance will be strongly influenced by the quality of the data because of the strong influence of local controls (topography, soil thickness, root strength, localized seepage forces and bedding or fractures) and their threshold dependency. Hillslope hydrology studies recently have shown the topography maybe the most important factor on moving of subsurface flow, distribution of soil thickness and soil properties related with topography were one of the important factors to shallow landslide prediction.

Objectives of this study are to evaluate the impact of topography effect by using physically based models in S. Korea and to explain the mechanism of shallow landslide for suggesting improving shallow landslide prediction modeling. To accomplish these objectives, I investigated detailed topography and soil thickness at specific study site in S. Korea and performed a large flume experiment using artificial rainfall in National Research Institute Earth Science and Disaster Prevention (NIED), Japan.

In chapter 2, the physically based H-slider model was accomplished to calculate steady-state critical rainfall intensity (mm/h) for shallow landslide modeling by using diverse topographic data in small scale study site located on Jinbu, Kangwon prefecture, Republic of Korea. To evaluate diverse factors for shallow landslide prediction using H-slider, 1) the two kinds of DEMs, i.e. ground surface topographic (GSTO) and bedrock surface topographic (BSTO), were established. 2) The three-soil thickness, i.e. average soil thickness 1m (AST), weathered soil thickness (WST) and bedrock soil thickness (BST), were established 125 points by using knocking pole test. 3) The soil parameters collected in study area were analyzed by using a triaxial compress test. The each prediction results simulated by H-slider model were evaluated by ROC analysis for accuracy of the effect of topography.

In chapter 3, the seemingly random occurrence of shallow landslides to spatial varia-

tion in topography, soil depth, cohesion of the soil and roots, hydraulic conductivity, ground water response, and the angle of internal friction. Unfortunately, these variables are exceedingly difficult to measure, and few studies have attempted to measure their spatial variation at the scale that influences slope stability. I performed predictions of shallow landslides induced by rainfall by using a SHALSTAB model and interpreted the importance of soil parameters such as cohesion and internal friction angle according to changes in soil thickness to improve the accuracy of shallow landslide prediction. I used a knocking pole test in the study area to measure soil thickness data and, the three soil parameters, which were collected at study area and analysed using two methods (direct shear tests and one triaxial compression test), used in SHALSTAB model.

In chapter 4, shallow landslide initiation was related to various hydrological processes and recently, hillslope hydrology studies have shown topography may be the most important controlling factor in the routing of subsurface flow on steep, wet and soil-mantled hillslopes. Thus, this study is to present the effect of topography and bedrockflow by piping flow on hydrological processes related to landslide initiation. A large flume experiment using artificial rainfall in the National Research Institute for Earth Science and Disaster Prevention (NIED), Japan have been conducted to evaluate the initiation process of rainfall-induced shallow landslide and seepage-induced shallow landslide by topography effect and bedrock flow in model hillslope.

The topography effect and seepage change were evaluated by using large flume experiment during rainfall experiment and bedrockflow effect was evaluated by using water injection experiment. To analysis topography effect and seepage effect by the hydraulic responses during both experiment, the numerical modeling and factor of safety applied to this experiment.

In chapter 5, the results obtained are summarized and evaluated. Limitation of the study methods is presented, together with suggestions for future study and conclusions of this study were presented.

Reference

Acharya, G., De Smedt, F., Long, N.T., (2006) Assessing landslide hazard in GIS: a case study from Rasuwa, Nepal. Bull Eng Geol Environ, **65** (1), 99–107.

Anderson, M.G., Burt, T.P., 1990. Subsurface runoff. In Process Studies in Hillslope Hydrology, Anderson MG, Burt TP (eds).Wiley: Chichester, 365–400.

Anderson, M. G. Kemp, M. J., 1991. Towards an improved specification of slope hydrology in the analysis of slope instability problems in the tropics. Progress in Physical Geography, **15**, 29–52.

Aleotti, P., 2004. A warning system for rainfall-induced shallow failures, Engineering Geology, **73**, 247–265.

Barling, R.D., Moore, I.D., Grayson, R.B., 1994. A quasi-dynamic wetness index for charac terrizing the spatial distribution of zones of surface saturation and soil-water content, Water Resource Research, **30** (4), 1029-1044.

Baum, R. L., Savage, W. Z., Godt, J. W., 2002. TRIGRS – a FORTRAN program for transient rain fall infiltration and grid-based regional slope stability analysis, US Geological Survey OpenFile Report 2002-424.

Brand, E.W., Dale, M.J., Nash, J.M., 1986. Soil pipes and slope stability in Hong Kong. Quarterly Journal of Engineering Geology, **19**, 301–303.

Caine, N., 1980. The rainfall intensity-duration control of shallow landslides and debris flows, Geog. Ann. Series A., **62**, 23–27.

Cannon, S. H., Gartner, J. E., Wilson R. C., Bowers J. C., Laber J. L., 2008. Storm rainfall conditions for floods and debris flows from recently burned areas in southwestern Colorado and southern California, Geomorphology, **96**, 250–269.

Casadei, M., Dietrich, W. E., Miller, N. L., 2003. Testing a model for predicting the timing and

location of shallow landslide initiation in soil mantled landscapes. Earth Surf. Proc. Land., **28**, 925–950.

Claessens, L., Heuvelink, G.B.M., Schoorl, J.M., Veldkamp, A., 2005. DEM resolution effects on shallow landslide hazard and soil redistribution modeling. Earth Surface Processes and Landforms, **30**, 461–477.

Coe, J. A., Kinner, D. A., Godt, J. W., 2008. Initiation conditions for debris flows generated by runoff at Chalk Cliffs, Central Colorado. Geomorphology, **96**, 270–297.

Dahal, R. K., Hasegawa, S., 2008. Representative rainfall thresholds for landslides in the Ne pal Himalaya, Geomorphology, **100**, 429–443.

Dietrich, W. E., Reiss, R., Hsu, M., Montgomery, D. R., 1995. A process-based model for colluvial soil depth and shallow landsliding using digital elevation data. Hydrol.Process., **9**, 383–400.

Dietrich, W. E., Montgomery, D. R., 1998. SHALSTAB- A Digital Terrain Model for Mapping Shallow Landslide Potential. National Council of the Paper Industry for Air and Stream Improvement, Technical Report, Berkeley. February, 29.

Duan, J., Grant, G.E., 2000. Shallow landslide delineation for steep forest watersheds based on topographic attributes and probability analysis. In: Wilson, J.P., Gallant, J.C. (Eds.), Terrain Analysis — Principles and Applications. John Wiley & Sons, 311–329.

Fannin, R.J., Jaakkola, J., Wilkinson, J.M.T., Hetherington, E.D., 2000. Hydrologic response of soils to precipitation at Carnation Creek, British Columbia, Canada. Water Resources Research, **36**, 1481–1494.

Freer, J., McDonnell, J.J., Beven, K.J., Peters, N.E., Burns, D.A., Hooper, R.P., Aulenbach, B., Kendall C., 2002. The role of bedrock topography on subsurface storm flow. Water Resource Research, **38**, doi: 10.1029/2001WR000872.

Giannecchini, R., 2006. Relationship between rainfall and shallow landslides in the southern

Apuan Alps (Italy). Natural Hazards and Earth System Science, **6**, 357–364,

Giannecchini R., Naldini D., D'Amato A. G., Puccinelli A., 2007. Modeling of the initiation of rainfall-induced debris flows in the Cardoso basin (Apuan Alps, Italy). Quaternary International, **171**, 108–117.

Guzzetti, F., Peruccacci, S., Rossi, M., Stark, C. P., 2007 Rainfall thresholds for the initiation of landslides in central and southern Europe. Meteorology and Atmospheric Physics, **98**, 239–267.

Harp, E.L., Wells, W.G., Sarmiento, J.G., 1990. Pore pressure response during failure in soils. Geological Society of America Bulletin, **102**, 428–438.

Hiramatsu, S., Mizuyama, T., Ishikawa, Y., 1990. Study of a method for predicting hillside land slides by analysis of transient flow of water in saturated and unsaturated soils. Journal of the Japan Society of Erosion Control Engineering, **43**, 5-15 (in Japanese).

Iverson, R.M., Reid, M.E., LaHusen, R.G., 1997. Debris-flow mobilization from landslides. Annual Review of Earth and Planetary Sciences, **25**, 85 – 138.

Jenkins, A., Ashworth, P.J., Ferguson, R.I., Grieve, I.C, Rowling, P., Stott, T.A., 1988. Slope failures in the Ochil hills, Scotland, November 1984.Earth Surface Processes and Landforms, **13**, 69–76.

Johnson, K.A., Sitar, N., 1990. Hydrologic conditions leading to debris-flow initiation. Canadian Geotechnical Journal, **27**, 789–801.

Kitahara, H., 1994. A study on the characteristics of soil pipes influencing water movement in forested slopes. Bulletin of the Forestry and Forest Products Research Institute, **367**, 63–115 (in Japanese with English summary).

Lanni, C., McDonnell, J.Hopp, L., Rigon, R., 2013 Simulated effect of soil depth and bedrock topography on near-surface hydrologic response and slope stability, Earth Surface Processes and Landforms, **38**, 146–159.

Minder, J.R., Roe, G.H., Montgomery, D.R., 2009. Spatial patterns of rainfall and shallow landslide susceptibility. Water Resource Research, **45**, W04419. doi:10.1029/2008WR 007027.

Montgomery, D.R., Dietrich, W.E., 1994. A physically based model for the topographic control on shallow landsliding. Water Resources Research, **30** (4), 1153–1171.

Montgomery, D.R., Dietrich, W.E., Torres, R., Anderson, S.P., Loague, K., 1997. Subsurface flow paths in a steep unchannelled catchment. Water Resources Research, **33**, 91–109.

O'Loughlin, E. M., Prediction of surface saturation zones in natural catchments by topographic analysis. Water Resources Research, **22**, 794–804, 1986.

Onda, Y., Okunishi, K., Iida, T., Tsujimura, M., 1996. In Hydrogeomorphology: The Interaction of Hydrological and Geologic Processes. Kokonshoin: Tokyo; 267 (in Japanese).

Onda, Y., Tsujimura, M., Tabuchi, H., 2004. The role of subsurface water flow paths on hillslope hydrological processes, landslides and landform development in steep mountains of Japan. Hydrological Processes, **18**, 637–650.

Okimura, T., Ichikawa, R., Fujii, I., 1985. Methods to Predict Failures on Granite Mountain Slopes by a Infiltrated Water Movement Model in a Surface Layer. Journal of the Japan Society of Erosion Control Engineering, **37**, 44–49 (in Japanese).

Ohta, T., Tsukamoto, Y., Noguchi, H., 1981. An analysis of pipeflow and landslide. In Proceedings of Annual Meeting of the Japan Society of Erosion Control Engineering, 92–93 (in Japanese).

Pack, R.T., Tarboton, D.G., Goodwin, C.N., 1998. The SINMAP Approach to Terrain Stability Mapping. 8th Congress of the International Association of Engineering Geology, Vancouver, British Columbia, Canada.

Pierson, T.C., 1980. Piezometric response to rainstorms in forested hillslope drainage depressions. Journal of Hydrology (NZ), **19**, 1–10.

Reid, M.E., Iverson, R.M., 1992. Gravity-driven groundwater flow and slope failure potential. 2. Effects of slope morphology, material properties, and hydraulic heterogeneity. Water Resources Research, **22**, 939–950.

Reid, M.E., LaHunsen, R.G., Iverson, R.M., 1997. Debris flow initiation experiments using diverse hydrologic triggers. In Debris Flow Hazards Mitigation: Mechanics, Prediction and Assessment, Chen CL (ed.). ASCE Proceedings. ASCE, 1–11.

Roering, J.J., Schmidt, K.M., Stock, J.D., Dietrich, W.E., Montgomery, D.R. 2003. Shallow landsliding,root reinforcement, and the spatial distribution of trees in the Oregon Cost Range. Canadian Geotechnical Journal, **40**, 237-253.

Rosso, R., Rulli, M.C., Vannucchi, G., 2006. A physically based model for the hydrologic control on shallow landsliding. Water Resources Research, **42**, W06410. http:// dx.doi.org / 10.1029/2005WR004369.

Savage, W.Z., Godt, J.W., Baum, R.L., 2003. A model for spatially and temporally distributed shallow landslide initiation by rainfall infiltration, in Rickenmann, D. and Chen, C., eds., Debris-Flow Hazards Mitigation-Mechanics, Prediction, and Assessment: Rotterdam, Millpress (Proceedings of the 3rd International conference on Debris Flow Hazards, Davos, Switzerland, September 10-13, 2003), 179-187.

Selby, M. J., 1993. In Hillslope Materials and Processes. Oxford University Press: Oxford; 451.

Shimokawa, E., Jitouzono, T., Takano, S., 1989. Periodicity of shallow landslide on Shirasu (Ito pyroclastic flow deposits) steep slopes and prediction of potential landslide sites. Trans., Jpn. Geomorphol. Union, **10**, 267– 284.

Sidle, R.C., 1984. Shallow groundwater fluctuations in unstable hillslopes coastal Alaska. Zeitschrift f¨ur Gletscherkunde und Glazialgeologie, **20**, 79–95.

Simoni, S., Zanotti, F., Bertoldi, G., Rigon, R., 2008. Modeling the probability of occurrence of shallow landslides and channelized debris flows using GEOtop-FS, Hydrolog. Process., **22**,

532–545.

Schmidt, K. M., J. J. Roering, J. D. Stock, W. E. Dietrich, Montgomery, D. R., Shaub T., 2001. Root cohesion variability and shallow landslide susceptibility in the Oregon Coast Range. Canadian Geotechnical Journal, **38**, 995– 1024.

Shindo, S., 1993. Convergent flow of subsurface water concerned with slope failure. The Quaternary Research, **32**, 315–322 (in Japanese with English summary).

Sidle, R.C., Pearce, A.J., O'Loughlin, C.L., 1985. In Hillslope Stability and Land Use. American Geophysical Union: Washington, DC, 140.

Sidle, R.C., 1994. Hydrological process related to landslide initiation. In Proceeding of the SABO Workshop on Experimental Research on Landslide Mechanism, 19–27.

Sidle, R.C., Tsuboyama, Y., Noguchi, S., Hosoda, I., Fujieda, M., Simizu, T., 1995a. Seasonal hydrologic response at various spatial scales in a small forested catchment, Hitachi Ohta. Journal of Hydrology, **168**, 227–250.

Talebi, A., Troch, P. A., Uijlenhoet, R., 2008. A steady-state analytical hillslope stability model for complex hillslopes. Hydrological Process, **22**, 546–553.

Terajima, T., Sakura, Y., 1993. Effect of subsurface flow on a topographic change at a valley head of granitic mountains. Transactions, Japanese Geomorphological Union, **14**, 365–384 (in Japanese with English summary).

Teragima, T., Miyahira, E., Miyajima, H., Ochiai, H., Hattori, K., 2014. How hydrological factors initiate instability in a model sandy slope. Hydrological Process, **28**, 5711-5724.

Torres R, Dietrich WE, Montgomery DR, Anderson SP, Loague K., 1998. Unsaturated zone processes and the hydrologic response of a steep, unchannelled catchment. Water Resources Research, **34**, 1865–1879.

Tsuboyama, Y., Sidle, R.C., Noguchi, S., Hosoda, I., 1994. Flow and solute transport through the soil matrix and macropores of a hillslope segment. Water Resources Research, **30**, 879–

890.

Uchida, T., Kosugi, K., Ohte, N., Mizuyama, T., 1996. The influence of pipe flow on slope stability. Journal of Japan Society of Hydrology and Water Resources, **9**, 330–339 (in Japanese with English summary).

Uchida, T., Tamur, K., and Akiyama, K., 2011. The role of grid cell size, flow routing algorithm and spatial variability of soil depth on shallow landslide prediction. Ital. J. Engi. Geol. and Environ., 149-157. doi: 10.4408/IJEGE.2011-03.B-018.

van Beek, L.P.H., 2002. The impact of land use and climatic change on slope stability in the Alcoy region, Spain. Doctoral Thesis. Utrecht University: Utrecht.

Wieczorek, GF., 1993. Assessment and prediction of debris-flow hazards. Proceedings of Hydraulic Engineering'93, **2**, 1272–1283.

Wilkinson, P. L., Anderson M. G., Lloyda, D. M., Renaudb J.P., 2002. Landslide hazard and bioengineering: towards providing improved decision support through integrated numerical model development. Environmental Modeling & Software, **17**, 333–344.

Wu, W. and Sidle, R. C., 1995. A distributed slope stability model for steep forested basins. Water Resource Research, **31**, 2097–2110.

Yoshinaga, S., and Saijo, K., 1989. Slope development during Holocene reconstructed from alluvial cone and talus cone aggradation process (in Japanese with English Abstract), Trans. Jpn. Geomorphol. Union, **10**, 285–301

Chapter 2. The Effect of Topography and Soil Parameterization Represented the Effect of Soil Thickness for Shallow Landslide Modeling

2.1 Introduction

Shallow landslides pose a significant hazard to mountain communities because they are frequent, difficult to predict and can develop into debris flows, which are potentially destructive due to their velocity and bulking capability during propagation (Campbell, 1975; Rickenmann and Zimmermann, 1993; Iverson et al., 1997; Reid et al., 2000; Crosta and Dal Negro, 2003). Moreover, the initiation of shallow landslides is frequently related to rainfall intensity and duration (Caine, 1980; Aleotti, 2004; Giannecchini, 2006; Guzzetti et al., 2007, 2008; Cannon et al., 2008; Coe et al., 2008; Dahal et al., 2006).

One of the simplest approaches to analyse shallow landsliding combines an infinite slope stability analysis with a steady-state shallow subsurface flow model (e.g. Okimura et al., 1985; Montgomery and Dietrich, 1994; Pack et al., 1998). The topography factor influences the initiation of shallow landslides through both the concentration of subsurface flow and the effect of the slope gradient on slope stability (Montgomery and Dietrich, 1994). Shallow landslides often occur in areas where the subsurface soil water flow increases the pore-water pressure (Anderson et al., 1991; Wilkinson et al., 2002; Talebi et al., 2008). In particular, hillslopes with a convergent plan shape tend to concentrate subsurface water into small areas of the slope, thereby generating a rapid increase in pore-water pressure during rainstorms (e.g. Montgomery et al., 1997; Tsuboyama et al., 2000; Troch et al., 2002; Fernandes et al., 2004; Hilberts et al., 2004).

Physically based models generally use a digital elevation model (DEM) of the

ground surface to compute a steady-state (Montgomery and Dietrich, 1994; Wu and Slide, 1995; Pack et al., 1998; Uchida et al., 2011) or a quasi-dynamic (Borga et al., 1998; Casadei et al., 2003) wetness index, when the specific (steady-state or time-variable) upslope area derived from the surface topography is assumed to be a surrogate measure of the subsurface flow in response to a rainfall of specified duration. Although hydrological models have been coupled with infinite slope stability models (Montgomery and Dietrich, 1994; Wu and Slidle, 1995; Pack et al., 1998; Casadei et al., 2003; Uchida et al., 2011), almost all such models have assumed that the soil–bedrock interface is a simple topographic surface paralleling the soil surface. Recently, more complex processes of shallow landslide occurrence have been incorporated into physically based models predicting the spatial patterns of shallow landslide susceptibility (e.g. Hiramatsu et al., 1990; Wu and Sidle, 1995; Rosso et al., 2006; Talebi et al., 2008; Uchida et al., 2011), such as SHALSTAB (Dietrich and Montgomery, 1998), SHETRAN (Ewen et al., 2000), TRIGRS (Baum et al., 2002), PROBSTAB (van Beek, 2002), GEOtop FS+ (Simoni et al., 2008) and H-slider (Uchida et al., 2011).

However, some issues regarding steady-state models remain unsolved. For example, one such issue is a time-scale discrepancy in the supposed hydrological process. The concept of steady groundwater flow parallel to the slope above an impermeable bed can predict only the long-term distribution of groundwater pressure—a predisposition to landsliding. A second concern is that the model cannot be applied to hillslopes underlain by highly permeable bedrock, where near-surface lateral water movement becomes unfeasible. Additionally, these mostly physically based models have used a factor of safety (FS) concept combined with a simple hydrology model related to groundwater increase within a soil layer by hydraulic conductivity, and they have expressed the output as stable and/or unstable using FS values where the shallow landslide area is sensitive. Thus, to perform shallow landslide prediction, weaknesses in steady-state shallow landslide models, as well as the timing of shallow landslides caused by rainfall, must be

considered.

The physically based models described above allow only a complete parameterisation, especially when considering rainfall-induced landslides for which definitions of components, such as the hydrological response of the soil and the soil's geotechnical properties, are needed (Duan and Grant, 2000; Schmidt et al., 2001; Giannecchini et al., 2007; Minder et al., 2009; Uchida et al., 2011; Lanni et al., 2013). Many researchers have variously attributed the seemingly random occurrence of landslides to spatial variation in topography, soil depth, cohesion of soil and roots, hydraulic conductivity, groundwater response and the angle of internal friction (e.g. Dietrich et al. 1995; Wu and Sidle, 1995; Montgomery et al., 1997). These physical parameters, however, can change as a result of topography and the distribution of soil depth due to local conditions and may affect shallow landslide modelling through one of the important factors (Dietrich et al., 1995; Claessens et al., 2005; Rosso et al., 2006; Uchida et al., 2011).

Spatial variability of soil depth is likely to be important for determining shallow landslide susceptibility on various steep landscapes. Soil depth, the parameter with the greatest influence on model uncertainties, is the variable having the greatest effect on the results (Melchiorre and Frattini, 2012). Wu and Sidle (1995) used some soil-thickness sampling data in their analysis, and Dietrich et al. (1995) proposed a soil-thickness estimation model based on the mass balance between soil production from underlying bedrock and the divergence of diffusive soil transport. The linear correlations between soil thickness and elevation (Saulnier et al., 1997), and between soil thickness and slope gradient (Ho et al., 2012), have been applied to shallow landslide prediction. Previous studies have shown only large spatial variability with low resolution in soil depth on individual hillslopes or mountains (Okimura, 1989, Heimsath et al., 1997; Iida and Tananka, 1997; Freer et al., 2002; Tesfa et al., 2009, Uchida et al., 2011), and soil thickness information from landslide-prone areas remains very limited (Okimura, 1989; DeRose et al., 1991). Unfortunately, the variables of soil properties are exceedingly difficult to measure, and few stud-

ies have attempted to measure their spatial variation at a scale that influences slope stability.

Soil properties, which comprise an important factor for shallow landslide modelling, can affect local conditions such as topography, soil thickness, subsurface flow, bedrock flow and vegetation. In particular, physical soil properties are affected by the topography and soil thickness at local sites. Iida (1999) suggested that the distribution of soil thickness and topography are important parameters for the return period of shallow landslides and calculated various factors related to shallow landslides using a stochastic hydro-geomorphological model to evaluate the return period of shallow landslides. Some researchers have suggested that the two-layer model of soil and bedrock, which assumes a potential landsliding (soil) layer, is suitable for slope stability analysis of shallow landslides by using a probabilistic model modified from the stochastic hydro-geomorphological model suggested by Iida (1999) (e.g. D'Odorico and Fragherazzi, 2003; Talebi et al., 2008). These researchers noted that the internal friction angle and soil cohesion had an effect on soil thickness and topography and that these values are difficult to measure in the field. Kim et al. (2015) also applied the method suggested by Iida (1999) to the SHALSTAB model (i.e. using the soil parameterization), which reflected the effects of topography and soil thickness, and showed an improvement in modelling accuracy for shallow landslides.

Many physically based models are used for shallow landslide prediction. In this study, I applied the physically based H-slider (hillslope-scale shallow landslide-induced debris flow risk evaluation method) model developed by the Public Works Research Institute in Japan (PWRI). Although H-slider assumes a steady state, similar to SHALSTAB, this model can calculate the steady-state rainfall intensity (mm/h), determined in combination with topography and soil thickness and based on the hydrology concept by considering pore-water pressure and specific contributing area. The H-slider model has also been applied to various regions in Japan and evaluated using various soil thicknesses and various DEM resolutions to predict shallow land-

slides induced by rainfall (Uchida et al., 2011). Although some physically based models, such as SHALSTAB and TRIGER, have been applied to regions incurring shallow landslides in Korea (e.g. Park et al., 2013; Kim et al., 2011; Kim et al., 2015), these studies did not consider detailed soil thickness values and topography based on the hydrology concept. Therefore, the H-slider model can be useful for evaluating shallow landslides caused by rainfall in Korea by using the various soil properties, topography and soil thicknesses of Korea.

Recent hillslope hydrology studies have shown that the bedrock surface topography rather than the ground surface topography may be the most important controlling factor in the routing of subsurface flow on steep, wet and soil-mantled hillslopes (e.g. Freer et al., 2002; Uchida et al., 2011) because the landslide slip surface can also be strongly affected by the bedrock surface topography. To better predict shallow landslides, modelling must consider the topography and detailed information about soil thicknesses. However, most landslide prediction studies have used a ground surface DEM to calculate the values of parameters used as topographic indices, such as the local slope angle and upslope contributing area, because detailed ground information on soil thickness is generally lacking. Although detailed information on soil thickness can affect subsurface water routing and shallow landslide initiation, studies regarding the effects of detailed soil thickness on the prediction of shallow landslides are still few. Therefore, I need to compare the prediction accuracies for shallow landslides using ground topographic surface and bedrock topographic surface while considering the effects of soil parameterisation reflecting the soil depth.

In this context, the physically based H-slider model was applied to a specific study site located in Jinbu-Myeon, Pyeongchang-gun and Kangwon prefectures in the Republic of Korea. This study area is an ideal field site to test the performance of the landslide model because the occurrence of shallow landslides has been accelerated by a recent increase in heavy rainstorms. Therefore, I did not need to consider the impact of past landslides. The effects of soil

thickness and two DEMs (ground surface topography and bedrock surface topography) on the accuracy of shallow landslide prediction were investigated and a stochastic hydro-geomorphological model (Iida, 1999) was applied to the parameterisation of soil properties reflecting soil thickness for improved model performance.

2.2 Study Area

The specific hillslope-scale study area located in the Jinbu-Myeon, Pyeongchang-gun and Kangwon prefectures in the Republic of Korea has a subtropical climate with year-round precipitation. The average annual precipitation from 1978 to 2008 was 1400 mm (Korea Meteorological Administration). The rainfall occurs mainly in the summer season (June–September) as a result of the East Asian monsoon, during which time the territory of Korea is also impacted by the passage of severe tropical typhoons. Most of the heavy rainfall in Korea can be attributed to typhoons passing over the territory. In particular, on 16 July 2006, more than 1200 shallow landslides occurred and triggered many debris flows. The total rainfall amount and maximum rainfall intensity of the triggering event were 417 mm/day and ~45 mm/h, respectively (Korea Meteorological Administration).

The study area ranges from ~383 to 533 m a.s.l., and the average area and average slope angle of hillslopes in the study area are ~1.2 ha and 40°, respectively. The study area is underlain only by well-weathered granite and is covered mainly by Korean red pine, Japanese larch and acacia. The average soil depth on hillslopes in the study area is ~1 m, with the landslide scars in the study area ranging from 9 to 20 m in width (Fig. 2.1).

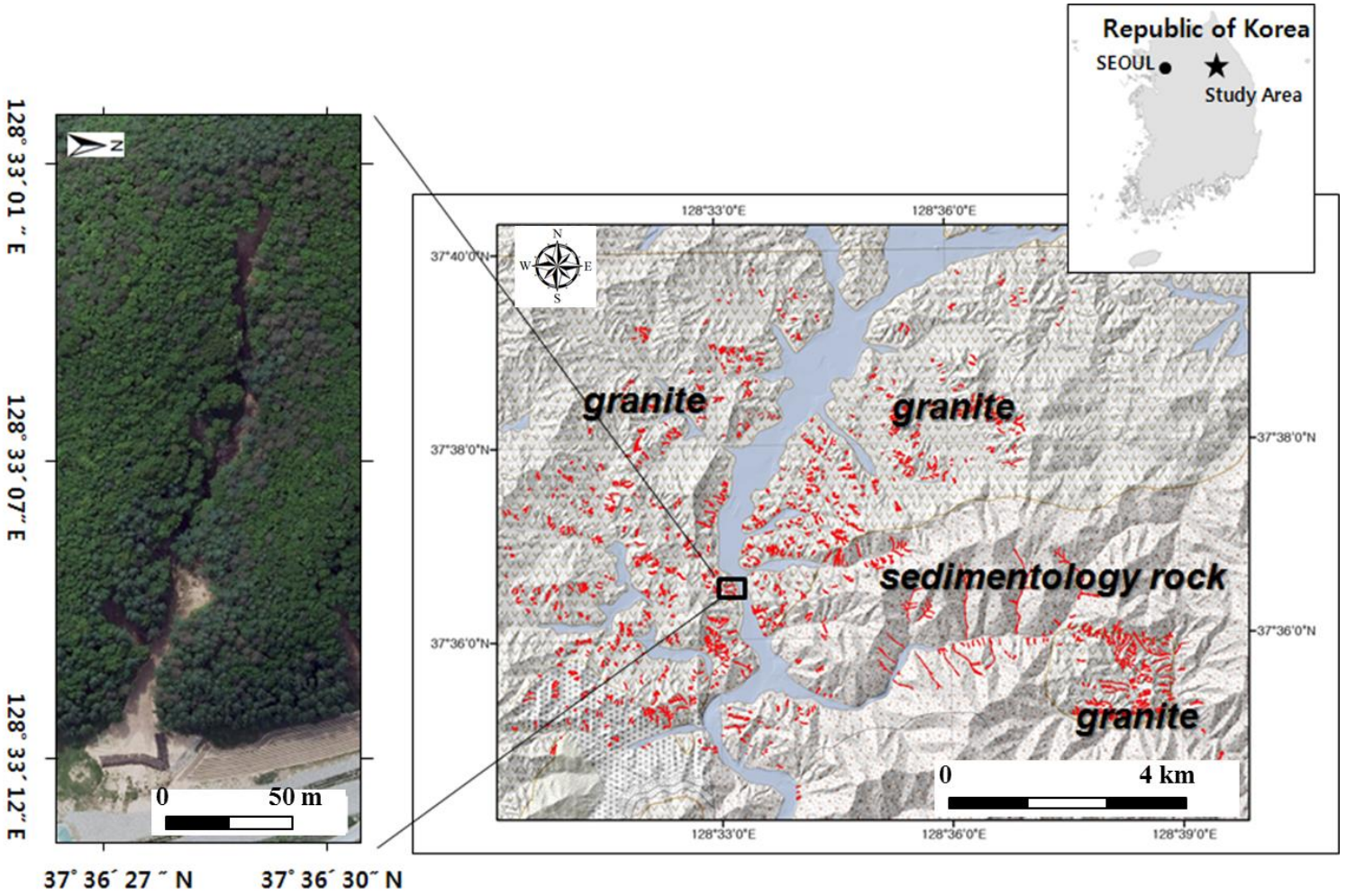

Fig. 2.1 Location and lithology map of the study site. Red colour indicates areas covered by shallow landslides that occurred on July 16, 2006.

2.3 Study Method

2.3.1 Description of r_c (H-slider)

H-slider is based on the infinite slope form of the Mohr–Coulomb failure law expressed by the ratio of stabilising forces (shear strength) to destabilising forces (shear stress) on a failure plane parallel to the ground surface (Fig. 2.2). To calculate the critical steady-state rainfall required to cause shallow landsliding, H-slider follows the methods of Okimura et al. (1985) and Montgomery and Dietrich (1994). An infinite planar slope can be used as a good approximation of a hillslope when soil thickness is small with respect to the length of the slope, as in the case of a hillslope (e.g. Okimura et al., 1985; Montgomery and Dietrich, 1994; Wu and Sidle, 1995; Rosso et al., 2006; Uchida et al., 2011). Thus, if the saturated depth is less than the soil depth, an infinite slope stability analysis can be used to compute the FS as follows:

$$\mathrm{FS} = \frac{c + \left(\gamma h cos^2 I - u(t)\right) tan\emptyset}{\gamma h cos I sin I} \qquad (2.1)$$

where c is effective cohesion (kN/m^2), $u(t)$ is pore pressure (cmH_2O), $\emptyset$ is the friction angle of the soil mantle (°), I is the angle of the bedrock surface (°), h is soil thickness (m) and γ is the specific weight of the soil mantle (kN/m^3).

Subsurface flow within saturated soil can be expressed using the law of Darcy as

$$\mathrm{Q(t)} = K_s \frac{u(t)}{\gamma_w} tan I \qquad (2.2)$$

where Q(t) is total discharge at the outlet point (m^2/s), K_s is saturated hydraulic conductivity

(m/s), and γ_w is the weight of water (kN/m^3). If Eq. (2.2) is combined with the law of conservation of mass in water, it can be expressed as

$$\mathrm{Q(t)} = \mathrm{r(t)A} + \frac{dv}{dt} \quad (2.3)$$

where r(t) is the rainfall intensity (m/s), A is the contributed area (m^2/m) and *v* is the water storage within a contour length (m^3/m) point. If we assume a steady state (dv/dt = 0) and from Eqs (2.2) and (2.3), u(t) is

$$\mathrm{u(t)} = \frac{r(t)A\gamma_w}{K_s tanI} \quad (2.4)$$

Substituting Eq. (4) into Eq. (1), we obtain

$$\mathrm{FS} = \frac{c + \left(\gamma h cos^2 I - \frac{r(t)A\gamma_w}{K_s tanI}\right) tan\emptyset}{\gamma h cosI sinI} \quad (2.5)$$

According to Darcy's law, the saturated water depth h_s (m) for calculating the steady-state rainfall intensity can be described as follows:

$$h_s = \frac{rA}{K_s sinI cosI} \quad (2.6)$$

if $h_s \leq h$, then one can obtain the critical steady-state rainfall (mm/h) required to cause shallow landsliding. Here, by setting $h_s = h$ in Eq. (2.3) and rearranging, the fully saturated condition can

be described as follows:

$$\mathrm{r} = \frac{hK_s sinIcosI}{A} \quad (2.7)$$

Thus, if a grid cell satisfies the equation

$$\frac{c}{\gamma_w cos^2 tan\emptyset + \gamma_s cosI(sinI - cosItan\emptyset)} > h \quad (2.8)$$

even if the soil mantle is fully saturated, the FS is larger than 1.0.

r_c, the critical steady-state rainfall required to cause shallow landsliding, can be determined with Eqs (2.5)–(2.8) by setting FS = 1 as follows:

$$r_c = \frac{K_s tanI\ cosI\{c - \gamma_t hcosI(sinI - cosItan\emptyset)\}}{A\{\gamma_w cosItan\emptyset + (\gamma_s + \gamma_t)(sinI - cosItan\emptyset)\}} \quad (2.9)$$

Where, γ_s is the specific weight of the saturated soil [kN/m^3] and γ_t is the specific weight of the unsaturated soil [kN/m^3].

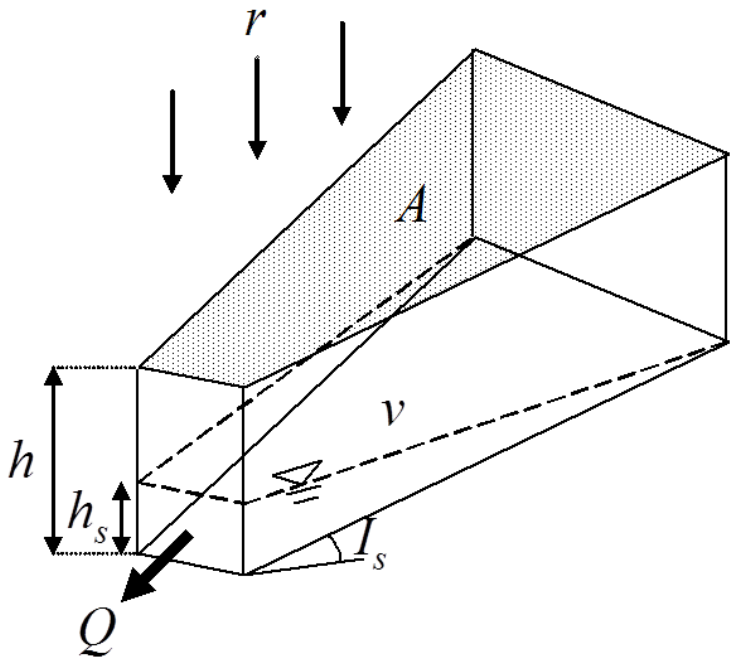

Fig. 2.2 Concept of H-slider

2.3.2 A stochastic hydro-geomorphologic concept for shallow landslide

Topography influences shallow landslide initiation through both the concentration of subsurface flow and the effect of the slope gradient on slope stability (Montgomery and Dietrich, 1994; Talebi et al., 2008). Failure often occurs in areas of convergent topography in which subsurface soil water flow paths give rise to excess pore-water pressures downslope (Anderson et al., 1991; Wilkinson et al., 2002; Talebi et al., 2008). Planar infinite slope analysis has been applied widely to the determination of natural slope stability, particularly when the thickness of the soil mantle is small compared to the slope length and when shallow landslides are due to failure of a soil mantle that overlies a sloping drainage barrier (Borga et al., 1998; Talebi et al., 2008). Some researchers have suggested that the two-layer model of soil and bedrock, which assumes a potential landsliding (soil) layer, is suitable for slope stability analysis of shallow landslides (Iida, 1999; D'Odorico and Fragherazzi, 2003; Talebi et al., 2008). Iida (1999) applied the same ap-

proach in his stochastic hydro-geomorphological model for shallow landslides due to rainstorms (Fig. 2.3).

$$H_{cr} = \frac{c - \gamma_t cos^2\beta(tan\beta - tan\emptyset)D}{cos^2\beta\{(\gamma_{sat} - \gamma_t)(tan\beta - tan\emptyset) + \gamma_w tan\emptyset\}} \quad (2.10)$$

where c is cohesion, $\emptyset$ is the internal friction angle, β is the slope angle, γ_t is the weight per unit volume of unsaturated soil, γ_{sat} is the weight per unit volume of saturated soil and γ_t is the weight of water per unit volume.

When the soil depth D is equal to in Fig.3, the critical soil depth D_{cr} can be expressed as

$$D_{cr} = \mathrm{c}/cos^2\beta\{\gamma_{sat}(tan\beta - tan\emptyset) + \gamma_w tan\emptyset\} \quad (2.11)$$

When the soil depth D is less than D_{cr} ($H_{cr} > D$), the depth H of saturated throughflow cannot reach the critical D_{cr}, even in the event of rainstorms with no shallow landsliding because the water table of saturated throughflow cannot rise beyond the ground surface. In this case, the saturation overland flow occurs. In the case of a relatively steep slope ($\emptyset < \beta$), D_{cr} decreases linearly with an increase in soil depth D and D_{cr} becomes zero. This means that shallow landsliding can occur on the slope without saturated throughflow if a critical ("upper limit") soil depth D exists:

$$D_{max} = \mathrm{c}/\gamma_t cos^2\beta(tan\beta - tan\emptyset) \quad (2.12)$$

The implications for modelling soil evolution are important because without cohesion, soils could never form on slopes greater than $\emptyset$, and even thin soils on slopes in the range $\beta < \emptyset$ would be extremely unstable because light rainfall would provide a saturated water depth H sufficient to cause landslides. Both of these implications are contrary to observations and suggest that soil cohesion (and hence the concept of "immunity depth") are needed in slope stability models (Iida, 1999; D'Odorico and Fragherazzi, 2003; Talebi et al., 2008).

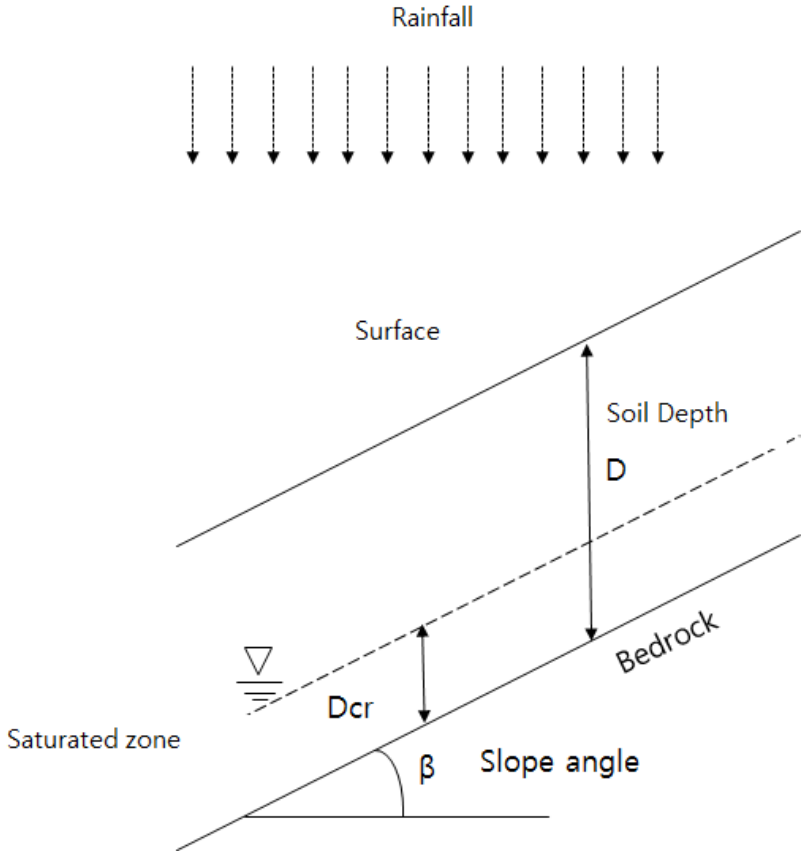

Fig. 2.3 Concept of stochastic hydro-geomorphology model

When soil properties data (e.g. cohesion) and topography data (e.g. slope angle) are substituted into Eqs (2.12) and (2.13), the results can be expressed, such as in Fig. 2.4, with soil thickness. The D_{cr} curves of the completely unsaturated state and D_{max} of the fully saturated state

in Fig. 2.4 perform important roles in obtaining the optimal values of cohesion and the internal friction angle, and we are able to control the two curves by controlling the internal friction angle and especially cohesion. When we control the curves of D_{cr} of the unsaturated state and D_{max} of the fully saturated state for calculating the soil parameters (i.e. internal friction angle and cohesion), an important point is that the distribution of soil thickness against slope angle comprises very sensitive input parameters and the curves can be changed, especially according to cohesion and the internal friction angle according to the distribution of soil thickness against the slope angle, which is related to topography.

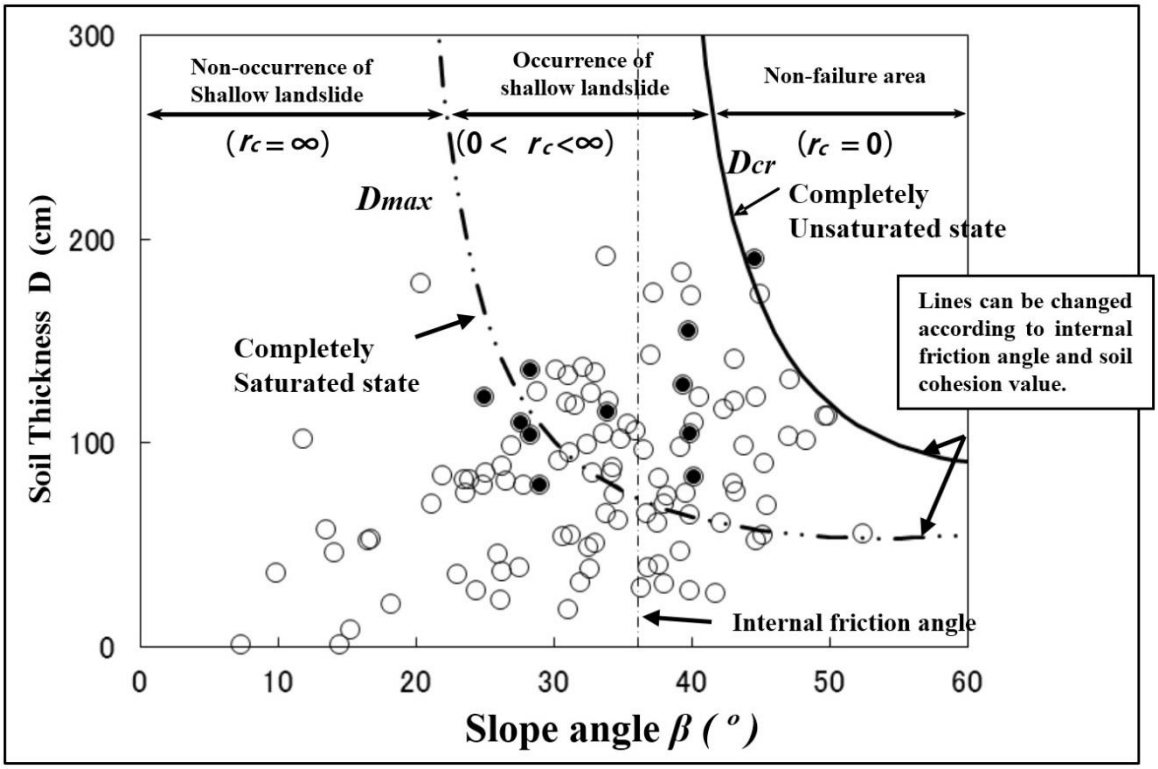

Fig. 2.4 D_{cr} (solid line) and D_{max} (dash line) calculated using Eqs (2.11) and (2.12), respectively. Shallow landslides can occur between D_{cr} and D_{max}. White circles indicate soil thickness measured with the knocking pole test outside of the shallow landslide area, and black circles indicate soil thickness measured by the knocking pole test inside the shallow landslide scar..

2.3.3 Soil thickness measurement and topography data

Unsaturated and saturated subsurface flows on a hillslope or in a catchment are affected by topography, soil depth and hydraulic properties in a complex manner. These properties serve as input data for numerical simulations and have significant implications for simulation accuracy. Although detailed surface topographic data can usually be readily obtained from DEMs, the soil depth and hydraulic properties for an entire hillslope or catchment are often lacking. The topography data used were from a 5 × 5-m DEM based on a digital elevation map (1:5000) from the National Geographic Information Institute in the Republic of Korea. The locations of shallow landslide areas were back-filled to represent the topography of the study area before landsliding (Fig. 2.5a, b).

The dynamic cone penetrometer (25 mm diameter with 60° tip angle), also known as a knocking pole (Yoshinaga and Ohnuki, 1995), consists of several 0.5 m flights of 15 mm diameter stainless steel rods with etched graduations every 10 cm. The penetration resistance value, *Nd* (drop/10 cm), was computed by the number of blows required for 10 cm of penetration. Liang et al., (2013) compared vertical *Nd* distributions between locations outside and inside shallow slope failures and found that soil layers with *Nd* values ranging from 5 to 20 were not detected at locations inside slope failures at their study site. They suggested that soil depths with an $Nd \leq 20$ could be defined as weathered soil layers (Fig. 2.5c) with the potential to fail, and that soil depths with an $Nd \geq 20$ could be defined as bedrock layers (Fig. 2.5d) in which failure would not occur. Penetration tests were conducted at 125 points (10 – 15 m intervals) along the slope, and the soil distribution was calculated by using the *Nd* values (Fig. 2.5).

I made a 5 × 5 m DEM of the ground surface from a digital elevation map (1:5000). It was then applied to make a 5 × 5 m DEM of the bedrock surface topography using the TIN [Triangulated Irregular Network] interpolation scheme and in situ soil thickness data (Freer et al.,

2002). Data sets of slope angle and upslope drainage area were calculated from the DEMs of both ground surface topography and bedrock surface topography, respectively, using the D-infinity method suggested by Tarboton (1997).

Additionally, soil samples were collected within the boundary between weathered soil and bedrock of the failure scars of two landslides in the study area. Testing of soils to understand their behaviour during shallow failure requires a method that mimics a stress field under natural conditions. Shallow landslides are triggered by elevated pore pressures that decrease the effective normal stress (i.e. the normal load minus the pore pressure) rather than by an increase in the shear stress. Whereas typical triaxial shear testing is done by increasing the shear stress, the CD [Consolidated Drained] test approximates the conditions that exist during rainfall-induced failure by holding the shear stress constant while reducing the effective stress. Hydraulic conductivity (*Ks*) tests were performed in the laboratory with "constant head" and "falling head" permeameters using soil cores extracted in the field. I calculated the *Ks* of the hillslope at the study area to be 5.0×10^{-2} m/s, which was 12 times the average soil-saturated conductivity measured in the undisturbed 100-cm^3 soil samples (Table 2.1).

Table 2.1 Soil parameters for shallow landslide modeling from tri-axal compression test method

Model input parameters	Values
Saturated soil density (kN/m^3)	17.4
Dry density (kN/m^3)	14.9
Water density (kN/m^3)	10
Hydraulic conductivity (m/h)	0.05
Cohesion (kPa)	1.6
Internal Friction Angle (˚)	36.5

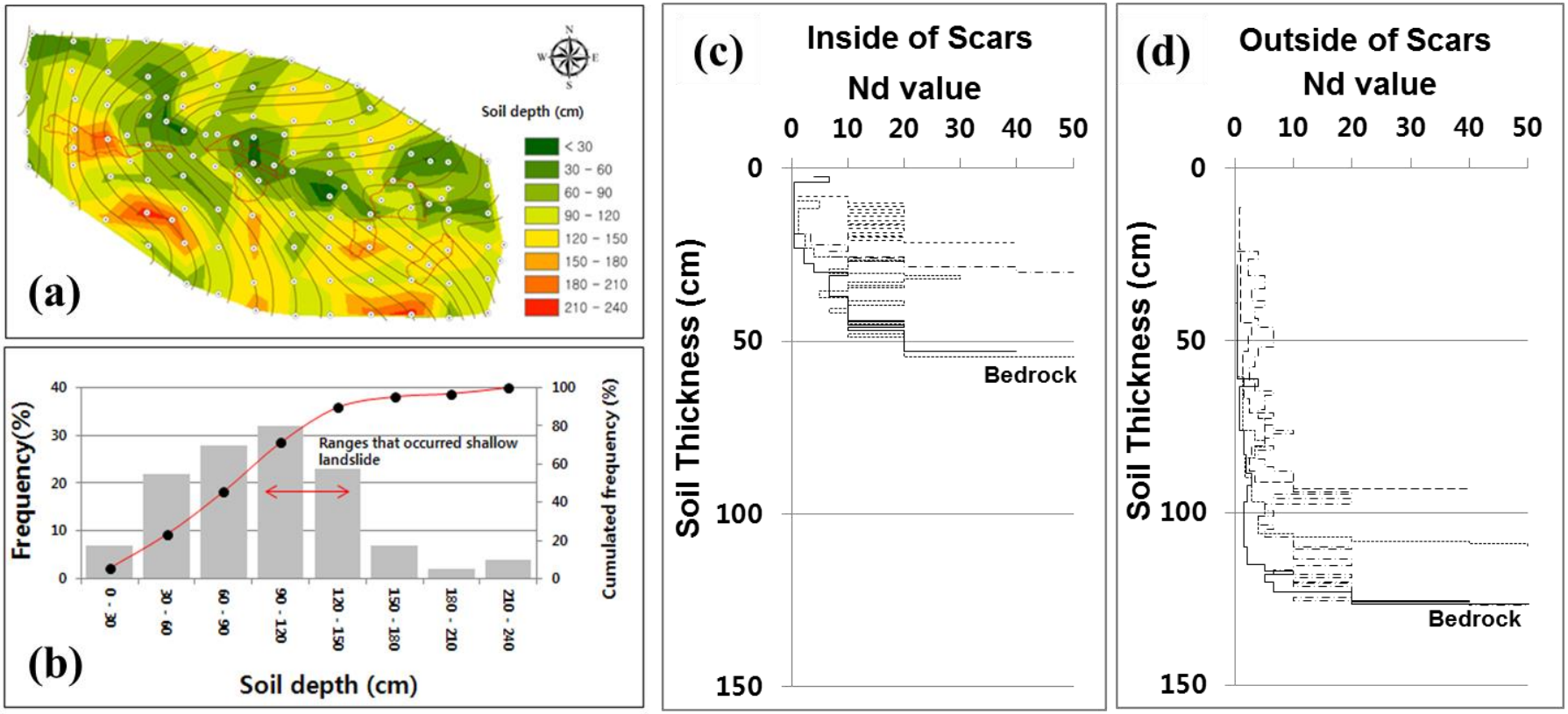

Fig. 2.5 This figure shown that soil distribution in study area (a), frequency of shallow landslide within soil thickness(b), Nd values of inside of landslide scar (c) and Nd values of outside of landslide scar (d) measured by using knocking pole test.

2.3.4 Accuracy analysis of model results

Shallow landslide prediction models commonly have the advantage of allowing for extensive analyses of hydrological responses without requiring a large number of observational items. However, these shallow landslide models combined with a simple hydrological model, which is extensively applied for the prediction of shallow landslides, tend to overpredict due to the input parameters. To objectively determine the accuracy of landslide prediction using different soil-thickness data, six criteria (three ground surface topographic and three bedrock surface topographic) were applied to check the model's performance.

The reliability of the model was assessed by overlying the digitised landslide map onto the map of predicted simulation results of the critical rainfall necessary for slope instability and comparing the resulting patterns. The prediction accuracy of regional landslide susceptibility models has typically been evaluated by comparing the locations of the known landslides with simulation results from the model (Montgomery et al., 1998, 2001; Godt et al., 2008). Receiver operating characteristics (ROCs), which are used in various studies including weather forecasting and landslide susceptibility mapping, represent a technique for comparing the performance of models for which results can be assigned to one of two classes or states (Swets, 1988; Fawcett, 2006; Van Den Eeckhaut et al., 2006; Godt et al., 2008). The model with the higher percentage provides the better prediction of shallow landslides.

The least critical test of prediction accuracy would be to count a successful prediction when a single grid cell is located within a mapped landslide polygon. More critical tests of prediction accuracy involve more detailed assessment of 1) the capability of the model to correctly identify mapped landslides (TP, true positive), 2) the frequency of errors when mapped landslides are not correctly identified (FN, false negative), 3) overprediction (FP, false positive) and 4) the model's ability to correctly identify an area that does not include mapped landslides

(TN, true negative). An ideal landslide susceptibility map simultaneously maximises the agreement between known and predicted landslide locations and minimises the area outside known landslides predicted to be unstable (FP). To perform the ROC analysis, two quantities were calculated: sensitivity (the true positive rate), defined as the ratio between TP and the sum of TP and FN, and specificity (the false positive rate), defined as the ratio between FP and the sum of TN and FP. Accuracy was defined as the ratio of TP + TN to the sum of all values (TP + FP + FN + TN) (Fig. 2.6).

Many previous studies have applied ROC analysis to estimate the accuracy of shallow landslide predictions (e.g. Begueria, 2006; Fawcett, 2006; Park et al., 2013), and ROC analysis was also applied in this study. For the ROC analysis of this study, I used *rc*, the critical steady-state rainfall amount (mm/h), as an index for assessing shallow landslide susceptibility. Under low rainfall amounts, grid cells with lower *rc* values denote areas unstable for shallow landsliding while those with higher *rc* values indicate stable areas.

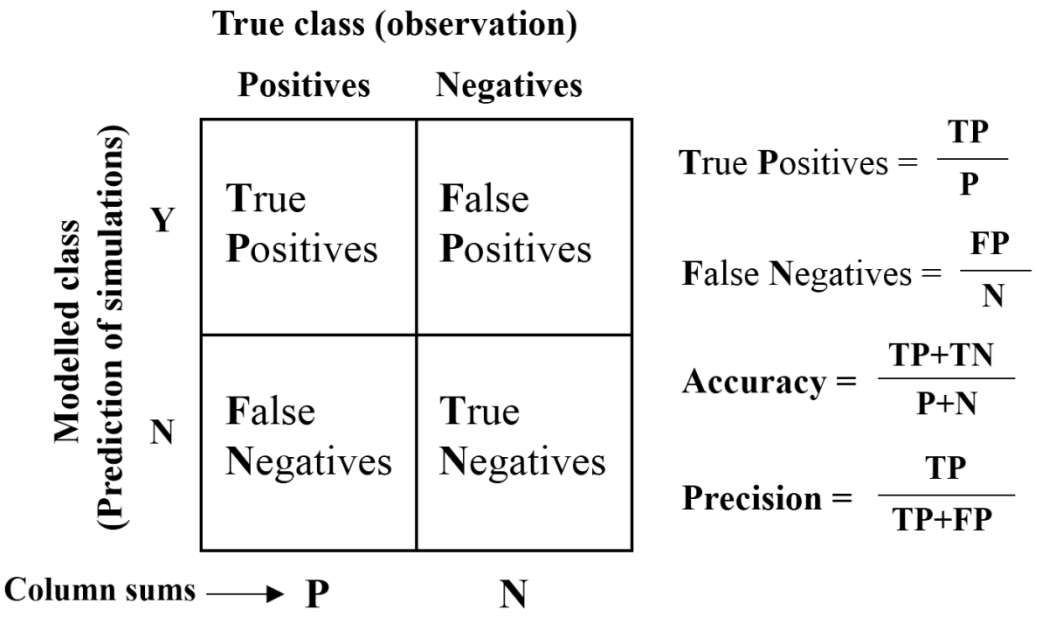

Fig. 2.6 Reciever operating characteristic (ROC) analysis method for determining the accuracy of shallow landslide prediction in this study (modified from Godt et al., 2008).

2.4 Results

2.4.1 Simulation results of H-slider

Our first simulation using H-slider considered two types of categories (Case I and Case II), i.e. GSTO and BSTO, respectively. Each category was divided into three simulation cases: average soil thickness (a), weathered soil thickness (b) and bedrock soil thickness (c). To input soil parameters into the H-slider model, I used soil parameters collected with the triaxial compression test method (Table 2.1).

Fig. 2.7 shows the results (Case I) of the spatial distribution of simulated critical rainfall intensity (mm/h) based on the GSTO using H-slider with the three soil thickness cases (a, b and c). The locations and boundaries of shallow landslides from air-photo imagery in 2006 were overlapped onto the Case I result. Fig. 2.7a presents the results of the spatial distribution of critical rainfall (mm/h) using average soil thickness (1 m) (Case I (a)). In Case I (a), 44% of the possible occurrences of shallow landslides were under a rainfall intensity of 20 mm/h (Table 2.2) and distributed evenly on the simulated area. The possible occurrences of shallow landslides under a rainfall intensity of more than 80 mm/h were 33.6% and distributed along the boundary of the watershed in the simulated area. Fig. 2.7b presents the results of the spatial distribution of critical rainfall (mm/h) using the distribution of weathered soil thickness (Case I (b)) from the knocking pole tests (Fig. 2.5). In Case I (b), 20.8% of the possible occurrences of shallow landslides were in the rainfall intensity of less than 20 mm/h (Table 2.2) and distributed evenly on the simulated area, and 62.4% of the possible occurrences of shallow landslides were in the rainfall intensity of more than 80 mm/h and distributed along the boundary of the watershed in the simulated area. Fig. 2.7 (c) presents the results of the spatial distribution of critical rainfall (mm/h) using the distribution of bedrock soil thickness (Case I (c)) from the knocking pole tests (Fig. 2.5). In Case I (c), 30.4% of the possible occurrences of shallow landslides were in the rainfall

intensity of less than 20 mm/h (Table 2.2) and distributed evenly on the simulated area, and 48.8% of the possible occurrences of shallow landslides were in the rainfall intensity of more than 80 mm/h and distributed along the boundary of the watershed in the simulated area.

To evaluate the accuracy of the simulated critical rainfall (mm/h) based on the GSTO (Case I) for the occurrence of shallow landslides, the reliability of each model result was evaluated using ROC analysis. The accuracy values from ROC for Case I of shallow landslide prediction, presented in Table 2.2, were 0.42, 0.67 and 0.54 for Cases I (a), I (b) and I (c), respectively. The results of the ROC analysis indicated that the accuracy of the modelling results for shallow landslides had a high value when the weathered soil distribution (Case I (b)) was used. Although Cases I (b) and I (c) used in situ soil thickness data, their ROC values were a little higher than that of Case I (a), implying that real soil thickness data can provide a small improvement to the accuracy of shallow landslide prediction based on the GSTO. Using the BSTO, the results well explained the movement of subsurface water flow compared to the GSTO. I used the BSTO to investigate how much the accuracy of shallow landslide prediction improves compared to the GSTO results.

Fig. 2.8 shows the results (Case II) of the spatial distribution of simulated critical rainfall intensity (mm/h) from H-slider based on the BSTO and the three soil thickness cases (a, b and c). The locations and boundaries of shallow landslides from air-photo imagery acquired in 2006 were overlapped on the result of Case II. Fig. 2.8a presents the results of the spatial distribution of critical rainfall (mm/h) using the average soil thickness (1 m) (Case II (a)). In Case II (a), 44% of the possible occurrences of shallow landslides were in the rainfall intensity of less than 20 mm/h (Table 2.2) and distributed evenly on the simulated area. Possible occurrences of shallow landslides at a rainfall intensity greater than 80 mm/h accounted for 40% of the incidences and were distributed along the boundary of the watershed in the simulated area. Fig. 2.8b presents the results of the spatial distribution of critical rainfall (mm/h) using the distribution of

weathered soil thickness (Case II (b)) from the knocking pole test (Fig. 2.5). In Case II (b), 28.8% of the possible occurrences of shallow landslides were in the rainfall intensity of less than 20 mm/h (Table 2.2) and distributed evenly on the simulated area, and 57.6% of the possible occurrences were in the rainfall intensity of more than 80 mm/h and distributed along the boundary of watershed. Fig. 2.8c presents the results of the spatial distribution of critical rainfall (mm/h) using the distribution of bedrock soil thickness (Case II (c)) from the knocking pole test (Fig. 2.5). In Case II (c), 24% of the possible occurrences of shallow landslides were in the rainfall intensity of less than 20 mm/h (Table 2.2) and distributed evenly on the simulated area, and 56.8% of the possible occurrences were in the rainfall intensity of more than 80 mm/h and distributed along the boundary of the watershed.

To evaluate the accuracy of the simulated critical rainfall (mm/h) based on the BSTO (Case II) for the occurrence of shallow landsliding, the reliability of each model result was evaluated using ROC analysis. The accuracy values using ROC for Case II of shallow landslide predictions, presented in Table 2.2, were 0.43, 0.58 and 0.52 for Cases II (a), II (b) and II (c), respectively. The results of the ROC analysis for the three cases indicate that the accuracy of the modelling results for shallow landslides had a high value when the weathered soil distribution (Case II (b)) was used. Although Cases II (b) and II (c) used in situ soil thickness data, their ROC values were a little higher than that of Case II (a), which implies that real soil thickness data can slightly improve the accuracy of shallow landslide prediction based on the BSTO. The results of the ROCs based on the GSTO (Case I) were almost the same as those based on the BSTO (Case II). This result implies that the combination of BSTO and the three soil thicknesses could not improve the accuracy of shallow landslide prediction compared to the accuracies of Case I.

However, both the results of Case I and Case II showed that the accuracy when soil thickness data were inputted (b and c) was higher compared to that of average soil thickness (a),

indicating that soil thickness may contribute to improvements in shallow landslide prediction. Additionally, when the weathered soil layer was used, the accuracy of shallow landslide prediction clearly improved compared with using the other soil layers in these simulation cases.

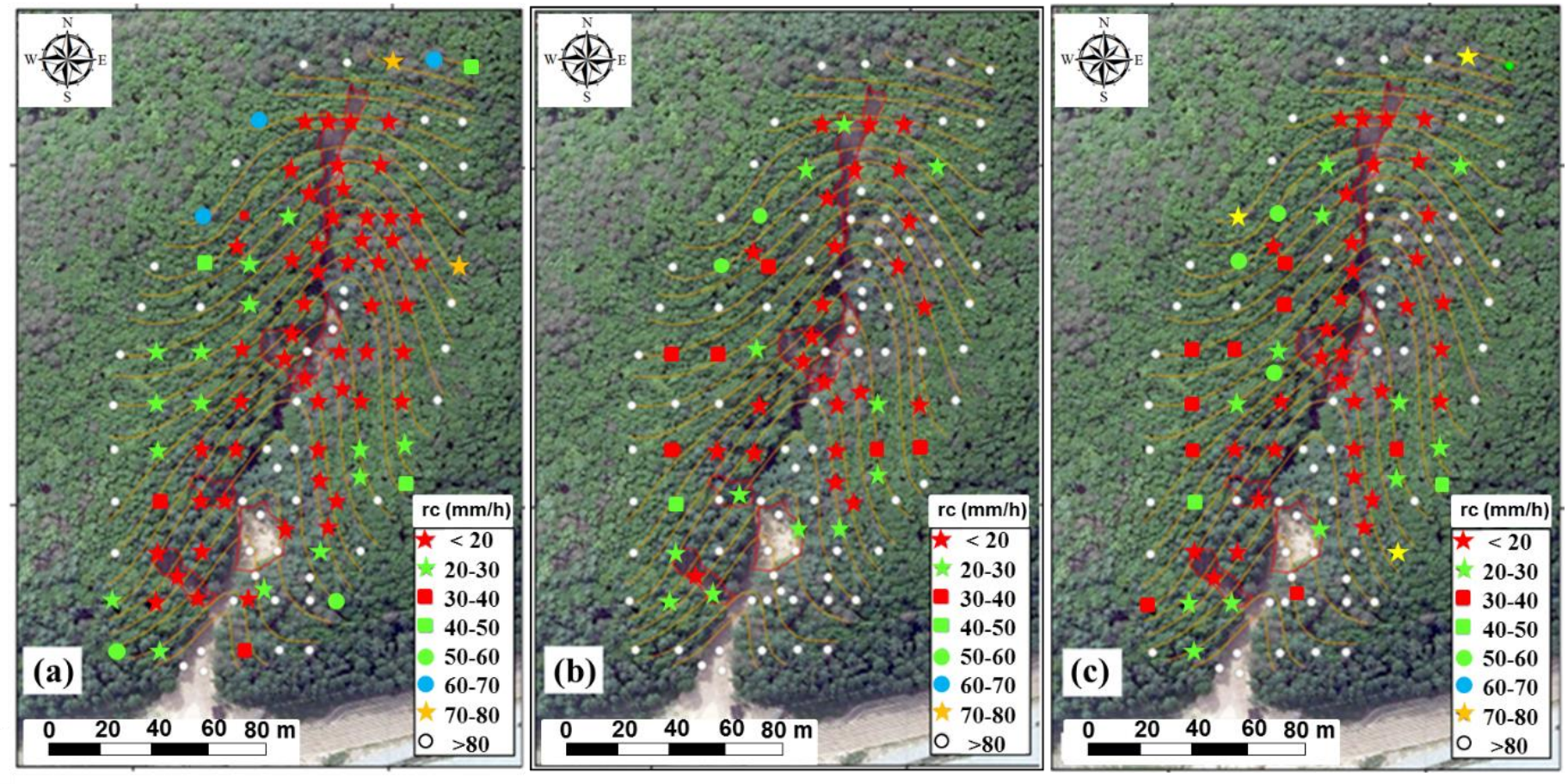

Fig. 2.7 Maps of the simulation results showed steady-state critical rainfall intensity (mm/h) caused shallow landslide using Ground surface topography and various soil thickness ((a) average soil thickness 1m, (b) weathered soil thickness and (c) bedrock soil thickness). Observed shallow landslides (in red line) that occurred on July 16, 2006, are also shown mapped shallow landslides

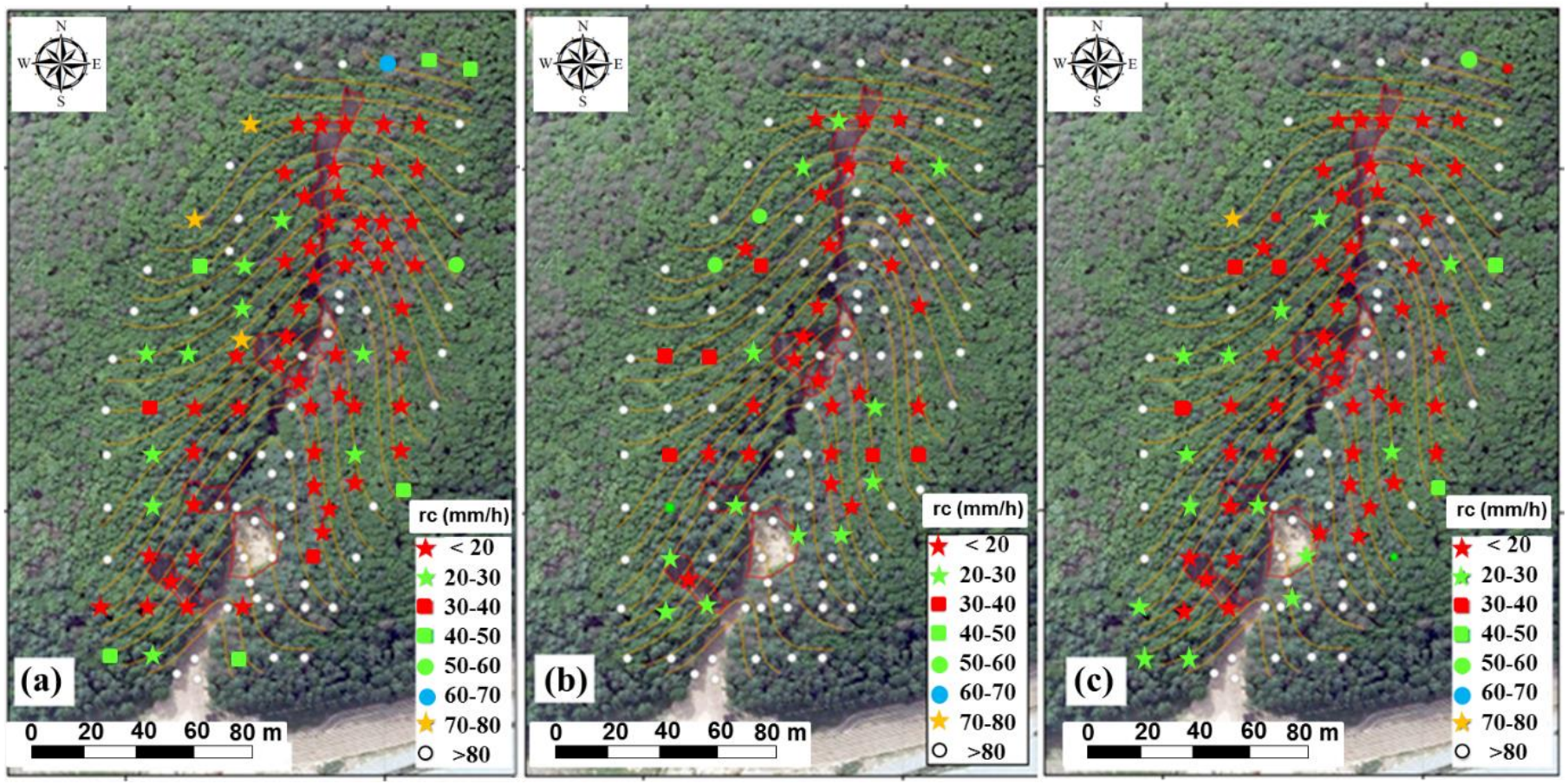

Fig. 2.8 Maps of the simulation results showed steady-state critical rainfall intensity (mm/h) caused shallow landslide using Bedrock surface topography and various soil thickness ((a) average soil thickness 1m, (b) weathered soil thickness and (c) bedrock soil thickness). Observed shallow landslides (in red line) that occurred on July 16, 2006, are also shown mapped shallow landslides.

Table 2.2 The results of distribution of steady state critical rainfall intensity using two DEMs (GSTO – Case I and BSTO – Case II) and three soil thickness ((a) Average Soil thickness (b) Weathered Soil thickness and (c) Bedrock Soil thickness). ROC values indicated the accuracy of prediction results.

Ground Surface Topography (GST) - Case I						
critical rainfall intensity	AST (a)	ratio (%)	WST (b)	ratio (%)	BST (c)	ratio (%)
< 20	55	44	26	20.8	38	30.4
20 - 30	15	12	12	9.6	12	9.6
30 - 40	3	2.4	6	4.8	8	6.4
40 - 50	3	2.4	1	0.8	2	1.6
50 - 60	2	1.6	2	1.6	3	2.4
60 - 70	3	2.4	0	0	0	0
70 - 80	2	1.6	0	0	1	0.8
> 80	42	33.6	78	62.4	61	48.8
Sum	125	100	125	100	125	100
Accuracy	0.42		0.67		0.54	
Bedrock Surface Topography (BST) - Case II						
critical rainfall intensity	AST (a)	ratio (%)	WST (b)	ratio (%)	BST (c)	ratio (%)
< 20	55	44	36	28.8	30	24
20 - 30	10	8	10	8	14	11.2
30 - 40	2	1.6	4	3.2	5	4
40 - 50	6	4.8	1	0.8	1	0.8
50 - 60	1	0.8	1	0.8	3	2.4
60 - 70	1	0.8	0	0	0	0
70 - 80	0	0	1	0.8	1	0.8
> 80	50	40	72	57.6	71	56.8
Sum	125	100	125	100	125	100
Accuracy	0.43		0.58		0.52	

2.4.2 Soil parameterization using hydro-geomorphology concept

To evaluate the topography effect by H-slider, I considered two DEMs and three soil thicknesses. However, the accuracy of the modelling results was generally low (Table 2.2), even when various model (e.g. BSTO and three soil thicknesses) parameters were used. Thus, I checked the soil parameters, which showed that cohesion had a low value of 1.6 and that the internal friction angle also had a low value of 36.5, rather than average hillslope angle of 40°. Therefore, I calculated the soil parameters to improve the accuracy of model performance.

To generate the model input data, a stochastic hydro-geomorphological model was used (see Section 2.3.2) and the soil parameters were calculated. Fig. 2.9 shows the results of the soil parameters for the three soil thicknesses and with the slope angle for shallow landslide prediction using the soil parameters in Table 2.1 and the soil thickness data measured in this study area (Fig. 2.4). The occurred shallow landslides were usually found between the curves of D_{cr} and D_{max} calculated from Eqs (2.11) and (2.12) because of the assumption that shallow landslides can occur only between D_{min} and D_{max}. The curves of D_{cr} and D_{max} in Fig. 2.9 performed an important role in obtaining the optimal values of cohesion and internal friction angle, which enabled calculations of the soil parameters. Table 2.3 shows the results of the calculated soil parameters considering cohesion, the internal friction angle and the effects of various soil thickness measured with the knocking pole test.

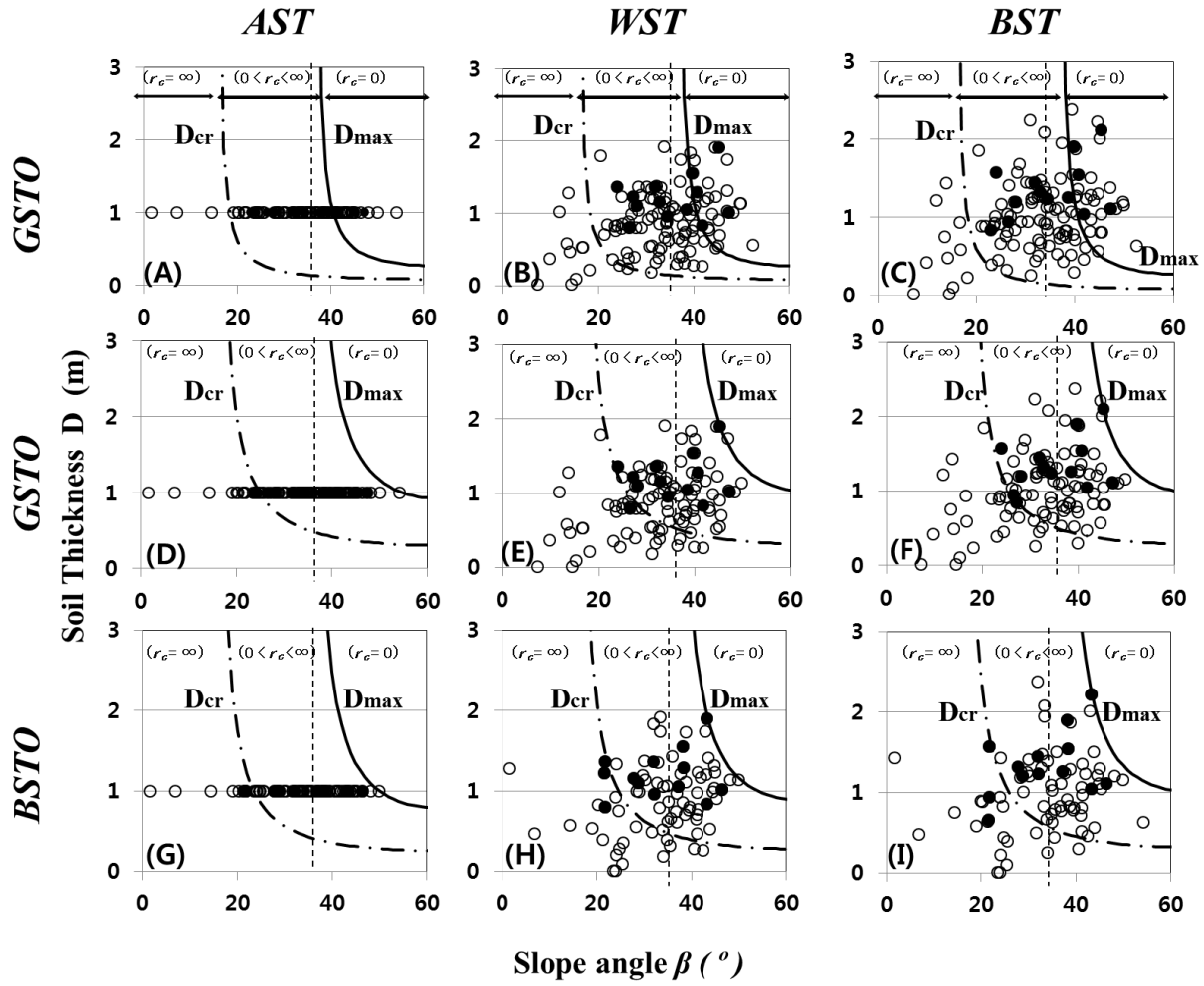

Fig. 2.9 D_{cr} (dashed line) and D_{max} (solid line) calculated using equations 2.12 and 2.13, respectively. Shallow landslides can be occurred between D_{cr} and D_{max}. From (A) to (C) used tri-axial compression test data and three distribution of soil thickness, i.e. (A) AST, (B) WST and (C) BST, based on GSTO. From (D) to (F) controlled by cohesion and internal friction angle, and GSTO and three distribution of soil thickness, i.e. (A) AST, (B) WST and (C) BST, used. From (G) to (I) controlled by cohesion and internal friction angle, and BSTO and three distribution of soil thickness, i.e. (A) AST, (B) WST and (C) BST, used

2.4.3 Re-assessment of H-slider using soil parameters reflected effect of soil thickness

Our second simulation for improving the modelling accuracy of shallow landslide prediction was also divided into two categories (GSTO for Case III and BSTO for Case IV). Each category was divided into three simulation cases: AST (a), WAS (b) and BST (c), like the first simulations (Cases I and II). In this simulation for predicting the critical rainfall intensity (mm/h) causing shallow landslides, I used soil parameters that represented the effect of the three soil thicknesses presented in Table 2.3.

Fig. 2.10 shows the results (Case III) of the spatial distribution of simulated critical rainfall intensity (mm/h) based on the GSTO and the modified soil parameters (GSTO in Table 2.3) by H-slider based on the three cases of soil thickness (a, b and c). The locations and boundaries of shallow landslides from air-photo imagery acquired in 2006 were overlapped onto the result of Case III. Fig. 2.10a presents the results of the spatial distribution of critical rainfall (mm/h) using average soil thickness (1 m) (Case III (a)) and the modified soil parameters (AST (a) in Table 2.4). In Case III (a), possible occurrences of shallow landslides at rainfall intensity of less than 20 mm/h accounted for 4.8% of occurrences (Table 2.4) and were distributed in the upper part and right slope of the simulated area. Possible occurrences of shallow landslides at rainfall intensity greater than 80 mm/h accounted for 90.4% and were distributed evenly over the simulated area.

Fig. 2.10b presents the results of the spatial distribution of critical rainfall (mm/h) using the modified soil parameters (WST (b) in Table 2.4) and the distribution of weathered soil thickness (Case III (b)) from the knocking pole tests (Fig. 2.5). In Case III (b), possible occurrences of shallow landslides at a rainfall intensity of less than 20 mm/h were 3.2% of the occurrences and distributed in the middle part of the simulated area. Possible occurrences of shallow landslides at rainfall intensity greater than 80 mm/h were 84.8% and distributed evenly over the

simulated area. Fig. 2.10c presents the results of the spatial distribution of critical rainfall (mm/h) using the modified soil parameters (BST (c) in Table 2.4) and the distribution of bedrock soil thickness (Case III (c)) from the knocking pole tests (Fig. 2.5). In Case III (c), possible occurrences of shallow landslides at rainfall intensity of less than 20 mm/h were 4% of the occurrences (Table 2.4) and distributed in the upper and middle parts of the simulated area. Possible occurrences of shallow landslides at rainfall intensity greater than 80 mm/h were 90.4% of occurrences and distributed evenly over the simulated area.

To evaluate the accuracy of simulated critical rainfall (mm/h) based on the GSTO (Case III) for the occurrence of shallow landslides, the reliability of each model result was evaluated using ROC analysis. In the ROC analysis for Case III of shallow landslide prediction (presented in Table 2.4), the accuracy values were 0.80, 0.81 and 0.83 for Cases III (a), III (b) and III (c), respectively. The results of the ROC analysis for the three cases indicate that the accuracy of the modelling results for shallow landslides had a high value when using the modified soil parameters BST (c) (shown in Table 2.3) and BST (Case III (c)). In the Case III simulation using the modified soil parameters, the simulation results for the initiation of shallow landslides showed improved accuracy, indicating that the results of the critical rainfall simulation were affected by the soil parameters, i.e. the internal friction angle and especially cohesion.

To evaluate the effect of the BSTO and the modified soil parameters, I simulated the distribution of the critical rainfall intensity (mm/h) causing shallow landslide initiation using H-slider. Fig. 2.11 shows the results (Case IV) of the spatial distribution of simulated critical rainfall intensity (mm/h) using H-slider based on the BSTO, the three cases of soil thickness (a, b and c) and the modified soil parameters shown in Table 2.3d–f. Fig. 2.11a presents the results of the spatial distribution of critical rainfall (mm/h) using the average soil thickness (1 m) (Case IVa). In Case IV (a), the possible occurrences of shallow landslides at a rainfall intensity of less than 20 mm/h were 19.2% of the occurrences (Table 2.4) and distributed evenly over the simu-

lated area. The possible occurrences of shallow landslides at a rainfall intensity of more than 80 mm/h were 66.4% of occurrences and distributed along the boundary of the watershed in the simulated area. Fig. 2.11b presents the results of the spatial distribution of critical rainfall (mm/h) using the distribution of weathered soil thickness (Case IV (b)) from the knocking pole tests (Fig. 2.5). In Case IV (b), the possible occurrences of shallow landslides at a rainfall intensity of less than 20 mm/h were 22.4% and distributed evenly over the simulated area. Possible occurrences of shallow landslides at rainfall intensity greater than 80 mm/h accounted for 60% of occurrences and were distributed along the boundary of watershed in the simulated area. Fig. 2.11c presents the results of the spatial distribution of critical rainfall (mm/h) using the distribution of bedrock soil thickness (Case IV (c)) from the knocking pole tests (Fig. 2.5). In Case IV (c), the possible occurrences of shallow landslides at rainfall intensity of less than 20 mm/h were 20% of occurrences (Table 2.2) and distributed evenly over the simulated area. Possible occurrences of shallow landslides at rainfall intensity of more than 80 mm/h were 59.2% and distributed along the boundary of the watershed in the simulated area.

To evaluate the accuracy of simulated critical rainfall (mm/h) based on the BSTO (Case IV) for occurrences of shallow landslides, the reliability of each model result was evaluated using ROC analysis. In the ROC analysis for Case IV of shallow landslide prediction (BSTO in Table 2.4), the accuracy values were 0.68, 0.60 and 0.50 for Cases IV (a), IV (b) and IV (c), respectively. The results of the ROC analysis for the three cases indicate that the accuracy of the modelling results for shallow landslides had a high value when the average soil distribution (Case IV (a)) was used. In the results of the critical rainfall intensity (mm/h) simulation using the two DEMs, three soil thicknesses and the modified soil parameters (shown in Figs 2.10 and 2.11), I found that the soil parameters, especially cohesion, improved the accuracy of shallow landslide prediction even though I applied three soil thickness and two DEMs to input parameters to H-slider in the simulation. By comparing the first simulation (Cases I and II) and the second simu-

lation (Cases III and IV) in this study, the effect of the soil parameters, rather than the effects of topography or soil thickness, may have contributed to improve the prediction of shallow landslides. However, the simulation using the modified soil parameters, the GSTO and the three soil thicknesses (Case III) indicated that if the shallow landslide simulation is performed after soil parameterization, the effect of the soil thicknesses, especially bedrock soil thickness, rather than the effect of topography, may be an important factor for shallow landslide prediction.

Table. 2.3 Calculated soil property results from the stochastic hydrogeomorphological model.

Model input parameters	Ground Surface Topographic (GST)			Bedrock Surface Topographic (BST)		
	Average	Soil layer	Bedrock	Average	Soil layer	Bedrock
Saturated soil density (kN/m3)	17.4	17.4	17.4	17.4	17.4	17.4
Dry density (kN/m3)	14.9	14.9	14.9	14.9	14.9	14.9
Cohesion (kPa)	3.5	3.8	3.5	3	3.3	3.8
Internal Friction Angle (˚)	36.5	37	37	36.5	39	38.5
Soil depth (m)	1m	Weathered	Bedrock	1m	Weathered	Bedrock

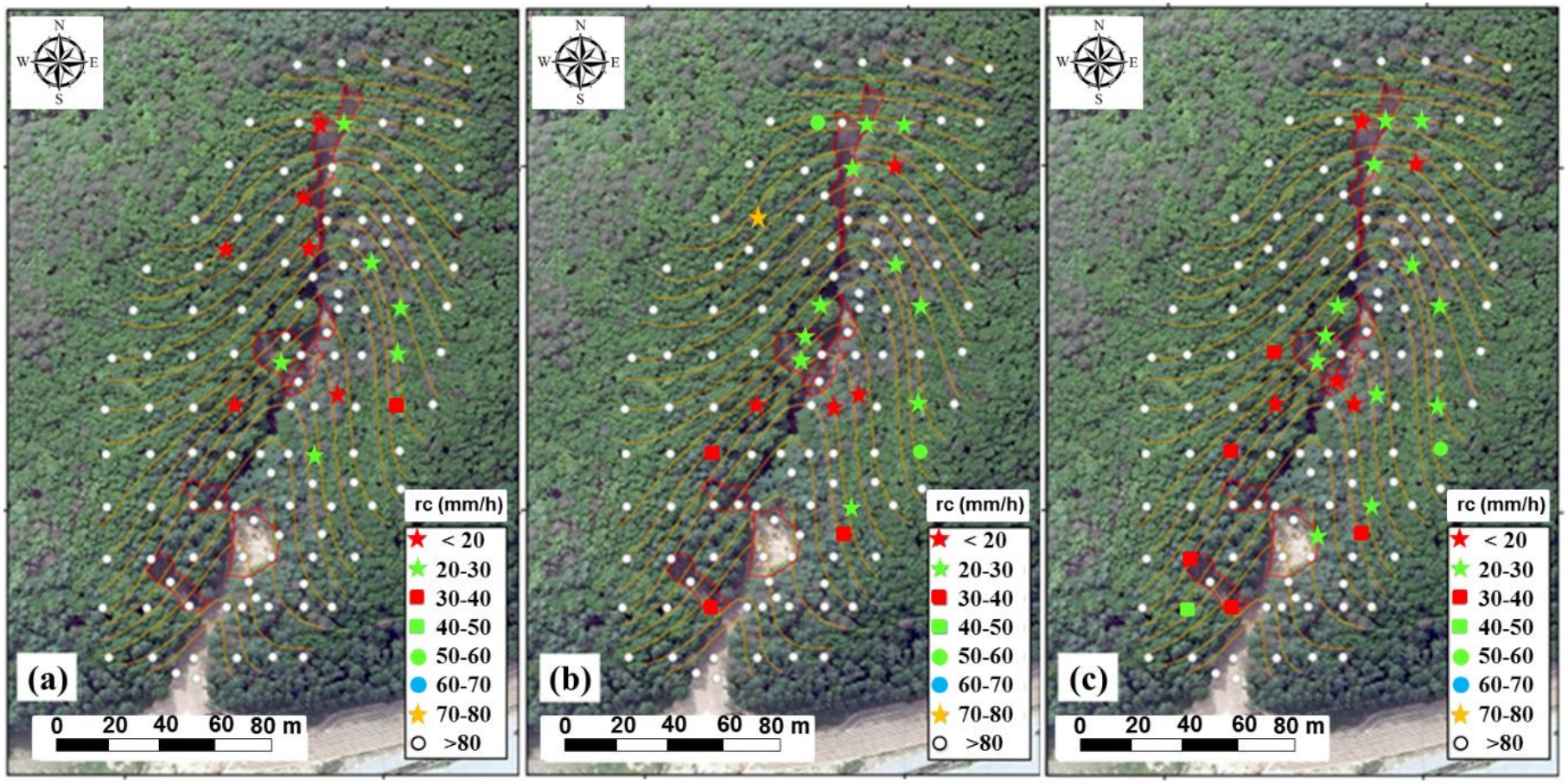

Fig. 2.10 Maps of the simulation results showed steady-state critical rainfall intensity (mm/h) caused shallow landslide using Ground surface topography, various soil thickness ((a) average soil thickness 1m, (b) weathered soil thickness and (c) bedrock soil thickness) and soil data based on GSTO from table 2.3.

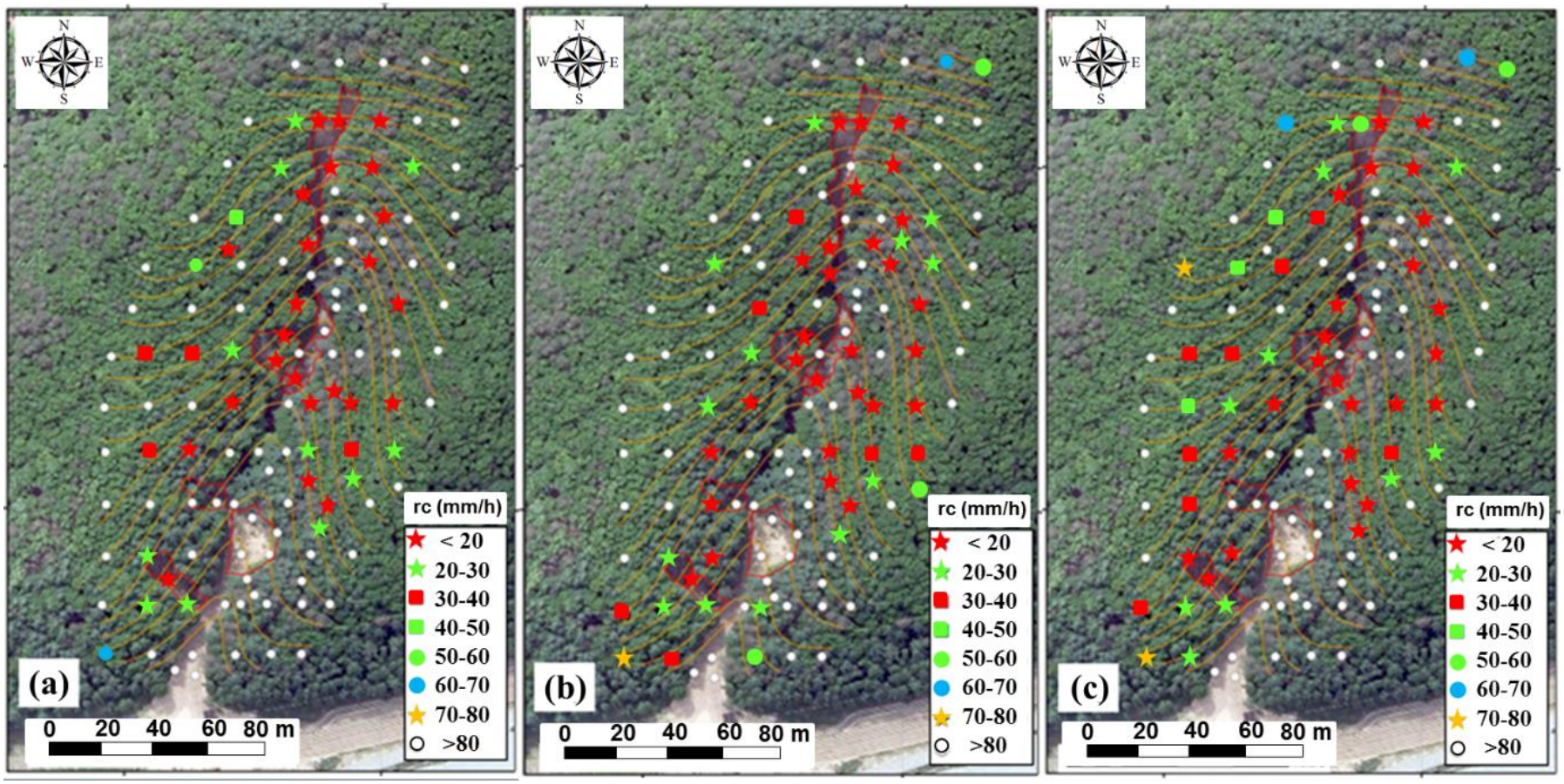

Fig. 2.11 Maps of the simulation results showed steady-state critical rainfall intensity (mm/h) caused shallow landslide using Ground surface topography, various soil thickness ((a) average soil thickness 1m, (b) weathered soil thickness and (c) bedrock soil thickness) and soil data based on BSTO from table 2.3.

Table 2.4 The results of distribution of steady state critical rainfall intensity using two DEMs (GSTO – Case III and BSTO – Case IV), three soil thickness ((a) Average Soil thickness (b) Weathered Soil thickness and (c) Bedrock Soil thickness) and soil data represented the effect of three soil thickness. ROC values indicated the accuracy of prediction results.

Ground Surface Topography (GST) - Case III						
critical rainfall intensity	AST (a)	ratio (%)	WST (b)	ratio (%)	BST (c)	ratio (%)
< 20	6	4.8	0	0	5	4
20 - 30	6	4.8	10	8	0	0
30 - 40	0	0	3	2.4	4	3.2
40 - 50	0	0	0	0	2	1.6
50 - 60	0	0	1	0.8	1	0.8
60 - 70	0	0	0	0	0	0
70 - 80	0	0	1	0.8	0	0
> 80	113	90.4	110	88	113	90.4
Sum	125	100	125	100	125	100
Accuracy	0.8		0.81		0.83	
Bedrock Surface Topography (BST) - Case IV						
critical rainfall intensity	AST (a)	ratio (%)	WST (b)	ratio (%)	BST (c)	ratio (%)
< 20	24	19.2	28	22.4	25	20
20 - 30	11	8.8	12	9.6	10	8
30 - 40	4	3.2	6	4.8	8	6.4
40 - 50	1	0.8	0	0	3	2.4
50 - 60	1	0.8	3	2.4	3	2.4
60 - 70	1	0.8	1	0.8	2	1.6
70 - 80	0	0	0	0	0	0
> 80	83	66.4	75	60	74	59.2
Sum	125	100	125	100	125	100
Accuracy	0.68		0.6		0.59	

2.5 Discussions

2.5.1. Effects of topography and soil thickness on prediction accuracy

Recent hillslope hydrology studies have shown that the subsurface topography has a strong effect on controlling the connectivity of saturated areas at the soil–bedrock interface (e.g. Freer et al., 2002; Uchida et al., 2011; Lanni et al., 2013) because the landslide slip surface can be strongly affected by its relationship with the pore-water pressure and bedrock surface topography.

Freer et al. (2002) measured soil thickness to monitor pore-water pressure and subsurface flow using tensiometers on a hillslope (20 m in width, 48 m in length and 34° average slope). They made the two DEMs (i.e. ground surface and bedrock surface) and compared the relationship between the results of monitoring at the research site and those of modelling using the two kinds of DEMs. In their results, comparing monitoring data and modelling results using the topography wetness index ($\ln(a/\tan\beta)$,), the modelling result based on the bedrock surface topography was better than that based on the ground surface topography. A topographic index (TWI) given by the ratio between the specific upslope contributing area and the local slope was used as a surrogate for lateral subsurface flow processes. The slope stability component (i.e. infinite slope stability model) used this topographic index to analyse the stability of each topographic element.

Additionally, Lanni et al. (2013) examined the response of pore-water pressure using an experiment representing bedrock interface topography (width 1.7 m, length 3.9 m, soil depth 0–0.2 m and three slope angles) and compared their findings with observed experimental data and modelling data using the Hydras 3-D program. They concluded that topographic depressions at the bedrock layer induced localised zones of pore-pressure fields that led to rapid landslide propagation in an experiment and that a pore-water pressure spatial distribution based on the to-

pography of bedrock may significantly improve the ability of a landslide model. H-slider reflects pore-water pressure by using Eq. (2.4). Because monitoring and modelling (e.g. Freer et al., 2002; Lanni et al., 2013) were based on the monitoring of pore-water pressure, I applied bedrock surface topography to H-slider. Thus, I followed this concept to improve the shallow landslide prediction.

Figs 2.7 and 2.8 represent the results of the spatial distribution of simulated critical rainfall intensity (mm/h) based on the two DEMs (GSTO and BSTO), respectively, the three distributions of soil thicknesses and the physical soil parameters obtained by triaxial compression test. Figs 10 and 11 represent the results of the spatial distribution of simulated critical rainfall intensity (mm/h) based on the two DEMs (GSTO and BSTO), respectively, three distributions of soil thicknesses and the modified physical soil parameters by the stochastic hydro-geomorphological model. However, in the results based on the BSTO (Cases II and IV (a) – (c)), application of the BSTO was determined unsuitable in this study by comparing its findings with the distribution of modelling results based on the shallow landslide boundaries from air-photo imagery and the results of the ROC analysis (Tables 2.2 and 2.4). This means that the bedrock surface topography did not affect modelling performance by H-slider and that the ground surface topography may be more reasonable for the prediction of shallow landslide initiation.

The distribution of the DEM in the study of Freer et al. (2002) had values ranging between 222 and 279 m, and the difference in elevation was ~55 m. Lanni et al. (2013) used bedrock interface topography (width 1.7 m, length 3.9 m, soil depth 0–0.2 m and three slope angles). However, in our research, the difference in elevation was ~150 m, as in Fig. 2.4a. This means that the analysis of flow paths using the D-infinity method by Tarboton (1997) may affect flow path simulation results. For example, Zhu and Lin (2009) studied the relationship between a subsurface interface DEM and a land surface DEM using a hydrologic model and reported that result of flow paths in the hydrologic modelling had almost similar results with more than 90%

agreement. They then interpreted the distinction between the results of the GSTO and BSTO. First, the topography of the interfaces was dominated by variation in land surface elevation. Second, soil thickness points measured at their research site were lacking, which affected the results of the flow path simulation.

Additionally, Uchida et al. (2011) applied the H-slider model to the Hiroshima area in Japan, which is similar to our study site, and they also used a surface interface DEM and bedrock interface DEM, such as in our study. In their results of critical rainfall prediction, they noted that the precision of landslide susceptibility prediction showed little difference between the surface interface DEM and bedrock interface DEM. Because research on the effect of using a bedrock surface DEM for shallow landslide prediction is lacking, I am unable to evaluate this conclusion. However, the effect of using a bedrock interface DEM in our research did not increase the accuracy of the shallow landslide model, such as in other studies (e.g. Zhu and Lin, 2009; Uchida et al., 2011). Consequently, for areas in which the subsurface interface topography is dominated by the surface DEM, the surface DEM can be used sufficiently to simulate subsurface concentrated lateral flow paths. Otherwise, simulation based on a subsurface interface DEM may be more desirable (Zhu and Lin, 2009).

Many researchers have noted that soil depth may provide a way to derive bedrock topographic relief and lead to the coupling of physically based landslide models with quantitative soil–landscape methods to ultimately improve their ability to predict shallow landslide potential (e.g. Rosso et al., 2006; Uchida et al., 2011; Lanni et al., 2013). Commonly, slope failures (shallow landslides) often occur in areas of topography in which subsurface soil water flow paths give rise to excess pore-water pressures downslope (Anderson et al., 1991; Wilkinson et al., 2002; Talebi et al., 2008). The results of the comparison between Case I (Fig. 2.7) and Case II (Fig. 2.10) showed that the accuracy of the modelling results was affected by soil thickness, and especially that the weathered soil depth showed a high accuracy for shallow landslide prediction

modelling. In contrast, the results of the comparison between Case III (Fig. 2.10) and Case IV (Fig. 2.11) showed that the accuracy of the modelling results was affected by soil thickness, and especially that bedrock soil thickness showed a high accuracy for shallow landslide prediction modelling.

Here, I found that the distributions of the two soil thicknesses used as model input parameters influenced the results of the modelling in this study. Uchida et al. (2011) discovered the relationship between the weathered layer ($Nd < 20$) and bedrock layer ($Nd > 20$) in their study area under granite. They applied two soil thicknesses to shallow landslide prediction and the results showed that using bedrock soil thickness produced higher prediction results than when using weathered soil thickness. However, in the case of Uchida et al. (2011), soil thickness was on average 1.8 m and the deepest thickness was 5 m, and our study site showed an average thickness of 1 m with a deepest thickness of 2.4 m (Fig. 2.4b). Therefore, spatial variability in soil thickness is likely to be important in shallow landslide prediction on other steep landscapes (Keijsers et al., 2011).

2.5.2. Soil re-parameterisation for improving the prediction accuracy

Case I (Fig. 2.7) and Case II (Fig. 2.8) used soil parameters tested by the triaxial compression method because Frank et al. (2009) observed that the triaxial compression test is better than the direct shear test for predictive models of shallow landslides, as it represents the processes and characteristics of the superficial soil layers reasonably well. In this study, the soil parameters tested by the triaxial compression method were applied to shallow landslide predictions, and the accuracy of the prediction results by ROC analysis showed overprediction and overly low values in Figs 2.7 and 2.8. However, the results of Case III and Case IV, which used modified soil parameters from a hydro-geomorphological model, rather than those of Cases I and

II, showed high accuracy, which may be explained by two reasons from the viewpoint of physical soil properties. First, because the triaxial compression test method did not clearly reflect root cohesion, the cohesion value might have led to error. According to Montgomery and Dietrich (1994), the effect of roots on shear stress resistance can be taken into account by increasing the value of the shear stress resistance angle by 40%. Schmidt et al. (2001) and D'Odorico and Fagherazzi (2003) showed that soil and root cohesion is inherently necessary for soil to build up in steep hollows; otherwise, landslides would occur even with light rainfall (Rosso et al., 2006).

Additionally, some researchers have recently shown the effect of the dependence between cohesion and internal friction angle in slope stability analyses (Yucemen et al., 1973; Low and Tang, 1997; Liang et al., 1999; Cherubini, 2000; Hong and Roh, 2008; Wu, 2008; Babu and Singh, 2009; Cho, 2010; Cho and Park, 2010). Soil cohesion has sometimes been neglected in stability analyses of steep mantled slopes, while the angle of repose has been deliberately increased to realistic values to account for the overall shear strength of the aggregates (Montgomery and Dietrich, 1994; D'Odorico and Fagherazzi, 2003). For these reasons, cohesion is a sensitive parameter in shallow landslide models and one of the most difficult to quantify; empirical treatment of this parameter may lead to large errors in estimates of slope stability (Casadai et al., 2003; Wooten et al., 2007).

Second, cohesion has an influence on soil thickness and topography. In this study, the internal friction angle, and especially cohesion, had a high impact on model accuracy as many researchers have also explained (e.g. Montgomery and Dietrich, 1994; Rosso et al., 2002; Linni et al., 2013). To evaluate the physical soil properties reflecting the distribution of soil thickness, I used a hydro-geomorphological concept model to calculate the soil properties. From the hydro-geomorphological model, the internal friction angle and especially cohesion were determined to be sensitive values for shallow landslide prediction. Then, the two calculated values were applied to the H-slider model to evaluate the improvement of prediction. Figs 2.10 and 2.11

illustrate the results of the prediction of shallow landslides using the calculated soil parameters.

Model accuracy was improved after parameterisation and the results, plotted in Figs 2.10 and 2.11, showed a clear tendency for shallow landslides to occur much more frequently with high values of cohesion and internal friction angles. Several researchers have reported that soil depth, cohesion and internal friction angle often exhibit considerable differences between suitable values used in model calculation and those measured from field sampling (e.g. Dietrich et al., 1995; Chang and Chiang, 2009). In terms of modelling method, although triaxial compression tests were done, cohesion equals soil and plant root cohesion. With soil samples, calculating the root cohesion is technically difficult, which may bring inaccuracy to the model.

Additionally, Casadei et al. (2003) noted that cohesion is the most important parameter affecting sensitivity analysis and that internal friction affects it secondarily. Another case study was begun after taking different locations and habitats of soil samples and analysing the distribution of cohesion depending on soil depth and the phase of the different habitats, and it concluded that the results showed a pattern similar to that of previous cohesion tests (Guimaraes et al., 2003). In other words, many researchers have explained that when entering parameters of soil properties into a model, the result cannot include the real nature of landslides. Although all the strength and hydrological parameters in the slope stability model can be obtained from field measurements or laboratory analysis, some of these parameters are difficult to define in practise, particularly with regard to their spatial variation (Dietrich et al., 1995). Hence, a definition of the relationship between soil cohesion and internal friction angle must consider theoretical approaches to a result based on that modelling method.

2.5.3. Other effects on prediction accuracy

Figure. 2.10 shows the shallow landslide prediction results when using the modified soil parameters, bedrock soil thicknesses and ground surface topography. Shallow landslide prediction using this combination of parameters showed greater accuracy compared with the other combinations of other parameters from a comparison among the 12 simulation cases (i.e. Cases I, II, III and IV (a)–(c)).

The first major purpose of our study was to present the effects of topography by comparing the GSTO with BSTO, and the second purpose was to improve the accuracy of modelling performance by controlling various model input parameters. Thus, I did not consider the effect of DEM resolution. However, I constructed 5-m resolution DEMs by using a 5-m contour digital map because shallow landslide scars in the study area were larger than this resolution. Many researchers have noted that a fine DEM (<10 m) is better than a coarse DEM (>20-m pixels) in these shallow landslide simulations (e.g. Montgomery and Dietrich, 1994; Uchida et al., 2011; Lanni et al., 2013). In this study, using various factors controlling the accuracy of shallow landslide prediction, a combination of the GSTO, BST and modified soil parameters (Case III (c)) showed reasonable modelling results using H-slider compared with the combination of other parameters by ROC analysis among 12 simulation cases (Cases I, II, III and IV (a)–(c)). However, the distribution of critical rainfall prediction using H-slider still did not clearly express the distribution of shallow landslides simulated.

Claessens et al. (2005) carried out a computation of steady-state critical rainfall using different DEM resolutions and reported that even if using a high-resolution DEM, such as from lidar data, for shallow landslide prediction modelling, it is unable to describe the characteristics of a natural hillslope in detail. Furthermore, Uchida et al. (2011) analysed the grid size, which ranged from 5 to 25 m interpolated from lidar data, to evaluate model accuracy using H-

slider at their research site for shallow landslides, Japan, and concluded that the effects of grid size had little effect on the simulation results. Liang and Uchida (2013) also applied a high-resolution DEM based on inputted data to the simulation of unsaturated flow using the 2D Richard equation. However, they also were unable to obtain highly accurate simulation results, similar to the experience of other researchers (e.g. Claessens et al., 2005; Uchida et al., 2011).

Additionally, Casadei et al. (2003) noted that although their topographic data captured part of the valley network and hollows from which landslides most commonly occurred, many fine-scale slopes were missing. Furthermore, in general, such data neither capture local steps and gentle slope areas nor the strength of topographic convergences and divergences, which influence pore-water pressure built up due to shallow subsurface flow. In this study, to evaluate the effect of topography on shallow landslide prediction, I applied the physically based H-slider model to a hillslope-scale site using diverse factors for shallow landslide prediction. However, I considered only topography, and soil thickness and physical soil properties, in this study. Furthur study of other factors, including the effects of hydraulic conductivity and antecedent rainfall, will be needed to improve shallow landslide predictions.

2.2.6 Conclusion

To evaluate the effects of topography and soil parameterisation reflecting the soil depth on shallow landslide prediction accuracy using H-slider, in this study, I considered various input parameters, i.e. two DEMs (ground surface and bedrock surface), three soil thicknesses (average soil thickness, weathered soil thickness and bedrock soil thickness) and physical soil parameters (cohesion and internal friction angle). The results of the topographic effect on the prediction of shallow landslides (Cases I and II) showed that the accuracy when using the GSTO was higher than the accuracy when using the BSTO. The prediction of shallow landslides with

soil parameterisation (Cases III and IV) showed improvement in prediction accuracy compared with Cases I and II, especially for prediction with the GSTO and soil parameterisation (Case III), which had the highest accuracy. These results imply that the accuracy of shallow landslide prediction was highest with the combination of ground surface topography and the modified soil parameters, and that the effect of soil parameters on the prediction of shallow landslides in this study could be greater than the effect of topography or soil thickness. Therefore, using soil properties representing the effect of soil thickness can improve the accuracy of shallow landslide prediction, thus contributing to more accurate prediction of shallow landslides.

References

Aleotti, P., 2004. A warning system for rainfall-induced shallow failures. Engineering Geology **73**, 247–265.

Anderson, M.G., Kemp, M.J., 1991. Towards an improved specification of slope hydrology in the analysis of slope instability problems in the tropics. Progress in Physical Geography **15**, 29–52.

Babu, G.L.S., Singh, V., 2009. Reliability analysis of soil nail wall. Georisk **3**, 44–54.

Baum, R.L., Savage, W.Z., Godt, J.W., 2008. TRIGRS - a fortran program for transient rainfall infiltration and grid-based regional slope stability analysis, version 2.0. In Open File Report US Geological Survey, 81.

Begueria, S., 2006. Validation and evaluation of predictive models in hazard assessment and risk management. Natural Hazards **37**, 315–329.

Borga, M., Dalla Fontana, G., Gregoretti, C., Marchi, L., 1998. Shallow landslide hazard assessment using a physically based model and digital elevation data. Journal of Environmental Geology **35**, 81–88.

Caine, N., 1980. The rainfall intensity–duration control of shallow landslides and debris flows. Geografiska Annaler: Series A, **62**, 23–27.

Campbell, R.H., 1975. Soil slips, debris flows, and rainstorms in the Santa Monica Mountains and vicinity, Southern California. U.S. Geological Survey Prof. Paper 851, 1–20.

Cannon, S.H., Gartner, J.E., Wilson R.C., Bowers J.C., Laber J.L., 2008. Storm rainfall conditions for floods and debris flows from recently burned areas in southwestern Colorado and southern California. Geomorphology **96**, 250–269.

Casadei, M., Dietrich, W.E., Miller, N.L., 2003. Testing a model for predicting the timing and location of shallow landslide initiation in soil mantled landscapes. Earth Surface Processes and Landforms **28**, 925–950.

Chang, K.T., Chiang, S.H., 2009. An integrated model for predicting rainfall-induced landslides. Geomorphology **105**, 366–373.

Cherubini, C., 2000. Reliability evaluation of shallow foundation bearing capacity on c' and ϕ' soils. Canadian Geotechnical Journal **37**, 264–269.

Cho, S.E., 2010. Probabilistic assessment of slope stability that considers the spatial variability of soil properties. Journal of Geotechnical and Geoenvironmental Engineering **136**, 975–984.

Cho, S.E., Park, H.C., 2010. Effect of spatial variability of cross-correlated soil properties on bearing capacity of strip footing. International Journal for Numerical and Analytical Methods in Geomechanics **34**, 1–26.

Claessens, L., Heuvelink, G.B.M., Schoorl, J.M., Veldkamp, A., 2005. DEM resolution effects on shallow landslide hazard and soil redistribution modeling. Earth Surface Processes and Landforms **30**, 461–477.

Coe, J.A., Kinner, D.A., Godt, J.W., 2008. Initiation conditions for debris flows generated by runoff at Chalk Cliffs, central Colorado. Geomorphology **96**, 270–297.

Crosta, G.B., Dal Negro, P., 2003. Observations and modelling of soil slip-debris flow initiation processes in pyroclastic deposits: the Sarno 1998 event. Natural Hazards and Environmental System Sciences **3**, 53–69.

Dahal, R.K., Hasegawa, S., Yamanaka, M., Nishino K., 2006. Rainfall triggered flow-like landslides: understanding from southern hills of Kathmandu, Nepal and northern Shikoku, Japan. Proc. 10th Int. Congress of IAEG, The Geological Society of London, IAEG2006 Paper number **819**, 1–14 (CD-ROM).

DeRose, R.C., Trustrum, N.A., Blaschke, P.M., 1991. Geomorphic change implied by regolith slope relationships on steepland hillslopes, Taranaki, New Zealand. Catena **18**, 489–514.

Dietrich, W.E, Montgomery D.R., 1998. SHALSTAB: a digital terrain model for mapping shallow landslide potential. Technical Report, NCASI.

Dietrich, W.E., Reiss, R., Hsu, M., Montgomery, D.R., 1995. A process-based model for colluvial soil depth and shallow landsliding using digital elevation data. Hydrological Processes **9**, 383–400.

D'Odorico, P., Fagherazzi, S., 2003. A probabilistic model of rainfall-triggered shallow landslides in hollows: a long-term analysis. Water Resources Research **39**, 1262,

doi:10.1029/2002WR001595.

Duan, J., Grant, G.E., 2000. Shallow landslide delineation for steep forest watersheds based on topographic attributes and probability analysis. In: Wilson, J.P., Gallant, J.C. (Eds.), Terrain Analysis—Principles and Applications. John Wiley & Sons, New York, pp. 311–329.

Ewen, J., Parkin, G., O'Connell, P.E., 2000 SHETRAN: distributed river basin flow and transport modeling system. Journal of Hydrologic Engineering **5**, 250-258.

Fawcett, T., 2006. An introduction to ROC analysis. Pattern Recognition Letters **27**, 861–874.

Fernandes, N.F., Guimarães, R.F., Gomes, R.A.T., Vieira, B.C., Montgomery, D.R., Greenberg, M.H., 2004. Topographic controls of landslides in Rio de Janeiro: field evidence and modeling. Catena **55**, 163–181.

Frank G., Martin F. Albert B. 2009. Effects of vegetation on the angle of internal friction of a moraine, Forest Snow and Landscape Research, **82**, 61-77.

Freer, J., McDonnell, J.J., Beven, K.J., Peters, N.E., Burns, D.A., Hooper, R.P., Aulenbach, B., Kendall, C., 2002. The role of bedrock topography on subsurface stormflow. Water Resource Research **38**, doi:10.1029/2001WR000872.

Giannecchini, R., 2006. Relationship between rainfall and shallow landslides in the southern Apuan Alps (Italy). Natural Hazards and Earth System Science **6**, 357–364, doi:10.5194/nhess-6-357-2006.

Giannecchini, R., Naldini, D., D'Amato Avanzi, G., Puccinelli, A., 2007. Modelling of the initiation of rainfall-induced debris flows in the Cardoso basin (Apuan Alps, Italy). Quaternary International **171**, 108–117.

Godt, J.W., Baum, R.L., Savage, W.Z., Salciarini, D., Schulz, W.H., Harp, E.L, 2008. Transient deterministic shallow landslide modeling: requirements for susceptibility and hazard assessments in a GIS framework. Engineering Geology **102**, 214–226.

Guzzetti, F., Peruccacci, S., Rossi, M., Stark, C.P., 2007. Rainfall thresholds for the initiation of landslides in central and southern Europe. Meteorology and Atmospheric Physics **98**, 239–267.

Guzzetti, F., Peruccacci, S., Rossi, M., Stark, C.P., 2008. The rainfall intensity–duration control of shallow landslides and debris flows: an update. Landslides **5**, 3–17.

Heimsath, A.M., Dietrich, W.E., Nishiizumi, K., Finkel, R.C., 1997. The soil production function and landscape equilibrium. Nature **388**, 358– 361.

Hilberts, A., Van Loon, E.E., Troch, P.A., Paniconi, C., 2004. The hillslope-storage Boussinesq model for non-constant bedrock slope. Journal of Hydrology **291**, 160–173.

Hiramatsu, S., Mizuyama, T., Ishikawa, Y., 1990. Study of a method for predicting hillside landslides by analysis of transient flow of water in saturated and unsaturated soils. Journal of the Japan Society of Erosion Control Engineering **43**, 5–15 (in Japanese).

Ho, J.Y., Lee, K.T., Chang, T.C., Wang, Z.Y., Liao, Y.H., 2012. Influence of spatial distribution of soil thickness on shallow landslide prediction. Engineering Geology **124**, 38–46.

Hong, H.P., Roh, G., 2008. Reliability evaluation of earth slope. Journal of Geotechnical and Geoenvironmental Engineering **134**, 1700–1705.

Iida, T., 1999. A stochastic hydro-geomorphological model for shallow landsliding due to rainstorm. Catena **34**, 293–313.

Iida, T., Tanaka, K., 1997. The relationship between topography and soil depth measured with the portable penetration test apparatus. Japan Geomorphological Union **18**, 61–78.

Iverson, R.M., Reid, M.E., LaHusen, R.G., 1997. Debris-flow mobilization from landslides. Annual Review of Earth and Planetary Sciences **25**, 85–138.

Keijsers, J.G.S., Schoorl, J.M., Chang, K.-T., Chiang, S.H., Claessens, L., Veldkamp, A., 2011. Calibration and resolution effects on model performance for predicting shallow landslide locations in Taiwan. Geomorphology **133**, 168–177.

Kim, M.S., Kim. J.K., Cho, Y.C., Kim, S.W., 2011. Geomorphic-characteristics of debris flow induced by typhoon “RUSA” in 2002 using Shalstab Model and Remote Sensing: case study in Macheon region near Jiri-Mountain. Journal of the Korean Geomorphological Association **18**, 1-15. (English abstract)

Kim, M.S., Onda. Y., Kim, J.K., 2015. Improvement of shallow landslide prediction accuracy using soil parameterisation for a granite area in South Korea, 2015, Natural Hazards and Environmental System Sciences Discussion **3**, 227–267.

Lanni, C., McDonnell, J., Hopp, L., Rigon, R., 2013. Simulated effect of soil depth and bedrock topography on near-surface hydrologic response and slope stability. Earth Surface Pro-

cesses and Landforms **38**, 146–159.

Liang, R.Y., Nusier, O.K., Malkawi, A.H., 1999. A reliability based approach for evaluating the slope stability of embankment dams. Engineering Geology **54**, 271–285.

Liang, W., Uchida, T., 2013. Effects of topography and soil depth on saturated-zone dynamics in steep hillslopes explored using the three-dimensional Richards' equation. Journal of Hydrology **510**, 124–136.

Low, B.K., Tang, W.H., 1997. Efficient reliability evaluation using spreadsheet. Journal of Engineering Mechanics, ASCE **123**, 749–752.

Melchiorre, C., Frattini, P., 2012. Modelling probability of rainfall-induced shallow landslides in a changing climate, Otta, Central Norway. Climatic Change **113**, 413–436.

Minder, J.R., Roe, G.H., Montgomery, D.R., 2009. Spatial patterns of rainfall and shallow landslide susceptibility. Water Resource Research **45**, W04419, doi:10.1029/2008WR007027.

Montgomery, D.R., Dietrich, W.E., 1994. A physically based model for the topographic control on shallow landsliding. Water Resources Research **30**, 1153–1171.

Montgomery, D.R., Dietrich, W.E., Torres, R. Anderson, S.P., Loague, K., 1997. Subsurface flow paths in a steep unchannelled catchment. Water Resources Research **33**, 91–109.

Montgomery, D.R., Sullivan, K., Greenberg, M.H., 1998. Regional test of a model for shallow landsliding. Hydrological Processes **12**, 943–955.

Montgomery, D.R., Balco, G., Willett, S.D., 2001. Climate, tectonics, and the morphology of the Andes. Geology **29**, 579–582, doi:10.1130/0091-7613(2001)029<0579:CTATMO>2.0.CO;2.

Okimura, T., 1989. A method for estimating potential failure depth used for a probable failure predicting model. Journal of the Japan Society of Erosion Control Engineering **42**, 14–21 (in Japanese).

Okimura, T., Ichikawa, R., Fujii, I., 1985. Methods to predict failures on granite mountain slopes by an infiltrated water movement model in a surface layer. Journal of the Japan Society of Erosion Control Engineering **37**, 44–49 (in Japanese).

Pack, R.T., Tarboton, D.G., Goodwin, C.N., 1998. The SINMAP Approach to Terrain Stability

Mapping, 8th Congress of the International Association of Engineering Geology, Vancouver, BC, Canada.

Park, H.J., Lee, J.H., Woo, I., 2013. Assessment of rainfall-induced shallow landslide susceptibility using a GIS-based probabilistic approach. Engineering Geology **161**, 1–15.

Reid, M.E., Christian, S.B., Brien, D.L., 2000. Gravitational stability of three-dimensional stratovolcano edifices. Journal Geophysical Research **105**, 6043–6056.

Renato Fontes Guimarãesa, David R. Montgomery, Harvey M. Greenberg, Nelson Ferreira Fernandes, Roberto Arnaldo Trancoso Gomes, Osmar Abílio de Carvalho Júnior, 2003, Parameterization of soil properties for a model of topographic controls on shallow landsliding: application to Rio de Janeiro. Engineering Geology **69**, 99-108.

Rickenmann, D., Zimmermann, M., 1993. The 1987 debris flows in Switzerland: documentation and analysis. Geomorphology 8, 175–189.

Rosso, R., Rulli, M.C., Vannucchi, G., 2006. A physically based model for the hydrologic control on shallow landsliding. Water Resources Research **42**, W06410. http://dx.doi.org/10.1029/2005WR004369.

Saulnier, G.M., Obled, C., Beven, K., 1997. Analytical compensation between DTM grid resolution and effective values of saturated hydraulic conductivity within the TOPMODEL framework. Hydrological Processes **11**, 1331–1346.

Schmidt, K.M., Roering, J.J., Stock, J.D., Dietrich, W.E., Montgomery, D.R., Shaub T., 2001. Root cohesion variability and shallow landslide susceptibility in the Oregon Coast Range. Canadian Geotechnical Journal **38**, 995–1024.

Simoni, S., Zanotti, F., Bertoldi, G., Rigon, R., 2008, Modeling the probability of occurrence of shallow landslides and channelized debris flows using GEOtop-FS, Hydrological Process, 22, 532–545.

Swets, J.A., 1988. Measuring the accuracy of diagnostic systems. Science **240**, 1285–1293.

Talebi, A., Troch, P.A., Uijlenhoet, R., 2008. A steady-state analytical hillslope stability model for complex hillslopes. Hydrological Process **22**, 546–553.

Tarboton, D.G., 1997. A new method for the determination of flow directions and contributing areas in grid digital elevation models. Water Resources Research **33**, 309–319.

Tesfa, T.K., Tarboton, D.G., Chandler, D.G., McNamara, J.P., 2009. Modeling soil depth from topographic and land cover attributes. Water Resources Research **10**, W10438. http://dx.doi.org/10.1029/2008WR007474.

Troch, P.A., Van Loon, E.E., Hilberts, A., 2002. Analytical solutions to a hillslope-storage kinematic wave equation for subsurface flow. Advances in Water Resources **25**, 637–649.

Tsuboyama, Y., Sidle, R.C., Noguchi, S., Murakami, S., Shimizu, T., 2000. A zero-order basin—its contribution to catchment hydrology and internal hydrological processes. Hydrological Process **14**, 387–401.

Uchida, T., Tamur, K., Akiyama, K., 2011. The Role of Grid Cell Size, Flow Routing Algorithm and Spatial Variability of Soil Depth on Shallow Landslide Prediction. Italian Journal of Engineering Geology and Environment (book), doi:10.4408/IJEGE.2011-03.B-018.

van Beek, L.P.H., 2002. Assessment of the Influence of Changes in Landuse and Climate on Landslide Activity in a Mediterranean Environment. PhD Thesis, Utrecht University, Utrecht, 363.

Van Den Eeckhaut, M., Vanwalleghem, T., Poesen, J., Govers, G., Verstraeten, G., Vandekerckhove, L., 2006. Prediction of landslide susceptibility using rare events logistic regression: a case study in the Flemish Ardennes (Belgium). Geomorphology **76**, 392–410, doi:10.1016/j.geomorph.2005.12.003.

Wilkinson, P.L., Anderson, M.G., Lloyda, D.M., Renaudb, J.P., 2002. Landslide hazard and bioengineering: towards providing improved decision support through integrated numerical model development. Environmental Modelling & Software **17**, 333–344.

Wooten, R.M., Latham, R.S., Witt, A.C., Douglas, T.J., Gillon, K.A., Fuemmeler, S.J., Bauer, J.B., Nickerson, J.G., Reid, J.C., 2007. Landslide hazard mapping in North Carolina— geology in the interest of public safety and informed decision making. Geological Society of America Abstracts with Programs **39**, 76.

Wu, W., Sidle, R.C., 1995. A distributed slope stability model for steep forested basins. Water Resource Research **31**, 2097–2110.

Wu, T.H., 2008. Reliability analysis of slopes. In: Phoon, K.K. (Ed.), Reliability Based Design in Geotechnical Engineering. Taylor & Francis, London, UK, 413–447.

Yucemen, M.S., Tang, W.H., Ang, A.H.S., 1973. A probabilistic study of safety and design of earth slopes. Civil Engineering Studies, Structural Research Series, 402 (University of Illinois, Urbana).

Yoshinaga, S., Ohnuki, Y., 1995. Estimation of soil physical properties from a handy dynamic cone penetrometer test. Journal of the Japan Society of Erosion Control Engineering **48**, 200.

Zhu, Q., Lin, H. S., 2009. Simulation and validation of concentrated subsurface lateral flow paths in an agricultural landscape, Hydrology and Earth System Science, **13** 1503-1518.

Chapter 3. Improvement of shallow landslide prediction accuracy using soil parameterisation for a granite area in South Korea

3.1 Introduction

Rainfall-induced shallow landslides have been studied for practical and scientific reasons (Anderson and Sitar, 1995; Iverson et al., 1997; Gabet and Muss, 2006). Regardless of the various scales of shallow landslides, they pose a significant hazard to mountain communities because they are frequent and difficult to predict, and they can develop into debris flows that are potentially destructive due to their velocity and potential for sediment bulking during propagation (Campbell, 1975; Rickenmann and Zimmermann, 1993; Iverson et al., 1997; Reid et al., 2000; Crosta and Dal Negro, 2003; Crosta and Frattini, 2003).

The initiation of shallow landslides is often related to rainfall intensity and duration (Caine, 1980; Aleotti, 2004; Giannecchini et al, 2006, Giannecchini et al., 2007; Guzzetti et al., 2008; Cannon et al., 2008; Coe et al., 2008). It has been frequently observed that hillslope failures such as shallow landslides are often related to short (<1 hour) and intense rainfall rather than daily-averaged precipitation (Reid et al., 1997; Montgomery et al., 1997; Caine, 1980; Casadei et al., 2003). Previous rainfall, geological soil properties, soil thickness, and hydraulic conductivity play important roles in triggering landslides, and the rate of water infiltration and water movement below the surface are also important factors for landslide initiation (Iverson, 2000; Crosta and Frattini, 2003; Giannecchini et al., 2007).

Recent physically based models have revealed the amount of precipitation required to trigger slope failures and the locations and times of the expected landslides, making these models of interest for landslide warning systems. Others combine an instability model with a hydrological model to provide better general models for topographically controlled shallow slope failures (Montgomery and Dietrich, 1994; Dietrich et al., 1995; Casadei et al., 2003). Many shallow landslide modelling efforts have focused on more effective ways to describe flows from upslope using topographic index or dynamic topographic index approaches (i.e., Montgomery and Dietrich, 1994; Tarolli and Tarboton, 2006). However, these physically based models only allow complete parameterisations and do not consider rainfall-induced landslides where definitions are needed for components such as the hydrological response of the soil and its geotechnical properties (Giannecchini et al., 2007).

The infinite-slope concept in a physically based model analysis is usually adopted within the defined physical parameters of the study area, and data of the in situ spatial distribution of soil thickness are required to perform slope instability analysis. Soil thickness is of particular importance, as are the mechanical and hydrological properties related to hydraulic conductivity, transmissivity, and the angle of internal friction. A uniform soil thickness was used in previous analyses of shallow landslides (e.g., Montgomery and Dietrich, 1994; Wu and Slide, 1995), and some researchers included sparse soil thickness sampling data in the analysis of shallow landslides. Recently, however, Lee and Ho (2009) adopted the wetness index to determine the spatial distribution of soil thickness for slope instability analysis. Ho et al. (2012) also applied uniformly distributed soil thicknesses to assess the success rate for physically based shallow landslide prediction using different soil thickness assumptions for comparison.

Various soil factors such as vegetation, roots, and internal friction angle can also affect the occurrence of shallow landslides. Kuriakose et al. (2009) attempted to evaluate the sensitivity of slope stability to the hydrological effects of vegetation and root reinforcement together

with other intrinsic and extrinsic factors in their research area using a dynamic hydrological model combined with a slope stability model. Sidle and Ochiai (2006) noted that shallow landslides were affected by the friction angle not only when gradient exceeds the friction angle.

Researchers have variously attributed the seemingly random occurrence of landslides to spatial variation in topography, soil depth, cohesion of the soil and roots, hydraulic conductivity, groundwater response, and the angle of internal friction (e.g., Dietrich et al. 1995; Wu and Sidle, 1995; Montgomery et al., 1997). Unfortunately, these variables are exceedingly difficult to measure, and few studies have attempted to measure their spatial variation at the scale that influences slope stability. Although several researchers (Dietrich et al., 1995; Claessens et al., 2005; Rosso et al., 2006; Uchida et al., 2011) have observed that soil properties are important factors for shallow landslide modelling performance and have incorporated these factors into their work, studies considering changes in the physical characteristics of soil with varying thickness remain rare. Shallow landslide prediction could be affected by several characteristics of the study area, including slope steepness, soil properties, forest cover, and other factors. Soil sample location and the methods for determining the soil physical parameters for the model input data could also affect the prediction of shallow landslides.

The aim of study was to test the impact of soil strength parameters on model performance and to find a way to use observed landslide depth and slope data to calibrate these soil strength parameters. For this, I used SHALSTAB model and interpreted the importance of soil parameters such as cohesion and internal friction angle according to changes in soil thickness. To conduct the soil thickness, I used a knocking pole test in the small study area and, the three soil parameters, which were collected at study area and analysed using two methods (direct shear tests and one triaxial compression test), used in SHALSTAB model.

3.2 Study area

The approximately 70-km^2 study area is located in Jinbu-Myeon, Pyeongchang-gun, Kangwon Prefecture in the Republic of Korea; the centre of the study area is located at 128°33”29’E, 37°37”49’N (Fig. 3.1). The annual mean precipitation in this area during the last 40 years (1978–2008) was about 1400 mm (Korea Meteorological Agency). This region has a temperate climate with year-round precipitation. Rainfall primarily occurs during the summer season, from June to September, as part of the East Asian monsoon. Korea is also threatened by severe tropical typhoons during the summer season. Most of the heavy rainfall observed in Korea can be attributed to typhoon activity in the area. On July 16, 2006, over 1,200 shallow landslides occurred in the Jinbu region as a result of typhoon rains. The Korea Meteorological Administration measured the total rainfall amount at 450 mm/day and the maximum rainfall intensity of the triggering event at about 45 mm/h.

The prevalent geological units exposed in the study area are the Mesozoic Nokam Formation and igneous rocks including the Imgye granite. The Triassic Nokam Formation is composed of fine sandstone with grey sandy shale, originating from thick clastic successions of marginal marine to nonmarine environments. In contrast, the Jurassic plutonic rock, the Imgye granite, mainly occurs as a large batholith trending NW–SE and as small stocks consisting of granite with minor syenite and diorite distributed along the Ogcheon Belt. Additionally, the Ordovician Jeongseon limestone is mainly of shallow marine origin and consists predominantly of limestone with lesser amounts of sandstone and shale. This area has undergone extensive intrusion by granitoids due to the Daebo Orogeny, which lasted from the early Jurassic to the early Cretaceous. All of the previous geological units were intensely deformed as a result of this intense orogenic event (Geological Society of Korea, 1962; Park et al., 2013).

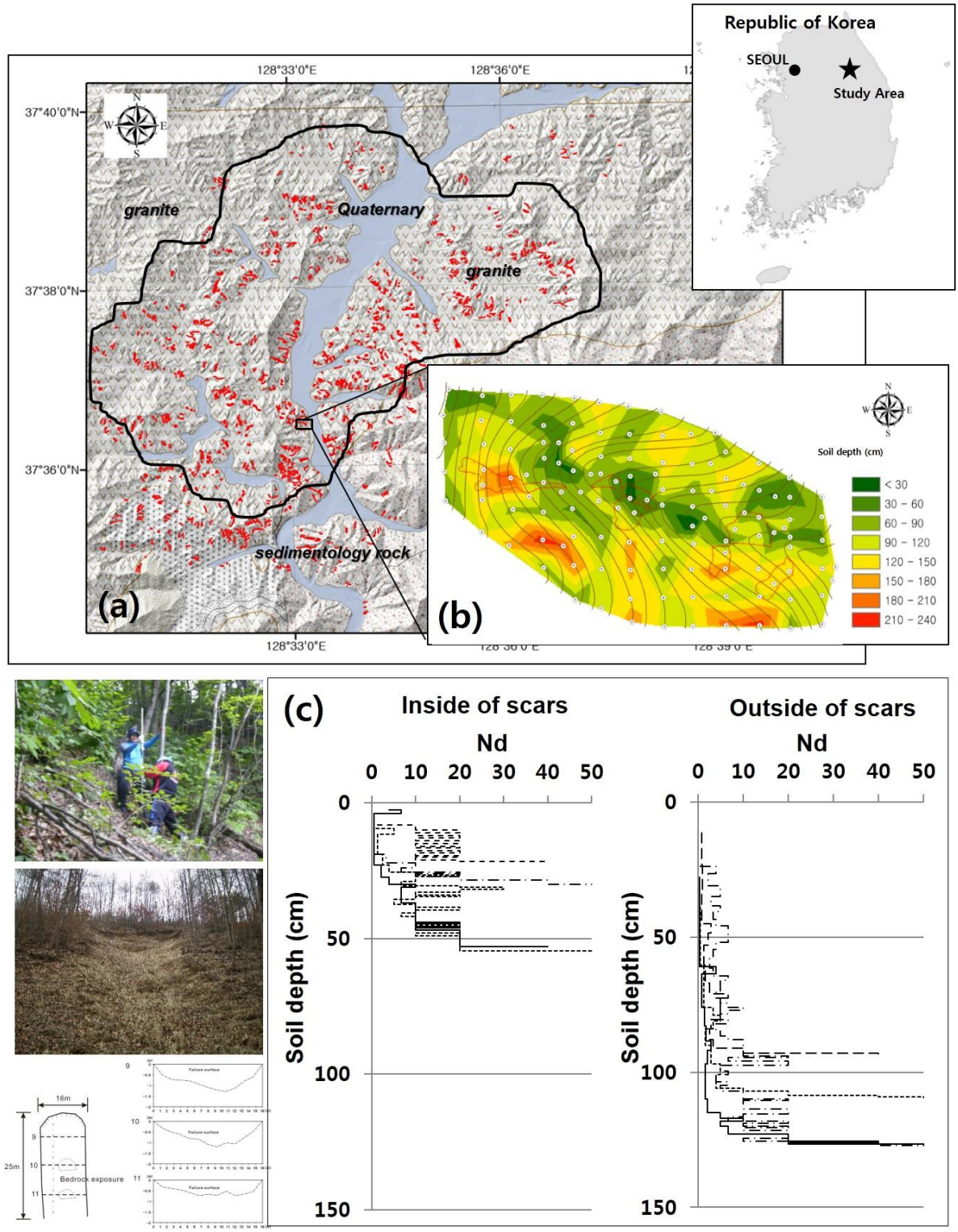

Fig. 3.1 Location and lithology map of the study site. Red indicates areas covered by shallow landslides that occurred on July 16, 2006. (A) soil thickness distribution and (B) histogram of soil depths measured by penetration tests for 125 points in a small watershed within the landslide study area.

3.3 Methods

3.3.1 Critical rainfall calculation

I used a SHALSTAB model combined with infinite slope stability equation and simple subsurface flow model for the shallow landslide hazard analysis (Fig. 3.2a). This method was described by Montgomery and Dietrich (1994) and is based on earlier formulations proposed by O'Loughlin (1986). The practicality of this approach and various adaptations of it have been demonstrated over the last decade, and it performs well for many applications (Dietrich et al., 1995; Dietrich and Montgomery, 1998; Wu and Sidle, 1995; Borga et al., 2002; Montgomery et al., 2000; Pack et al., 2001; Vanacker et al., 2003; Fernandes et al., 2004). Calculation of the *Rc* (slope stability index; Equation 1) is based on the infinite slope form of the Mohr–Coulomb failure law, expressed by the ratio of the stabilising force (shear strength) to the destabilising force (shear stress) on a failure plane parallel to the ground surface (e.g., Montgomery and Dietrich, 1994; Dietrich and Montgomery, 1998).

$$R_c = T sin\beta \left(\frac{b}{a}\right)\left(\frac{\rho_s}{\rho_w}\right)\left[1 - \frac{(sin\beta - C)}{(cos\beta tan\emptyset)}\right] \qquad (3.1)$$

where T is the saturated soil transmissivity (m^2h^{-1}), β is the local slope angle (°), θ is the internal friction angle of the soil (°), a is the upslope contributing area (m^2), b is the unit contour length [in our grid-based approach the grid resolution (m) is taken as the effective contour length, as in Pack et al. (2001)], ρ_s is the wet soil bulk density (g cm^{-3}), and ρ_w is the density of water (g cm^{-3}). C is the combined cohesion term (−), made dimensionless relative to the perpendicular soil thickness and defined as

$$C = \frac{C_r + C_s}{h\rho_s g} \qquad (3.2)$$

where C_r is the root cohesion (Nm^{-2}), C_s is the soil cohesion (Nm^{-2}), h is the vertical soil thickness (m), and g is the gravitational acceleration constant (9.81 ms^{-2}). Given the assumptions and boundary conditions used in deriving equation 1, it could be expressed using the conditions for the upper and lower thresholds of elements that can possibly fail. Unconditionally stable areas are predicted to be stable even when saturated, and they satisfy

$$\tan\theta \leq \left(\frac{C}{cos\theta}\right) + \left(1 - \frac{\rho_s}{\rho_w}\right) tan\emptyset \qquad (3.3)$$

Unconditionally unstable elements, which in most cases are bedrock outcrops, are unstable even when dry, and they satisfy

$$\tan\theta > tan\emptyset + \left(\frac{C}{cos\theta}\right) \qquad (3.4)$$

The predictive index of this model (i.e., the stability index) is expressed in mm day^{-1} of critical rainfall and is of variable scale, where lower values indicate a higher probability of instability, and higher values indicate a greater probability of stability. This scale also encompasses areas identified as unconditionally stable and unconditionally unstable based on the estimated rainfall value (Zizioli et al., 2013).

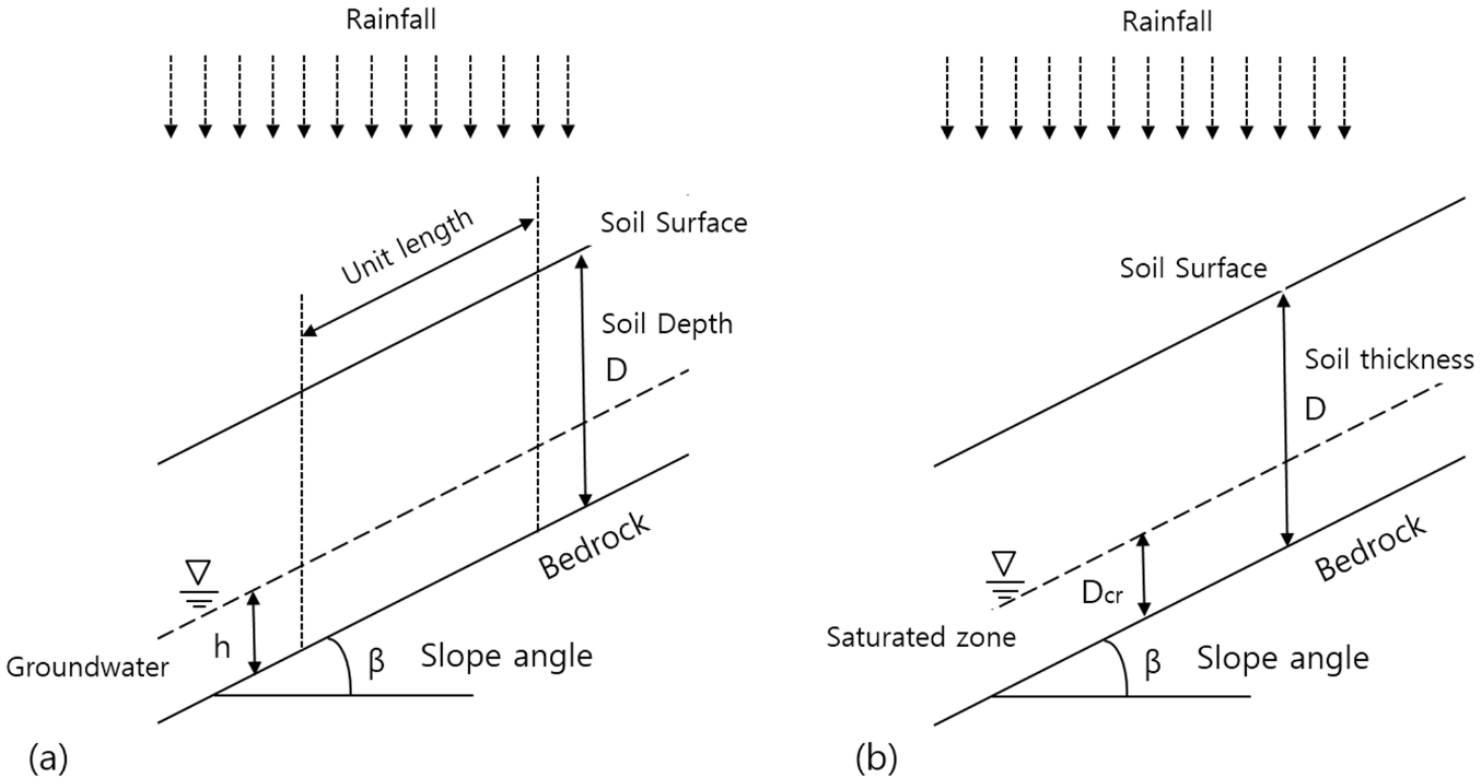

Fig. 3.2 SHALSTAB (a) and stochastic hydro-geomorphology conceptual models (b).

3.3.2 Stochastic model for soil parameterisation

Topography influences the initiation of shallow landslides through both the concentration of subsurface flow and the effects of slope gradient on slope stability (Montgomery and Dietrich, 1994; Talebi et al., 2008). Slope failure often occurs in areas of convergent topography, where subsurface soil water flow paths increase the excess pore water pressure downslope (Anderson et al., 1991; Wilkinson et al., 2002; Talebi et al., 2008). Planar infinite slope analysis has been widely applied to the evaluation of natural slope stability, particularly where the thickness of the soil mantle was small relative to slope length and where shallow landslides occurred due to the failure of a soil mantle overlying a sloping drainage barrier (Talebi et al., 2008).

Iida (1999) suggested that the two-layer model of soil and bedrock, which assumes a potential landslide (soil) layer, is suitable for the slope stability analysis of shallow landslides. Several researchers (Iida, 1999; D'Odorico andFragherazzi, 2002; Talebi et al., 2008) applied the same approach in a stochastic hydrogeomorphological model for shallow landslides resulting from rainstorms. This model in Fig. 3.2a is based on the Mohr–Coulomb failure law, and the failure condition can be expressed as (Iida, 1999)

$$H_{cr} = \frac{c - \gamma_t cos^2\beta(tan\beta - tan\emptyset)D}{cos^2\beta\{(\gamma_{sat} - \gamma_t)(tan\beta - tan\emptyset) + \gamma_w tan\emptyset\}} \qquad (3.5)$$

where β is the local slope angle (°), c is the cohesion, $\emptyset$ is the internal friction angle (°), γ_t is the weight per unit volume of unsaturated soil (g cm^{-3}), γ_{sat} is the weight per unit volume of saturated soil (g cm^{-3}), and γ_w is the weight of water per unit volume (g cm^{-3}).

In this model, shallow landslides occur when the soil thickness D is between D_{cr} and D_{max} (Talebi et al., 2008).

When the soil Depth D is equal to D_{cr}, the critical soil depth D_{cr} can be expressed as follows:

$$D_{cr} = c/cos^2\beta\{\gamma_{sat}(tan\beta - tan\emptyset) + \gamma_w tan\emptyset\} \qquad (3.6)$$

When the soil depth D is less than D_{max} (D_{max}>D), the depth D of saturated throughflow cannot reach the critical D_{cr} value, even in a rainstorm. Thus, shallow landslides do not occur because the water table of the saturated throughflow cannot rise above the ground surface, resulting in saturated overland flow. In the case of a relatively steep slope ($\emptyset < \beta$), D_{cr} decreases linearly with increased soil depth D, and D_{cr} becomes zero. This means that a shallow landslide can occur on the slope without saturated throughflow, given a critical ('upper limit') soil depth D.

$$D_{max} = \mathrm{c}/\gamma_t cos^2\beta(tan\beta - tan\emptyset) \qquad (3.7)$$

The modeling soil of evolution is important because without cohesion, soils could never form on slopes greater than $\emptyset$, and even thin soils on slopes in the range of β <$\emptyset$ would be extremely unstable because light rainfall would provide a sufficient saturated water depth H to cause landslides. These scenarios are contrary to observation, suggesting that soil cohesion must be considered in slope stability models (Iida, 1999).

3.3.3 Model input parameterisations

Unsaturated and saturated subsurface flow on hillslopes and/or catchments is affected by topography, soil depth, and hydraulic properties in a complex manner. These properties serve as input data for numerical simulations and have significant implications for simulation accuracy. Although detailed surface topography data can generally be readily obtained from digital elevation models (DEMs), soil depth and hydraulic properties for an entire hillslope and/or catchment are often lacking. The topographic data used in this study consisted of a 5 × 5-m DEM based on a digital elevation map (1:5,000) from the National Geographic Information Institute in the Republic of Korea. The locations of shallow landslide areas were back-filled to represent the topography of the study area before the landslides occurred.

The dynamic cone penetrometer (25-mm diameter with a 60° tip angle), also known as the knocking pole (Yoshinaga and Ohnuki, 1995), consists of several 0.5-m sections of 15-mm-diameter stainless steel rods with graduations etched every 10 cm. The penetration resistance value, Nd (drop/10 cm), was computed as the number of blows required for 10-cm penetration. Uchida et al. (2009) compared vertical Nd distributions among locations outside and inside areas of shallow slope failure and found that soil layers with Nd values of 5–20 were not detected as locations within areas of slope failure in their study area. They suggested that soil depths with Nd ≤20 could be defined as soil layers with failure potential, and soil depths with Nd ≥20 could be defined as bedrock layers not prone to failure. For our study, 125 penetration tests were performed at 10–15-m intervals along the slope, and the soil distribution was calculated using the Nd values (Fig. 3.1b). To compare actual shallow landslides with our shallow landslide simulation results, I used air photo images taken after shallow landslide occurrence and converted the shallow landslide area into polygons using the ArcGIS 10.1 program (ESRI, California, USA).

I collected soil samples from the study area and tested them using a triaxial compression test to determine the model input parameters. Testing soils to understand their behaviour during shallow failures normally requires a method that mimics the stress distribution under natural conditions. Shallow landslides are triggered by elevated pore pressure that decreases the effective normal stress rather than by increasing shear stress (Anderson and Reimer, 1995). Unlike typical triaxial shear testing that is accomplished by increasing the shear stress, the consolidated drained (CD) test approximates the conditions during rainfall-induced failure by maintaining constant shear stress while reducing the effective stress (Reimer, 1992). Lee et al. (2009) and Park et al. (2013) tested soil samples at the same study site for soil parameters using a direct shear test, and I used soil data from these studies, which were performed in the study area (Table 3.1).

Table 3.1 Soil parameters for shallow landslide modeling (a and bwere determined by direct shear test, and c was determined by triaxial compression test).

Model input parameters	a	b	c
Saturated soil weight (kg/m^3)	1790	1960	1740
Dry density (kg/m^3)	1550	1510	1490
Water density (kg/m^3)	1000	10	10
Hydraulic conductivity (m/h)	0.08	0.04	0.05
Cohesion (kPa)	3.8	4	1.6
Internal Friction Angle (°)	35.2	34	36.5
Slope degree (°)	DEM	DEM	DEM
Gravity velocity (m/s)	9.8	9.8	9.8
Average soil depth (m)	1m	1m	1m

3.3.4 Assessment of model results

The prediction accuracy of regional landslide susceptibility models has typically been evaluated by comparing the locations of the known landslides with simulation results from the model (Montgomery et al., 1998, 2001; Godt et al., 2008). Receiver operating characteristics (ROCs), which are used in various studies including weather forecasting and landslide susceptibility mapping, represent a technique for comparing the performance of models for which results can be assigned to one of two classes or states (Swets, 1988; Fawcett, 2006; Van Den Eeckhaut et al., 2006; Godt et al., 2008). The model with the higher percentage provides a better prediction of shallow landslides. The least critical test of prediction accuracy would be to count a successful prediction when a single grid cell is located within a mapped landslide polygon.

More critical tests of prediction accuracy involve more detailed assessment of 1) the capability of the model to correctly identify mapped landslides (TP; true positive), 2) the frequency of errors when mapped landslides are not correctly identified (FN; false negative), 3) over-prediction (FP; false positive), and 4) the model's ability to correctly identify the area that does not include the mapped landslides (TN; true negative). An ideal landslide susceptibility map simultaneously maximises the agreement between the known and predicted landslide locations and minimises the area outside the known landslides that is predicted to be unstable (FP). To perform the ROC analysis, two quantities were calculated: sensitivity (the true positive rate), defined as the ratio between TP and the sum of TP and FN, and specificity (the false positive rate), defined as the ratio between FP and the sum of TN and FP. Accuracy was defined as the ratio of TP+TN to the sum of all values (TP+FP+FN+TN) (Fig. 3.3). Relatively flat areas such as rivers including alluvia, rice paddies, etc. were excluded from the analysis because the mapped shallow landslides only occurred in the mountainous area.

A Receiver Operating Characteristics (ROC) plot (Fawcett, 2006), defined by the false alarm rate FPR and the hit rate TPR, plotted on the x and y axes, respectively. In the ROC space, a point located in the upper left corner represents a perfect prediction (TPR = 1 and FPR = 0), and points along the diagonal line for which TPR = FPR represent random predictions. The area under the ROC curve AUC is taken as a quantitative measure of the performance of the classification. If AUC = 0.5, a classification is poor and indistinguishable from a random classification, whereas a perfect classification has AUC = 1 and an acceptable prediction requires TPR/FPR > 1 (Fawcett, 2006; Rossi et al., 2010; Raia et al., 2014).

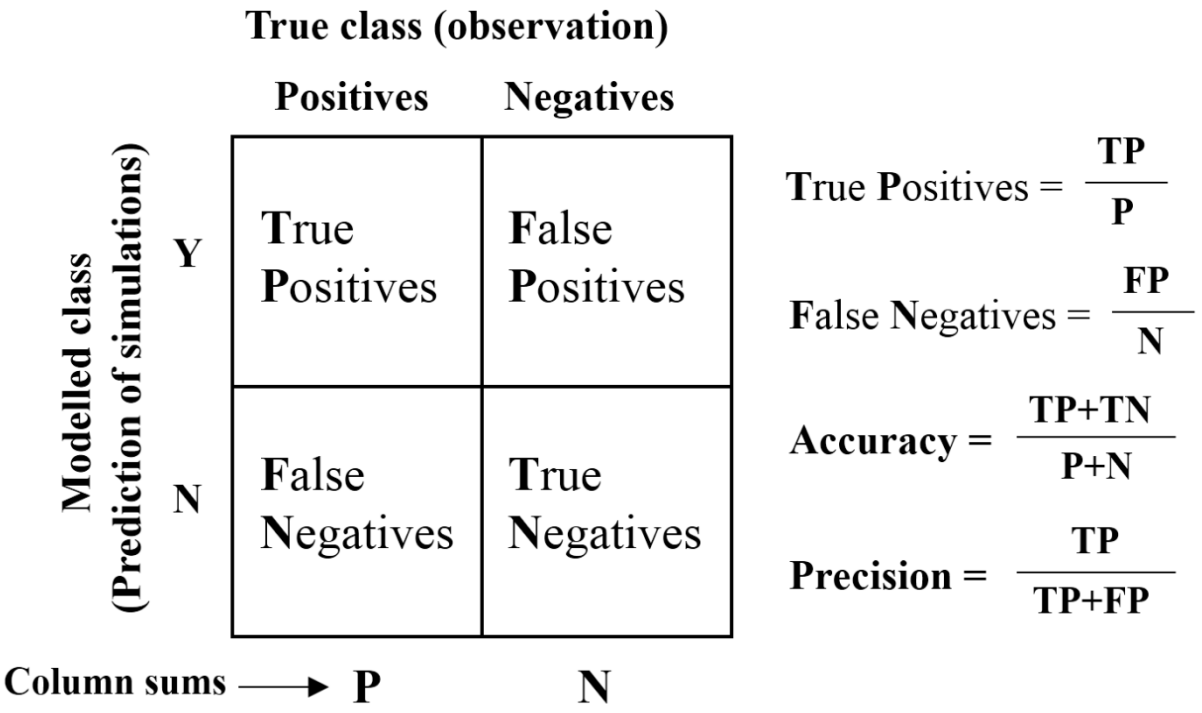

Fig. 3.3 Reciever operating characteristic (ROC) analysis method for determining the accuracy of shallow landslide prediction in this study (modified from Godt et al., 2008).

3.4 Results

3.4.1 Shallow landslide simulation using experimental data set (Case I)

The three different soil parameters (Table 3.1) used in the shallow landslide model for the July 16, 2006, event were further analysed to quantify the spatial discrepancy between the landslides triggered by the July 2006 rainfall event and the prediction results for the critical rainfall level that would trigger a shallow landslide in the area. The resulting map of steady-state critical rainfall (mm/day) that could trigger shallow landslides in the study area is shown in Fig. 3.5, where the shallow landslide-prone areas predicted by equation 1 are delineated by the steady-state rainfall intensity (mm/day) necessary for slope instability in each topographic element. These were also compared with the shallow landslides observed in air photo images.

In Fig. 3.5 a and b, which are based on the direct shear test data, the steady-state critical rainfall varied between 50 and 500 mm per day except in the stable area, and shallow landslides occurred near the high mountains in the simulated area. The landslide areas surveyed in 2006 showed a similar pattern to the critical rainfall simulation results, but these revealed an over-prediction, particularly around high mountain areas. The landslide occurrence based on triaxial compression test data also showed calculated critical rainfall levels at 50 – 500 mm/day except in the stable area (Fig. 3.5c). However, it was sensitive to rainfall levels of 50 – 200 mm/day, and most of the areas could be exposed to landslide risk when compared with mapped air photo images. Furthermore, in all three cases, the steep slope of the study area indicates relatively high possibility of a landslide triggered by a critical rainfall level of 0–50 mm/day.

I separated the steady-state critical rainfall (mm/day) data from the simulated grid data (Fig. 3.6) to obtain the distribution of steady-state critical rainfall levels (mm/day) from the three types of experimental soil data. In Fig. 3.6a, Cases I-a and I-b showed a large stable area (stable

cells and cells >500 mm/day), but Case I-c showed less than half the number of stable cells. The low values of Case I-c mean that the triaxial compression test soil data were more sensitive than the direct shear test soil data.

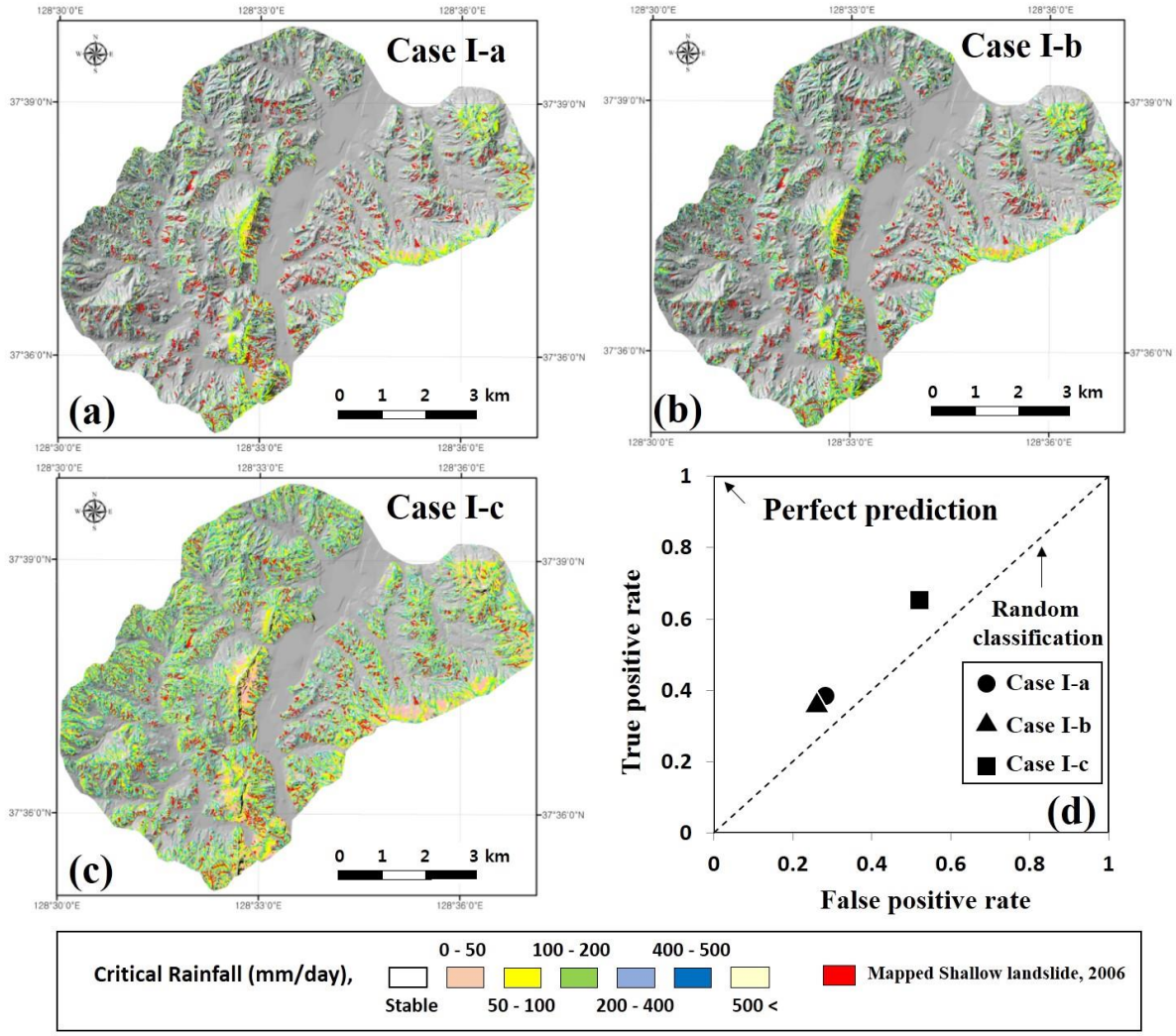

Fig. 3.5 Maps of study area showing steady-state rainfall intensity (mm/d) necessary for slope instability as predicted from equation 1 using several soil parameters tested by direct shear test and triaxial compression test (Table 1) for the shallow landslide-prone area. Observed shallow landslides (in red) that occurred on July 16, 2006, are also shown apped shallow landslides.

Table 3.2 Accuracy analysis of shallow landslide prediction using ROC analysis.

Model Class	True Positive Rate	False Positive Rate	TPR/FPR	Accuracy
CASE I-a	0.37	0.28	1.34	0.71
CASE I-b	0.35	0.26	1.34	0.73
CASE I-c	0.65	0.52	1.13	0.48

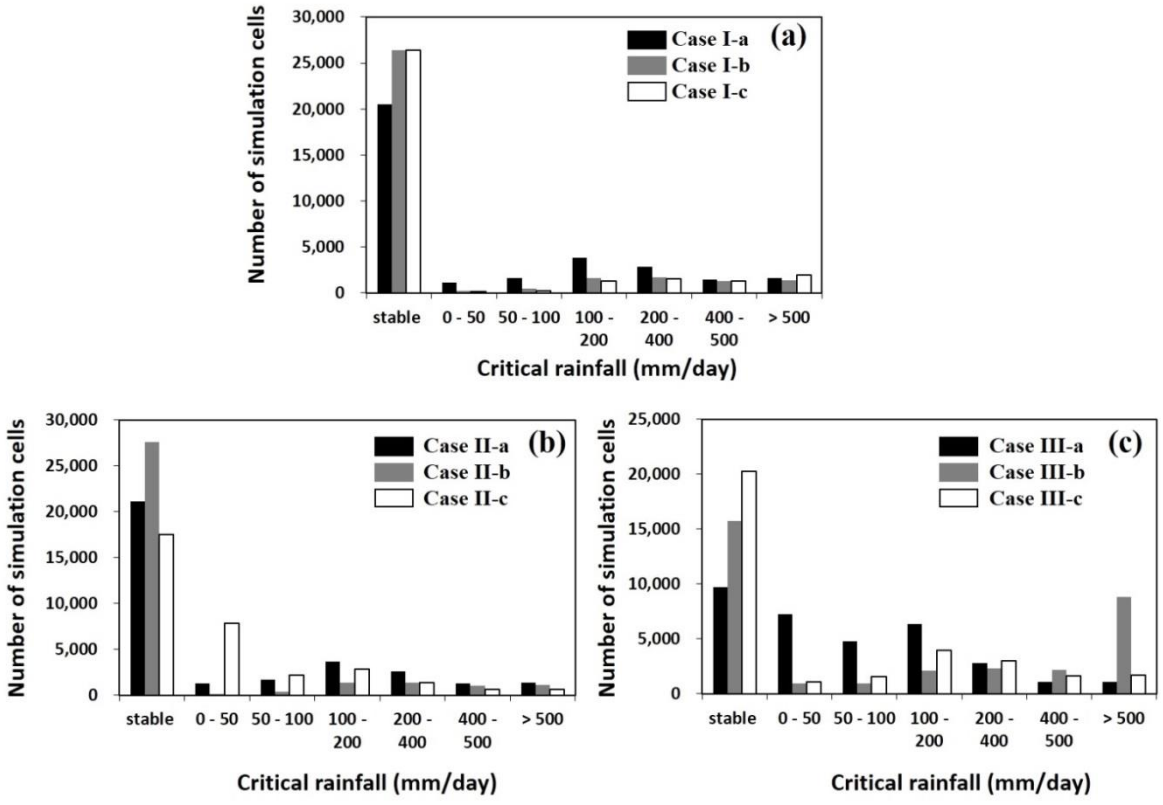

Fig. 3.6 Number of simulated cells and the distribution of critical rainfall intensity (mm/day) for Case I, Case II and Case III from the shallow landslide prediction based on the three soil parameters in Table 3.1.

I performed ROC analysis to evaluate the accuracy of the modelling results. The calculated accuracy values of Cases I-a, I-b, and I-c were 0.71, 0.73, and 0.48, respectively. The value of the TPR/FPR ratio, which is indicating the large value is a measure of the better predicting performance, were Case I-a, I-b, and I-c were 1.34, 1.34, and 1.13, respectively(Fig. 3.5d and Table 3.2). The ROC analysis indicated low overall model accuracy, with the accuracy of Case I-c (0.48) being the lowest of the three. The difference among the three cases can be attributed to the soil testing methods, specifically, the values for soil cohesion and internal friction angle that were determined by direct shearing and triaxial compression tests in this study.

3.4. 2 Calculation of soil strength parameters

I determined the shallow landslide distribution in the study area using equations 3.6 and 3.7 to calculate physical soil parameters such as cohesion and internal friction angle. Equation 3.6 but not equation 3.7 assumes that shallow landslides only occur when the soil was completely saturated. These equations together set the limits on the depth-slope space in which landslides can occur (Fig. 3.7). Fig. 3.7 shows the results of soil parameterisation, which reflect the effect of soil thickness (i.e., the measured soil thickness in Fig. 3.1 (a) and the average soil thickness of 1 m), using equation 3.6 (D_{cr}) and equation 3.7 (D_{max}) in the hydro-geomorphological model derived from the soil parameters in Table 3.1. Fig. 3.7a (Case I) shows an overlap with the distribution of measured soil thickness (y-axis) against the slope angle (x-axis) (black circles are located within the shallow landslide scar, and white circles are located external to the shallow landslide scar). The curves (D_{cr}) and (D_{max}) were calculated using the data in Table 3.1. The black circles are located outside D_{cr} and D_{max}, indicating that the cohesion and internal friction values used in the Case I simulation for shallow landslide prediction in Fig. 3.5 contain errors.

Accordingly, I changed the internal friction angle and cohesion values, resulting in values nested between D_{cr} and D_{max} in Fig. 3.7 for Cases II and III.

Case II (Fig. 3.7) shows an overlap with the distribution of measured soil thickness (*y*-axis) against slope angle (*x*-axis), and the curves were controlled using changes in the internal friction angle and cohesion. Case III (Fig.3. 7) shows an overlap with the distribution of the average soil thickness (1 m) (*y*-axis) against slope angle (*x*-axis), and the curves were also controlled using changes in the internal friction angle and cohesion. All values calculated by the hydro-geomorphological model are presented in Table 3.3.

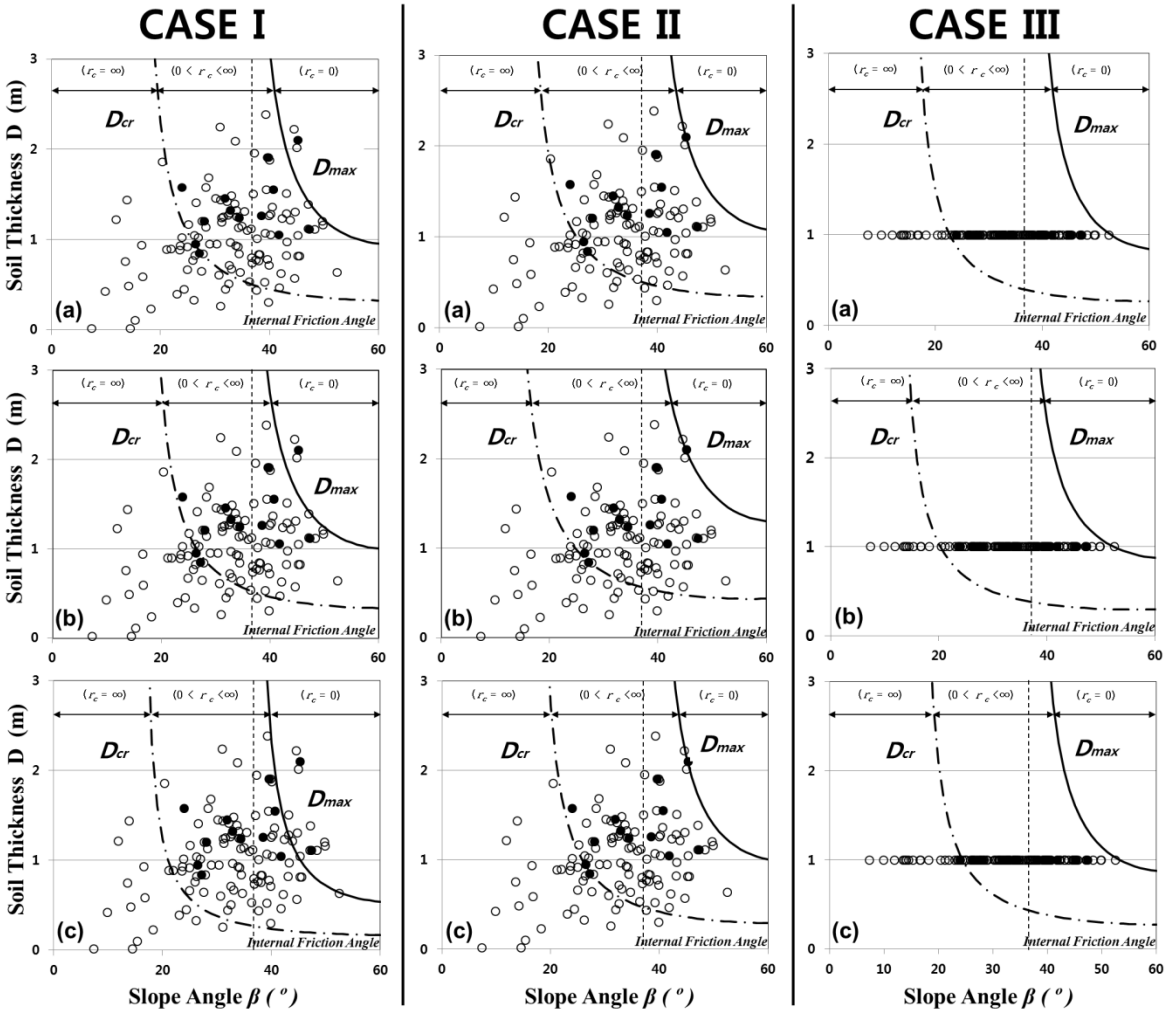

Fig. 3.7 D_{cr} (dashed line) and D_{max} (solid line) calculated using equations 3.6 and 3.7. Shallow landslides can occur between D_{cr} and D_{max}. White circles indicate soil thickness measured by knocking pole test outside of the shallow landslide area, and black circles indicate soil thickness measured by knocking pole test inside the shallow landslide scar. Case I was calculated using soil thickness and soil data shown in Table 3.1. Case II was calculated using soil thickness and by controlling the cohesion and internal friction angle based on data shown in Table 3.1. Case III was calculated using the average soil thickness and controlling for the cohesion and internal friction angle based on data shown in Table 3.1.

Table 3.3 Soil property calculation results from the stochastic hydrogeomorphological model (Measured soil thickness data were used for Case II, and average soil thickness data were used for Case III).

Model input parameters	Case II-a	Case II-b	Case II-c	Case III-a	Case III-b	Case III-c
Saturated soil density (kg/cm^3)	1,790	1,960	1,740	1,790	1,960	1,740
Dry density (kg/cm^3)	1,550	1,510	1,490	1,550	1,510	1,490
Water density (kg/cm^3)	1,000	1,000	1,000	1,000	1,000	1,000
Hydraulic conductivity (m/h)	0.08	0.08	0.04	0.04	0.05	0.05
Cohesion (kPa)	4.5	3.2	5.2	3.5	3.2	3.2
Internal Friction Angle (°)	37	34	37.2	37	34	37.2
Slope degree (°)	DEM	DEM	DEM	DEM	DEM	DEM
Gravity velocity (m/s)	9.8	9.8	9.8	9.8	9.8	9.8
soil thickness (m)	Measured	Measured	Measured	Average 1m	Average 1m	Average 1m

The internal friction angle and cohesion values in Table 3.3 were greater than those listed in Table 1. In particular, the soil cohesion value determined by triaxial compression test (Table 3.1) was almost doubled due to the influence of soil thickness (Table 3.3). To evaluate the effect of soil thickness on the soil parameters I applied altered soil parameters to the SHALSTAB model [i.e., measured soil thickness (Case II) and a constant soil thickness of 1 m (Case III)], and steady-state critical rainfall (mm/day) was re-calculated for shallow landslide prediction. The accuracy of this shallow landslide prediction was also evaluated using ROC analysis to assess any improvement in the prediction accuracy compared with the results for Case I.

3.4. 3 Application of soil parameters represented the measured soil thickness (Cases II)

Fig. 3.8 shows the distribution of the areas with rainfall values critical for the occurrence of shallow landslides. Fig. 3.8a (Case II-a) and Fig. 3.8b (Case II-b) show the critical rainfall distribution using soil parameters from the direct shear test, incorporating the effect of measured soil thickness distribution (Table 3.3). Fig. 3.8c (Case II-c) shows the critical rainfall distribution using soil parameters from the triaxial compression test, incorporating the effect of measured soil thickness distribution (Table 3.3). The critical rainfall simulation results in Fig. 3.8 were compared with the shallow landslide grid derived from air photo images from a post-event survey of the study area in 2006.

The distribution of the simulated critical rainfall (mm/day) in Fig. 3.8a and b based on the results for Cases II-a and II-b (Fig. 3.6b and Table 3.3) showed a similar pattern to the air photo images grid (red colour). The simulated critical rainfall values in Fig. 3.8a and 3.8b showed that the area of unconditionally stable cells increased. The critical rainfall values were 0–50 mm/day, which show decreased sensitivity for shallow landslide occurrence compared with

Fig. 3.5a and 3.5b. Fig. 3.8c shows the distribution of simulated critical rainfall (mm/day) based on the results for Case II-c (Fig. 3.8 and Table 3.3), and also shows a similar pattern to the air photo images grid (red colour). However, the critical rainfall simulation results in Fig. 3.8c differ from those in Fig. 3.8a and 3.8b. In Fig. 3.8c, the area of unconditionally stable cells increased, similar to those in Fig. 3.8a and 3.8b, but the critical rainfall value increased to over 500 mm/day. The distribution of critical rainfall in Fig. 3.8c matched well with the shallow landslide locations of 2006.

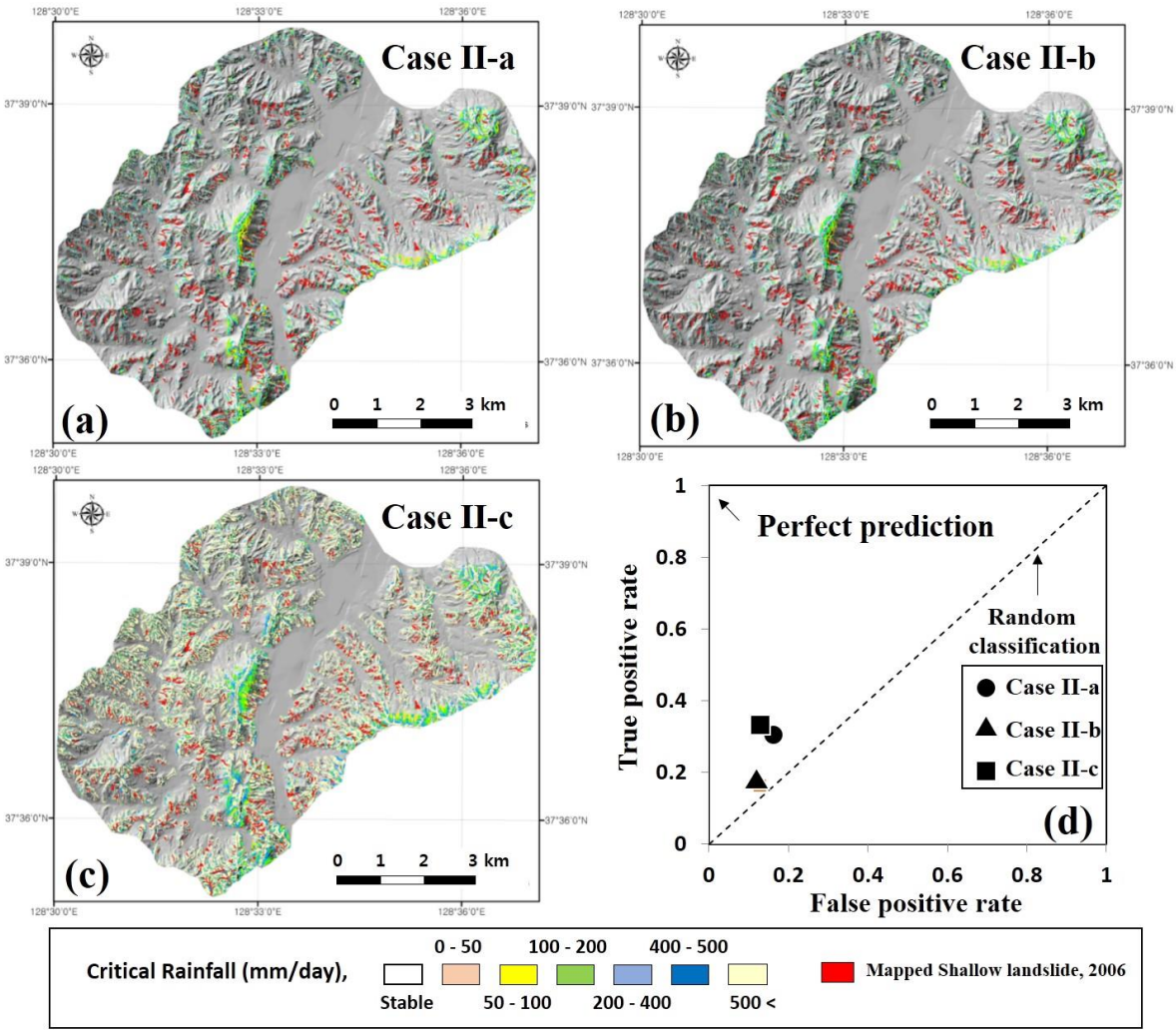

Fig.3.8 Maps of the simulation results showing the shallow landslide-prone area based on the steady-state rainfall intensity (mm/d) necessary for slope instability as predicted from equation 1 using measured soil thickness.

The distributions of the critical rainfall simulation using soil parameters reflected effects of measured soil thickness in Fig. 3.8 (Case II); the grid cells simulated in Fig. 3.8 are presented in Fig. 3.6b. The distribution patterns of critical rainfall cells in Cases II-a and II-b (Fig. 3.6b) were similar, and the number of stable cells increased, in contrast to Cases I-a and I-b, (Fig. 3.6a) based on the direct shear test method. The distribution of critical rainfall cells in Case II-c (Fig. 3.6b) showed that stable cells and cells of >500 mm increased, in contrast to Case I-c (Fig. 3.6a), based on the triaxial compression test method. This means that the over-prediction of shallow landslide occurrence under light rainfall conditions decreased.

The accuracy of the simulated critical rainfall prediction for Case II was evaluated by ROC analysis. The ROC analysis values for Case II are presented in Table 3.4. The ROC accuracy values for Cases II-a, II-b, and II-c were 0.83, 0.86, and 0.85, respectively. The value of the TPR/FPR ratio, which is indicating the large value is a measure of the better predicting performance, were Case II-a, II-b, and II-c were 1.95, 1.28, and 2.37, respectively. All simulation cases in Fig. 3.8, simulating the distribution of critical rainfall values (mm/day), clearly improved over those of Case I (Fig. 3.5). ROC analysis results are presented in Table 3.4; the increased ROC values for Case II (Fig. 3.8d) indicate improved predictive accuracy for the critical rainfall simulation. This also demonstrates that soil cohesion and internal friction angle may be important factors for shallow landslide modelling.

3.4. 4 Application of soil parameters represented the average soil thickness (CASE III)

To evaluate the impact of soil parameters other than soil thickness, I performed shallow landslide simulation using an average soil thickness of 1 m (Case III in Fig. 3.9 and Table 3.3). The critical rainfall simulation distribution for the effect of 1-m soil thickness on shallow landslide occurrence is shown in Fig. 3.9. The distribution of the critical rainfall value in Fig.

3.9a (Case III-a) was similar to that of Case II-a (Fig. 3.9), but it differed from the other cases in Fig. 3.9. The critical rainfall values of <50 mm/day (Fig. 3.9b) and 100–200 mm/day (Fig. 3.9c), were low, which differed from the sensitivity in Fig. 3.8. The low sensitivities of Cases III-b and III-c in Fig. 3.9 mean that soil cohesion and the internal friction angle can still influence the outcome of the critical rainfall simulation despite a constant average soil thickness of 1 m.

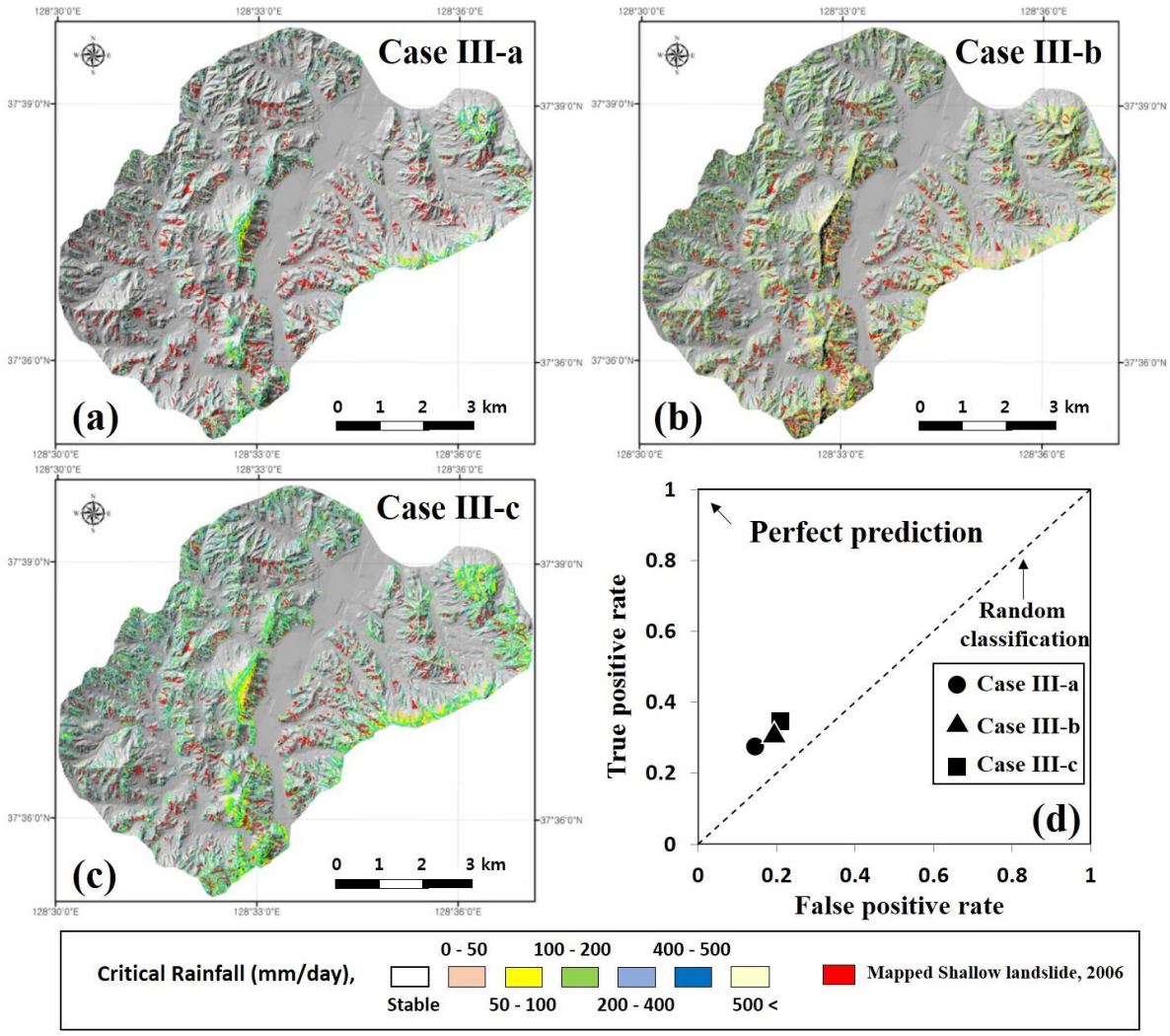

Fig. 3.9 Maps of the simulation results showing the shallow landslide-prone area based on the steady-state rainfall intensity (mm/d) necessary for slope instability as predicted from equation 3.1 using average soil thickness 1m.

The distribution of simulated critical rainfall cells (Fig. 3.9) is presented in Fig. 3.6c. The distribution patterns for Cases III-a and III-c are similar (Fig. 3.6c). However, the critical rainfall cells in Case III-b (Fig. 3.6c) show that the distribution of < 50 mm/day cells increased and stable cells decreased compared with the other simulations (Fig. 3.6). The critical rainfall simulation accuracy of Fig. 3.9 was evaluated by ROC analysis and is presented in Table 3.4. The accuracy values for Cases III-a, III-b, and III-c were calculated as 0.83, 0.79, and 0.78, respectively. The value of the TPR/FPR ratio, which is indicating the large value is a measure of the better predicting performance, were Case I-a, I-b, and I-c were 1.78, 1.50, and 1.60, respectively (Fig. 3.9d). The accuracy values of Case III were higher than those of Case I (Fig. 3.5), but lower than those of Case II (Fig. 3.8). Therefore, the accuracy of the shallow landslide prediction based on ROC analysis follows Case II > Case III > Case I. This indicates that soil parameterisation using soil thickness is important for improving the shallow landslide prediction accuracy of a model. These soil parameters (i.e., internal friction angle and soil cohesion) can greatly affect the prediction of shallow landslides.

Table 3.4 ROC accuracy analysis of shallow landslide prediction using soil parameterisation for two soil thickness parameters (measured soil thickness and average soil thickness of 1 m).

Class	Simulation case	True Positive Rate	False Positive Rate	TPR/FPR	Accuracy
Measured soil depth (m)	CASE II-a	0.30	0.16	1.95	0.83
	CASE II-b	0.16	0.13	1.28	0.86
	CASE II-c	0.32	0.14	2.37	0.85
Average soil depth (1m)	CASE III-a	0.27	0.15	1.78	0.84
	CASE III-b	0.30	0.20	1.50	0.79
	CASE III-c	0.34	0.21	1.60	0.78

3.5. Discussions

3.5.1 The effect of soil strength

I used soil parameters tested by the triaxial compression (Case I-c) method because Frank et al. (2009) observed that the triaxial compression test is better than the direct shear test for predictive models of shallow landslides, as it represents the processes and characteristics of the superficial soil layers reasonably well. In this study, the soil parameters tested by the triaxial compression method were applied to shallow landslide predictions, and the accuracy of the prediction results by ROC analysis showed over prediction and overly low values in Fig. 3.5c.

However, the results of Case II and Case III, which used modified soil parameters from a hydro-geomorphological model, rather than those of Cases I, showed high accuracy, which may be explained by two reasons from the viewpoint of physical soil properties. First, because the triaxial compression test method did not clearly reflect root cohesion, the cohesion value might have led to error. According to Montgomery and Dietrich (1994), the effect of roots on shear stress resistance can be taken into account by increasing the value of the shear stress resistance angle by 40%. Schmidt et al. (2001) and D'Odorico and Fagherazzi (2003) showed that soil and root cohesion is inherently necessary for soil to build up in steep hollows; otherwise, landslides would occur even with light rainfall (Rosso et al., 2006).

Additionally, some researchers have recently shown the effect of the dependence between cohesion and internal friction angle in slope stability analyses (e.g., Wu and Sidle, 1995; Cherubini, 2000; Hong and Roh, 2008; Cho and Park, 2010). Soil cohesion has sometimes been neglected in stability analyses of steep mantled slopes, while the angle of repose has been deliberately increased to realistic values to account for the overall shear strength of the aggregates (Montgomery and Dietrich, 1994; D'Odorico and Fagherazzi, 2003). For these reasons, cohesion is a sensitive parameter in shallow landslide models and one of the most difficult to quantify;

empirical treatment of this parameter may lead to large errors in estimates of slope stability (Casadai et al., 2003).

Second, cohesion has an influence on soil thickness and topography. In this study, the internal friction angle, and especially cohesion, had a high impact on model accuracy as many researchers have also explained (e.g. Montgomery and Dietrich, 1994; Rosso et al., 2002; Lanni et al., 2013). To evaluate the physical soil properties reflecting the distribution of soil thickness, I used a hydro-geomorphological concept model to calculate the soil properties. From the hydro-geomorphological model, the internal friction angle and especially cohesion were determined to be sensitive values for shallow landslide prediction.

Additionally, Casedei et al. (2003) noted that cohesion is the most important parameter affecting sensitivity analysis and that internal friction affects it secondarily. Another case study was begun after taking different locations and habitats of soil samples and analyzing the distribution of cohesion depending on soil depth and the phase of the different habitats, and it concluded that the results showed a pattern similar to that of previous cohesion tests. In other words, many researchers have explained that when entering parameters of soil properties into a model, the result cannot include the real nature of landslides. Although all the strength and hydrological parameters in the slope stability model can be obtained from field measurements or laboratory analysis, some of these parameters are difficult to define in practise, particularly with regard to their spatial variation (Dietrich et al., 1995). Hence, a definition of the relationship between soil cohesion and internal friction angle must consider theoretical approaches to a result based on that modeling method.

3.5.2 Infinite assumption on DEM resolution.

Fig. 3.8 and 3.9 show the shallow landslide prediction results using soil parameterisation

representing the effects of measured (Case II) and average (Case II) soil thickness (Fig. 3.7). Shallow landslide predictions using soil parameterisation showed greater accuracy than those using experimental soil parameters (Case I) (Fig. 3.5). The order of shallow landslide prediction accuracy based on ROC analysis was Case II > Case III > Case I. Although I performed soil parameterisation for shallow landslide prediction, over-prediction was still detected (Fig. 3.8 and Fig. 3.9).

I used a 5-m-resolution DEM with a 5-m contour digital map (see section 3.3) for shallow landslide prediction. I was unable to investigate the effect of DEM resolution in this study, but several authors (e.g., Zhang and Montgomery 1994; Claessens et al., 2005; Penna et al., 2014) have previously analysed the effect of DEMs on modelling results.

Claessens et al. (2005) calculated steady-state critical rainfall using different DEM resolutions and observed that even using high-resolution DEMs such as LIDAR data for shallow landslide prediction modelling, the model cannot describe the characteristics of the natural hillslope in detail. Many previous studies (e.g., Claessens et al., 2005; Tarolli and Tarboton, 2006) concluded that even if high-resolution DEMs are used to analyse shallow landslides, the complete prediction of the shallow landslide area is difficult.

In addition, Milledge et al. (2012) suggested that the infinite length assumption within the infinite slope stability model for DEM resolution is only valid for landslides with a high length/depth (L/H) ratio of 25 calculated by using the factor of safety from the finite element method. And they established a critical L/H ratio of 25, implying reasonable validity of the assumption for modelling when a coarse (>25 m) DEM resolution is used. If models with a finer resolution (< 10 m) DEM used, the assumption of infinite length proves to be less valid depending on the assumed landslide failure plane depth and on the material properties. To do this, they used SHALSTAB model to be compared with a coarse DEM (10 m) and a fine DEM (1 m) for verification of their assumption and explained that finer grid resolutions could be predicted on

shallow landslide long and predicted width is dramatically reduced.

That is, the limited validity of the assumption could be responsible for the under-prediction of landslides upslope, which in general have a somewhat smaller L/H ratio. However, they also concluded that the infinite length assumption can be valid for smaller DEM resolutions (e.g. 1 m). Because if lateral subsurface flow plays a role in defining pore water pressure then its spatial organization mitigates against predicting short landslides and minimizes the risk that predicted landslides will have length/depth ratios less than 25 (Milledge et al. 2012). Thus, in this study site, taking into consideration earlier arguments that more complex and localized processes play a role in landsliding and finer resolutions might capture those processes better (Milledge et al. 2012) and, the other factors could be affected on prediction of shallow landslide when I followed assumption of infinite in this study.

3.5. 3 Limitations

There are many reasons for such over-prediction in this study. Antecedent rainfall and DEM effects could be the primary factors resulting in over-prediction. Due to the difficulty of performing field tests for hydraulic conductivity (K_s) on high steep mountainous slopes, classical methods for measuring hydraulic conductivity have involved the laboratory test-based "constant head" and "falling head" parameters using soil core samples extracted from the field. Antecedent rainfall plays an important role in the initiation of landslides but SHALSTAB assumes hydrologic steady-state (i.e. all slopes are in equilibrium with infinite duration antecedent rainfall at the current rate). Because SHALSTAB model can calculate the critical rainfall occurring shallow landslide by one day [mm/day], it did not reflect the antecedent rainfall.

Antecedent rainfall plays an important role in the initiation of landslides (Wieczorek,

1987), but its influence is difficult to quantify. Soil water conditions from antecedent rainfall depend on several factors including local climatic conditions, slope angle, and the heterogeneity of the physical–mechanical properties and permeability of the soil (Aleotti, 2004). Therefore, I was unable to determine the in situ soil water conditions, and instead used the steady-state critical rainfall obtained from the SHALSTAB model.

To increase the accuracy of shallow landslide prediction, I performed soil parameterisations using three kinds of experimental soil data (two direct shear tests and one triaxial compression test) and applied them to a stochastic hydro-geomorphological model based on soil thickness. I achieved a more accurate critical rainfall modelling result for rainfall-induced shallow landslide prediction than that obtained prior to calibration of the soil strength parameters. Although I only considered physical soil properties in this study, further study of other factors including the effects of hydraulic conductivity and antecedent rainfall will be needed to improve shallow landslide prediction.

3.5 Conclusion

To improve the accuracy of shallow landslide prediction, I compared the results of shallow landslide predictions using a SHALSTAB model, varying the input soil data. Experimental soil data were used for the first simulation (Case I), whereas soil data represented the measured soil thickness (Case II) and represented average soil thickness (1 m, Case III) data were used in the second and third simulations, respectively. The accuracy of shallow landslide prediction was evaluated by ROC analysis. The order of accuracy as determined by ROC analysis was Case II > Case III > Case I, indicating that Case II showed the highest predictive accuracy. Therefore, the use of soil properties reflecting soil thickness may improve the accuracy of shallow landslide prediction.

References

Aleotti, P., 2004 A warning system for rainfall-induced shallow failures, Eng. Geol., **73**, 247–265.

Anderson, S. A.,Sitar, N., 1995 Analysis of rainfall-induced debris flows. J. Geotech. Engi., **121**, 544–552.

Anderson, S. A., Reimer, M. F., 1995 Collapse of saturated soil due to reduction in confinement. J. Geotech. Engi., **121**, 216– 220.

Baum, R. L., Savage, W. Z., Godt, J. W., 2010. TRIGRS - a fortran program for transient rainfall infiltration and grid-based regional slope stability analysis, version 2.0. In Open File Report US Geological Survey, **81**, 2010.

Borga, M., Dalla Fontana, G., Gregoretti, C., Marchi, L., 2002. Assessment of shallow landsliding by using a physically based model of hillslope stability. Hydrol.Process, **16**, 2833–2851.

Caine, N., 1980. The rainfall intensity-duration control of shallow landslides and debris flows, Geog. Ann. Series A., **62**, 23–27, 1980.

Campbell, R. H., 1975. Soil slips, debris flows, and rainstorms in the Santa Monica Mountains and vicinity, Southern California. US Geol. Surv. Prof. Paper., **851**, 1–20, 1975.

Cannon, S. H., Gartner, J. E., Wilson R. C., Bowers J. C., Laber J. L., 2008. Storm rainfall conditions for floods and debris flows from recently burned areas in southwestern Colorado and southern California, Geomorphology, **96**, 250–269.

Casadei, M., Dietrich, W. E., Miller, N. L., 2003. Testing a model for predicting the timing and location of shallow landslide initiation in soil mantled landscapes. Earth Surf. Proc. Land., **28**, 925–950.

Cherubini, C., 2000. Reliability evaluation of shallow foundation bearing capacity on *c*' and ϕ' soils, Can. Geotech. J., **37**, 264–269, 2000.

Cho, S. E., Park, H. C., 2010. Effect of spatial variability of cross-correlated soil properties on bearing capacity of strip footing. International J. for Numerical and Analytical Methods in Geomechanics, **34**, 1–26.

Claessens, L., Heuvelink, G. B. M., Schoorl, J. M., Veldkamp, A., 2005. DEM resolution effects on shallow landslide hazard and soil redistribution modeling. Earth Surf. Proc. Land.,**30**, 461–477.

Coe, J. A., Kinner, D. A., Godt, J. W., 2008. Initiation conditions for debris flows generated by runoff at Chalk Cliffs, Central Colorado. Geomorphology, **96**, 270–297.

Crosta, G.B., Dal Negro, P., 2003. Observations and modeling of soil slip-debris flow initiation processes in pyroclastic deposits: the Sarno 1998 event. Nat. Hazards Earth Syst. Sci., **3**, 53–69. 81–93, doi:10.5194/nhess-3-81-2003.

Crosta, G. B., Frattini, P., 2003. Distributed modeling of shallow landslides triggered by intense rainfall, Nat. Hazards Earth Syst. Sci., **3**, 81–93.

Dietrich, W. E., Reiss, R., Hsu, M., Montgomery, D. R., 1995. A process-based model for colluvial soil depth and shallow landsliding using digital elevation data. Hydrol.Process., **9**, 383–400.

Dietrich, W. E., Montgomery, D. R., 1998. SHALSTAB- A Digital Terrain Model for Mapping Shallow Landslide Potential. National Council of the Paper Industry for Air and Stream Improvement, Technical Report, Berkeley. February, 29.

D'Odorico, P., Fagherazzi, S., 2003. A probabilistic model of rainfall-triggered shallow landslides in hollows: a long-term analysis. Water Resource. Resources, **39**,

1262.doi:10.1029/2002WR001595.

Eyles, R. J., Crozier, M. J., Wheeler, R. H., 1978. Landslips in Wellington City. New Zealand Geographer **34**, 58–74.

Fawcett, T., 2006. An introduction to ROC analysis. Patt.Recog. Lett., **27**, 861–874.

Fernandes, N. F., Guimarães, R. F., Gomes, R. A. T., Vieira, B. C., Montgomery, D. R., Greenberg, M. H., 2004. Topographic controls of landslides in Rio de Janeiro: field evidence and modeling. Catena, **55**, 163–181.

Frank G., Martin, F., Albert, B., 2009. Effects of vegetation on the angle of internal friction of a moraine, For. Snow Landsc. Res., **82**, 61-77, 2009.

Gabet, E. J., Mudd, S. M., 2006. The mobilization of debris flows from shallow landslides, Geomorphology, **74**, 207–218.

Geological Society of Korea, Changdong–Hajinburi Geological Map Sheet.KIGAM, 1962.

Giannecchini, R., 2006. Relationship between rainfall and shallow landslides in the southern Apuan Alps (Italy). Nat. Hazards Earth Syst. Sci., **6**, 357–364, doi:10.5194/nhess-6-357-2006.

Giannecchini, R., Naldini, D., D'Amato Avanzi, G., Puccinelli, A., 2007. Modeling of the initiation of rainfall-induced debris flows in the Cardoso basin (Apuan Alps, Italy), Quat. Int., **171**, 108–117.

Godt, J. W., Baum, R. L., Savage, W. Z., Salciarini, D., Schulz, W. H., Harp, E. L., 2008. Transient deterministic shallow landslide modeling: requirements for susceptibility and hazard assessments in a GIS framework, Engi. Geol., **102**, 214–226.

Godt, J. W., McKenna, J. P., 2008. Numerical modeling of rainfall thresholds for shallow landsliding in the Seattle, Washington, area. In: Baum, R.L., Godt, J.W., Highland, L.M. (Eds.),

Landslides and Engineering Geology of the Seattle Washington Area. Geol. Soc. Am. Rev. in Engi.Geol., **20,** doi:10.1130/2008.4020(07).

Guzzetti, F., Peruccacci, S., Rossi, M., and Stark, C. P., 2008. The rainfall intensity-duration control of shallow landslides and debris flows: an update, Landslides, **5**, 3–17.

Ho, J. Y., Lee, K. T., Chang, T. C., Wang, Z. Y., Liao, Y. H., 2012. Influence of spatial distribution of soil thickness on shallow landslide prediction. Engi. Geol., **124**, 38–46.

Hong, H. P., Roh, G., 2008. Reliability evaluation of earth slope. J. Geotech. andGeoenviron. Engi., **134**, 1700–1705.

Iida, T., 1999. A stochastic hydro-geomorphological model for shallow landsliding due to rainstorm. Catena, **34**, 293–313.

Iverson, R. M., Reid, M. E., LaHusen, R. G., 1997. Debris-flow mobilization from landslides. Annual Review of Earth and Planetary Sci., **25**, 85–138.

Kuriakose, S. L., van Beek, L. P. H., van Westen, C. J., 2009. Parameterizing a physically based shallow landslide model in a data poor region. Earth Surf. Proc. Land., **34**, 867-881.

Lee, M. S., Ryu, J. C., Kim, K. S., 2009. Development of the Linear Regression Analysis Model to Estimate the Shear Strength of Soils, The J. Eng. Geol. in Korea., 19, 177–189.(In English Abstract)

Lee, K. T., Ho, J. Y., 2009. Prediction of landslide occurrence based on slope-instability analysis and hydrological model simulation, J. of Hydrol., **375**, 489–497.

Milledge, D. G., Griffiths, D. V., Lane, S. N., Warburton, J, 2012. Limits on the validity of infinite length assumptions for modelling shallow landslides, Earth Surf. Proc. Land., 37, 1158-1166.

Montgomery, D. R., Dietrich, W. E., 1994. A physically based model for the topographic control

on shallow landsliding. Water Resour. Res., **30**, 1153–1171.

Montgomery, D. R., Dietrich, W. E., Torres, R., Anderson, S. P., Loague, K., 1997. Subsurface flow paths in a steep unchannelled catchment. Water Resour. Res., **33**, 91–109.

Montgomery, D. R., Sullivan, K., Greenberg, M. H., 1998. Regional test of a model for shallow landsliding. Hydrol. Process., **12**, 943– 955.

Montgomery, D. R., Schmidt, K. M., Green Berg, H. M., Dietrich, W. E., 2000. Forest clearing and regional landsliding. Geology, **28**, 311–314.

Montgomery, D. R., Balco, G., Willett, S. D., 2001. Climate, tectonics, and the morphology of the Andes: Geology, **29**, 579–582. doi:10.1130/0091-7613(2001)029<0579:CTATMO> 2.0.CO;2.

O'Loughlin, E. M., 1986. Prediction of surface saturation zones in natural catchments by topographic analysis. Water Resour. Res., **22**, 794–804, 1986.

Pack, R. T., Tarboton, D. G. and Goodwin, C. N., 2001. Assessing terrain stability in a GIS using SINMAP. Presented at the 15th annual GIS conference, GIS, February, 19-22, Vancouver, British Columbia.

Park, H. J., Lee, J. H., Woo, I. k., 2013. Assessment of rainfall-induced shallow landslide susceptibility using a GIS-based probabilistic approach, Eng. Geol., **161**, 1–15.

Penna, D., Borgal, M., Aronica, G. T., Brigandì, G., Tarolli, P., 2014. The influence of grid resolution on the prediction of natural and road-related shallow landslides, Hydrol. Earth Sys.Sci., **18**, 2127–2139. doi:10.5194/hess-18-2127-2014.

Raia, S., Alvioli, M., Rossi M., Baum, R. L., Godt, J. W., Guzzetti, F., 2014. Improving predictive power of physically based rainfall-induced shallow landslide models: a probabilistic approach, Geosci. Model Dev., 7, 495-514.

Reid, M. E., LaHunsen, R. G., Iverson, R. M., 1997. Debris flow initiation experiments using diverse hydrologic triggers. In Debris Flow Hazards Mitigation: Mechanics, Prediction and Assessment, Chen CL (ed.). ASCE Proceedings.1–11.

Reimer, M.F., 1992. The effects of testing conditions on the constitutive behavior of loose, saturated sands under monotonic loading. PhD thesis, University of California, Berkeley.

Rickenmann, D., Zimmermann, M., 1993. The 1987 debris flows in Switzerland: documentation and analysis, Geomorphology, **8**, 175–189.

Rossi, M., Guzzetti, F., Reichenbach, P., Mondini, A., Peruccacci, S., 2010. Optimal landslide susceptibility zonation based on multiple forecasts, Geomorphology, **114**, 129–142.

Rosso, R., Rulli, M. C., Vannucchi, G., 2006. A physically based model for the hydrologic control on shallow landsliding. Water Resour. Res., **42**, W06410.http:// dx.doi.org / 10.1029/2005WR004369.

Schmidt, K. M., Roering, J. J., Stock, J. D., Dietrich, W. E., Montgomery, D. R., Shaub, T., 2001. Root cohesion variability and shallow landslide susceptibility in the Oregon Coast Range, Can. Geotech. J., **38**, 995– 1024.

Selby, M. J., 1976. Slope erosion due to extreme rainfall: a case study from New Zealand. Geog. Ann., **3A**, 131–138.

Sidle, R. C. and Ochiai, H., 2006. Landslides: processes, prediction, and land use. Am. Geophys. Union., Washington DC, 312.

Swets, J. A., 1988. Measuring the accuracy of diagnostic systems. Science, **240**, 1285–1293.

Talebi, A., Troch, P. A., Uijlenhoet, R., 2008. A steady-state analytical hillslope stability model for complex hillslopes. Hydrol.Process., **22**, 546–553.

Tarolli, P., Tarboton, D. G., 2006. A new method for determination of most likely landslide initia-

tion points and the evaluation of digital terrain model scale in terrain stability mapping. Hydrol. Earth Syst. Sci., **10**, 663–677.

Uchida, T., Mori, N., Tamura, K., Takiguchi, S., Kamee, K., 2009. The role of data preparation on shallow landslide prediction. J. the Jap. Soc. Eros. Cont. Engi., **62**, 23–31.

Uchida, T., Tamur, K., and Akiyama, K., 2011. The role of grid cell size, flow routing algorithm and spatial variability of soil depth on shallow landslide prediction. Ital. J. Engi. Geol. and Environ., 149-157. doi: 10.4408/IJEGE.2011-03.B-018.

Van Den Eeckhaut, M., Vanwalleghem, T., Poesen, J., Govers, G., Verstraeten, G., Vandekerckhove, L., 2006. Prediction of landslide susceptibility using rare events logistic regression: a case study in the Flemish Ardennes (Belgium). Geomorphology, **76**, 392–410. doi:10.1016/j.geomorph.2005.12.003.

Vanacker, V., Vanderschaeghe, M., Govers, G., Willems, E., Poesen, J., Deckers, J., De Bievre, B., 2003. Linking hydrological, infinite slope stability and land-use change models through GIS for assessing the impact of deforestation on slope stability in high Andean watersheds. Geomorphology, **52**, 299–315.

Wieczorek, G. F., 1987. Effect of rainfall intensity and duration on debris flows in central Santa Cruz Mountains, California, in: Debris Flows/Avalanches: Processes, Recognition and Mitigation, edited by: Costa, J. E. and Wieczorek, G. F., Reviews in Engineering Geology, Geol. Soc. of Am., **7**, 23–104.

Wilkinson, P. L., Anderson , M. G., Lloyda, D. M., Renaudb, J. P., 2002. Landslide hazard and bioengineering: towards providing improved decision support through integrated numerical model development. Environmental Modeling &Software., **17**, 333–344.

Wu, W., Sidle, R. C., 1995. A distributed slope stability model for steep forested basins. Water

Resour. Res., **31**, 2097–2110, 1995.

Yoshinaga, S., Ohnuki, Y., 1995. Estimation of soil physical properties from a handy dynamic cone penetrometer test. J. of the Jap.Soc. of Eros. Cont. Engi., **48**, 200.

Zhang, W., Montgomery, D. R., 1994. Digital elevation model grid size, landscape representation, and hydrologic simulations. Water Resources Research., **30**, 1019–1028.

Zizioli, D., Meisina, C., Valentino, R., Montrasio, L., 2013. Comparison between different approaches to modeling shallow landslide susceptibility. Nat. Hazards Earth Syst. Sci., **13**, 559–573.

Chapter 4. Analysis of subsurface flow by piping for landslide initiation and development using a large flume experiment

4.1 Introduction

Rainfall is a principal factor in the triggering of shallow landslides (Campbell, 1966; Starkel, 1976; Iverson, 2000). Shallow landslides induced by rainfall have been studied for practical and scientific reasons, because it is important to consider subsurface water when attempting to understand the processes involved in shallow landslide initiation (Anderson and Sitar, 1995; Iverson et al., 1997; Gabet and Mudd, 2006). Many landslide studies, however, have found it difficult to delineate potential landslides because of the strong influence of local controls, such as regolith, soil permeability, soil layering, root strength, localised seepage forces and preferential flow along bedrock surfaces due to piping (Casadei et al., 2003).

Previous studies have shown that the presence of groundwater in the soil mantle markedly affects rainwater discharge and slope stability on steep slopes (e.g., Anderson and Sitar, 1995; Iverson et al., 2000; Wang and Sassa, 2003; Onda et al., 2004; Kosugi et al., 2008). Therefore, one of the simplest approaches to analyse the effects of groundwater formation on shallow landslides involves a combination of infinite slope stability analysis with a steady-state shallow subsurface flow model (e.g., Okimura et al., 1985; Montgomery and Dietrich, 1994; Pack et al., 1998). In addition, many physical models assume that the soil–bedrock interface is a simple topographic surface paralleling the soil surface.

Recently, more complex processes have been considered in physically based models to predict the spatial susceptibility and patterns of shallow landslides (e.g., Hiramatsu et

al., 1990; Wu and Sidle, 1995; Rosso et al., 2006; Talebi et al., 2008; Uchida et al., 2011). However, some issues remain unresolved regarding steady-state models. For example, time-scale discrepancies in the modelled hydrological processes and the concept of steady groundwater flow slope parallel to an underlying impermeable bed can predict only the long-term distribution of groundwater pressure, which could be viewed as a predisposition to landslides (Teragima et al., 2014). Models can be used to calculate the topographically driven convergence of rainwater and the groundwater table in the soil mantle, thus providing a physically based estimate of the stream hydrograph and a spatially distributed prediction of shallow landslide occurrences. The accuracy of these physical models is still limited, mainly because they ignore storm responses in the underlying bedrock (e.g., Wilson and Dietrich, 1987; Kosugi et al., 2008; Lanni et al., 2013).

Several recent studies have suggested that flow via piping could contribute substantially to the rapid transfer of stormwater (e.g., Mosely, 1982; Kirkby, 1988; Tanaka et al., 1988; Tsukamoto and Ohta, 1988; McDonnell, 1990) and that evidence of the occurrence of increasing groundwater levels due to bedrock flow was often found in the scars of shallow landslides (e.g., Ohta et al., 1981; Brand et al., 1986; Jenkins et al., 1988; Selby, 1993; Onda et al., 2004). Theoretical analyses and observations have been presented regarding the movement of soil particles within slopes with an emerging subsurface flow to evaluate subsurface flow that may cause shallow landslides (Zaslavsky and Kassiff, 1965; O'Loughlin and Pearce, 1976; Wu et al., 1979; Kochel et al., 1985; Iverson and Major, 1986; Kohno et al., 1987; Selby, 1993; Terajima and Sakura, 1993; Terajima et al., 1997, 2001; Gabet and Dunne, 2002; Terajima et al., 2014).

The importance of seepage flow convergence by the groundwater table within hillslope hollows to shallow landslide initiation has also been studied. Many researchers have attempted to analyse subsurface flow for shallow landslide initiation using various methods. Pierson (1983) observed that a closed pipe raised the groundwater table downslope from the

pipe's outlet. Wilson and Dietrich (1987) measured piezometric responses along a hollow in a catchment underlain by arkosic greywacke and clarified the relations of these responses to spatial variations in bedrock permeability. Terajima and Moroto (1990) and Uchida et al. (2011) measured hydrostatic pressure propagation from the soil mantle through the bedrock in catchments underlain by weathered granite. Katsura et al. (2006) and Kosugi et al. (2006) showed that both saturated and unsaturated water flows in weathered granitic bedrock are important for the development of groundwater within the soil mantle.

In a large flume experiment and field observation study, Iverson and Major [1986] and Reid and Iverson (1992) showed that ascending subsurface flows at the toe of slopes or at geological boundaries were involved in the initiation of shallow landslides and subsequent debris flows. Sidle et al. (1995) conducted a series of flume experiments using a single drainage pipe composed of five segments, each with a different roughness coefficient. Some researchers developed numerical models to simulate soil–pipe flow within a hillslope and verified these results with flume experiments (e.g., Kosugi et al., 2004; Tsutsumi et al., 2005a). They mentioned that the direction and force of the subsurface flow during rainstorms is important to interpret mechanisms for the initiation of shallow landslides.

However, there have been few previous studies regarding shallow landslide initiation by subsurface hydrological processes, such as the effects of seepage direction and changes of seepage force by topographic characteristics, and monitoring of the factors of seepage direction and force is difficult. Moreover, assessment of the individual effects of seepage characteristics on shallow landslide processes due to local conditions is complicated. In this study, to evaluate the seepage failure mechanisms by piping, a large flume experiment and artificial rainfall simulation were conducted and hydraulic responses were monitored. I analysed the effects of subsurface flow by piping using factors of safety and numerical modelling.

4.2 Seepage direction modeling

Unsaturated and saturated flows within the slopes were modelled by finite element seepage analysis using SEEP/W (GeoStudio 2004 Software,Version 6.22). The model code is based on the equations of motion and mass conservation. Both saturated and unsaturated flows are simulated using a modified version of Darcy's law (Richards' equation). Darcy's law was originally derived for saturated soils, but later research showed that it can also be applied to the flow of water through unsaturated soils (Richards, 1931). Under unsaturated conditions, the hydraulic conductivity function is no longer a constant but varies with changes in water content (Brooks and Corey, 1964; Fredlund and Rahardjo, 1993) and the governing equation has been extended to incorporate unsaturated conditions (Richards, 1931; Fredlund and Rahardjo, 1993; Tofani et al., 2006). Differential controlling equations for simple saturation seepage are written for an anisotropic environment as follows:

$$\frac{\partial}{\partial \mathrm{x}}\left(-\mathrm{k_x}\frac{\partial \mathrm{H}}{\partial \mathrm{x}}\right)+\frac{\partial}{\partial \mathrm{y}}\left(-\mathrm{k_y}\frac{\partial \mathrm{H}}{\partial \mathrm{y}}\right)=0 \qquad (4.1)$$

where H = total head, k_x = hydraulic conductivity in the x direction, and k_y = hydraulic conductivity in the y direction. For unsteady or transient flow conditions, Equation 4.1 changes to Equation 4.2:

$$\frac{\partial}{\partial \mathrm{x}}\left(-\mathrm{k_x}\frac{\partial \mathrm{H}}{\partial \mathrm{x}}\right)+\frac{\partial}{\partial \mathrm{h}}\left(-\mathrm{k}_y\frac{\partial \mathrm{H}}{\partial \mathrm{y}}\right)+\mathrm{Q}=\frac{\partial \theta}{\partial \mathrm{t}} \qquad (4.2)$$

where Q=flow, θ=the water volume content and t= time.

Equation 4.2 shows that the difference between the flow entering and leaving an elemental volume at a point in time is equal to the change in the volumetric water content. More fundamentally, it shows that the sum of the rates of change of flows in the x- and y-directions plus the external applied flux is equal to the rate of change of the volumetric water content with respect to time.

4.3 Factor of safety analysis for seepage force and direction

Soil strength or the resisting force which is responsible for slope stability is usually defined using Mohr–Coulomb's equation:

$$\tau = c' + \left(\sigma_n - u_w\right) \tan \phi' \qquad (4.3)$$

where, τ is the shear strength, c' is the effective cohesion, ϕ' is the effective angle of internal friction, σ_n is the total normal stress, and u_w is the soil pore-water pressure (Whitlow, 1983; Fredlund and Rahardjo, 1993).

Under saturated conditions, effective normal stress is expressed as total normal stress minus pore water pressure. If pore water pressure exceeds total normal stress, the value of effective stress becomes negative, indicating that stress is acting in the upward rather than downward direction. In the cohesive matrix above the "normal" level of the groundwater table (phreatic surface) and capillary fringe, materials are unsaturated, pores are filled with water and air, and pore water pressure is negative (Simon and Collison, 2002). In unsaturated soils, de-

creasing matric suction has the effect of increasing the apparent cohesion of the soil, as described by Fredlund and Rahardjo (1993):

$$\tau = c^{'} + \left(\sigma_{n} - u_{a}\right) \tan \phi^{'} + (u_{a} - u_{w}) \tan \phi^{b'} \qquad (4.4)$$

where τ = shear strength on a potential failure plane (N/m^2), c' = effective cohesion, σ_n = normal stress, ϕ' = friction angle in terms of effective stress, $\phi^{b\prime}$ = angle expressing the rate of increase in strength relative to the matrix suction, $(\sigma_n - u_w)$ is the net normal stress state on the failure plane at failure, u_a is the pore air pressure on the failure plane at failure, $(u_a - u_w)$ is the matrix suction and $\varphi^{b\prime}$ is the angle indicating the rate of increase in shear strength relative to the matrix suction $(u_a - u_w)$, which is generally between 10° and 20° (Fredlund and Rahardjo, 1993; Simon et al., 1999). Therefore, an increase in pore water pressure decreases the effective stress of the soil, which in turn decreases the shear strength.

The safety factor F_s is defined as the ratio of the resisting forces to the driving forces. The driving forces are the vector components of the seepage force and weight perpendicular to the plane, whereas the resisting forces are equal to shear strength of the soil defined by the Mohr–Coulomb equation. The safety factor F_s is defined by the ratio between the stabilising action, T_s and destabilising action, T_d:

$$F_s = \frac{T_s}{T_d} \qquad (4.5)$$

In the infinite slope analysis of homogeneous slopes, the slip surface is assumed

to be a plane parallel to the ground surface where the end effects can be neglected (Huang 1982). This analysis is valid if the ratio of depth to length of the sliding mass is small (a ratio of 1/20 or less is commonly used). Ghiassian and Ghareh (2008) considered seepage conditions including seepage direction and force and, an infinite slope element subjected to both uniform seepage and gravitational forces is shown in Fig. 4.1.

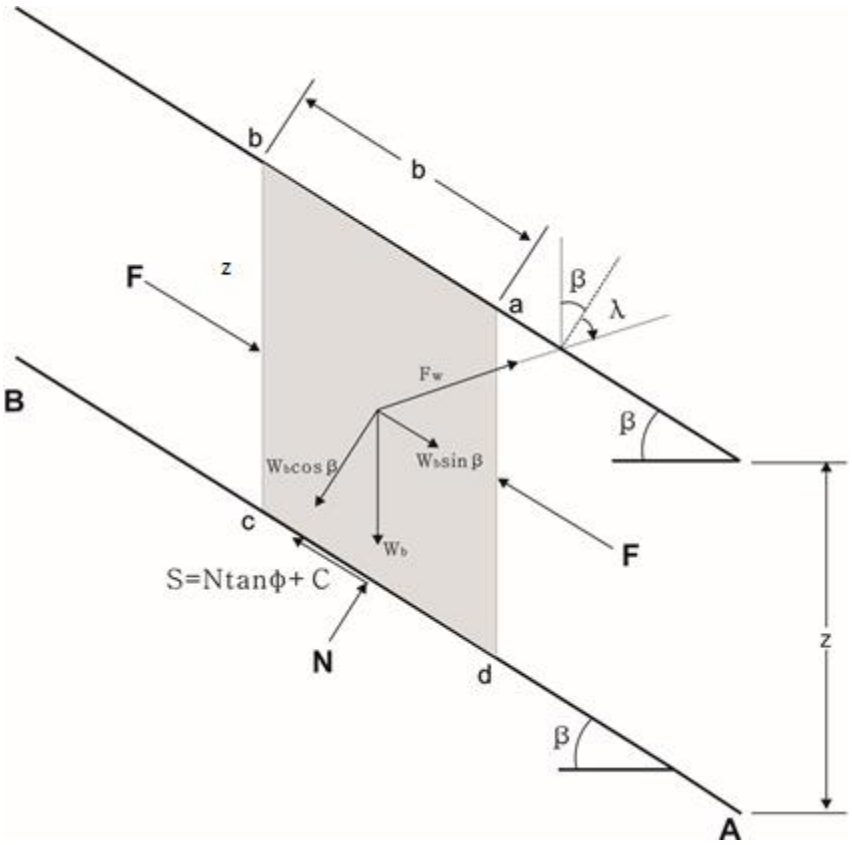

Fig. 4.1 Concept of factor of safety reflecting the seepage force and direction.

The equilibrium equations is derived using a rectangular block, W_b, (i.e. a-b-c-d in Fig. 4.1) and seepage force with a variable seepage direction, F_w, expressed, respectively, as:

$$W_b = V\gamma_b = zbcos\beta\gamma_b \qquad (4.6)$$

$$F_w = iV\gamma_w \qquad (4.7)$$

where W_b is the weight of block; V is the volume of rectangular block; γ_b is soil density, z is vertical soil depth; b is the length of the element parallel to the slope; β is slope angle; i is hydraulic gradient (the seepage vector of magnitude, i=sinβ/sinλ) and γ_w is water density. And normal stress N for the stabilising action and could be expressed as:

$$\mathrm{N} = W_b cos\beta - F_w cos\lambda \qquad (4.8)$$

And by substituting eq. (8), the stabilising action for shear strength (S) is expressed as:

$$\mathrm{S} = \mathrm{N}\tan\theta' + c'b = (W_b cos\beta - F_w cos\lambda)\tan\theta' + c'b \qquad (4.9)$$

where, λ is seepage direction measured clockwise from the inward normal to the slope and θ' is internal friction angle. In here, the shear stress (T_d) on destabilising action could be expressed:

$$T_d = W_b sin\beta + F_w sin\lambda \quad (4.10)$$

And substituting eq. (9) and eq. (10) into eq. (5) to calculate the factor of safety gives:

$$\mathrm{FS} = \frac{S}{W_b sin\beta + F_w sin\lambda} = \frac{(W_b cos\beta - F_w cos\lambda)\tan\theta' + c'b}{W_b sin\beta + F_w sin\lambda} \qquad (4.11)$$

By substituting eq. (6) and (7) to into eq. (11), the equation could be expressed as:

$$\mathrm{FS} = \frac{cos\beta - i\frac{r_w}{\gamma_b}cos\lambda}{sin\beta + i\frac{r_w}{\gamma_b}sin\lambda}\tan\theta' + \frac{\frac{c'b}{W_b}}{sin\beta + i\frac{r_w}{\gamma_b}sin\lambda} \qquad (4.12)$$

If A_b(the buoyant seepage) and m_b (buoyant cohesion coefficient) are defined as:

$$A_b = i\frac{\gamma_w}{\gamma_b} = \frac{sin\beta}{sin\lambda}\frac{\gamma_w}{\gamma_b}, \quad m_b = \frac{cb}{W_b} = \frac{c}{\gamma_b z cos\beta} \qquad (4.13)$$

By substituting eq. (12) and (13), the equation of FS could be simplified as:

$$\mathrm{FS} = \frac{cos\beta - A_b cos\lambda}{sin\beta + A_b sin\lambda}\tan\theta' + \frac{m_b}{sin\beta + A_b sin\lambda} \qquad (4.14)$$

For the sake of convenience and efficiency, the "seepage force" approach was used, although the "boundary pore pressure" gives identical results (Lambe and Whitman, 1969). The stability can decrease even more if seepage emerges from the slope with a smaller λ. The most critical seepage gradient is when the flow direction approaches zero, i.e., perpendicular to the slope (i → ∞).

4.4. Experiment method

4.4.1 Artificial rainfall simulating and large flume experiments

I used the artificial rainfall simulators (75 m in length, 50 m in width and 22 m in

height) at the National Research Institute for Earth Science and Disaster Prevention (NIED), Japan. This simulator can be moved between five experimental sites to efficiently conduct many experiments throughout the year. The height of the nozzles above the ground was 16 m, far enough for raindrops to reach the natural terminal velocity. The simulator can sprinkle water at intensities of 15 – 200 mm/h; for our experiment, the rainfall intensity was set at 80 mm/h (Table 1). Three cylindrical rain gauges were installed around the sides of the flume to monitor the rainfall amount and its spatial distribution during the experimental simulations.

In this study, a large flume experiment was conducted with a width of 1.5 m, length of 6 m and height of 3.4 m, with a soil depth of 0.6 m and slope angle of 30°. In this flume, one sidewall of the entire flume was made of clear reinforced glass to enable direct observation of soil deformation. To evaluate the effects of piping on shallow landsliding potential, the water tank was installed on top of the flume for the maximum hydraulic gradient (seepage force). Two hoses (2.5 cm in diameter) were connected between the water tank and two holes (2.5 cm in diameter) 50 cm from the flume bottom.

Fig. 4.2 A large flume experiment and artificial rainfall in NIED.

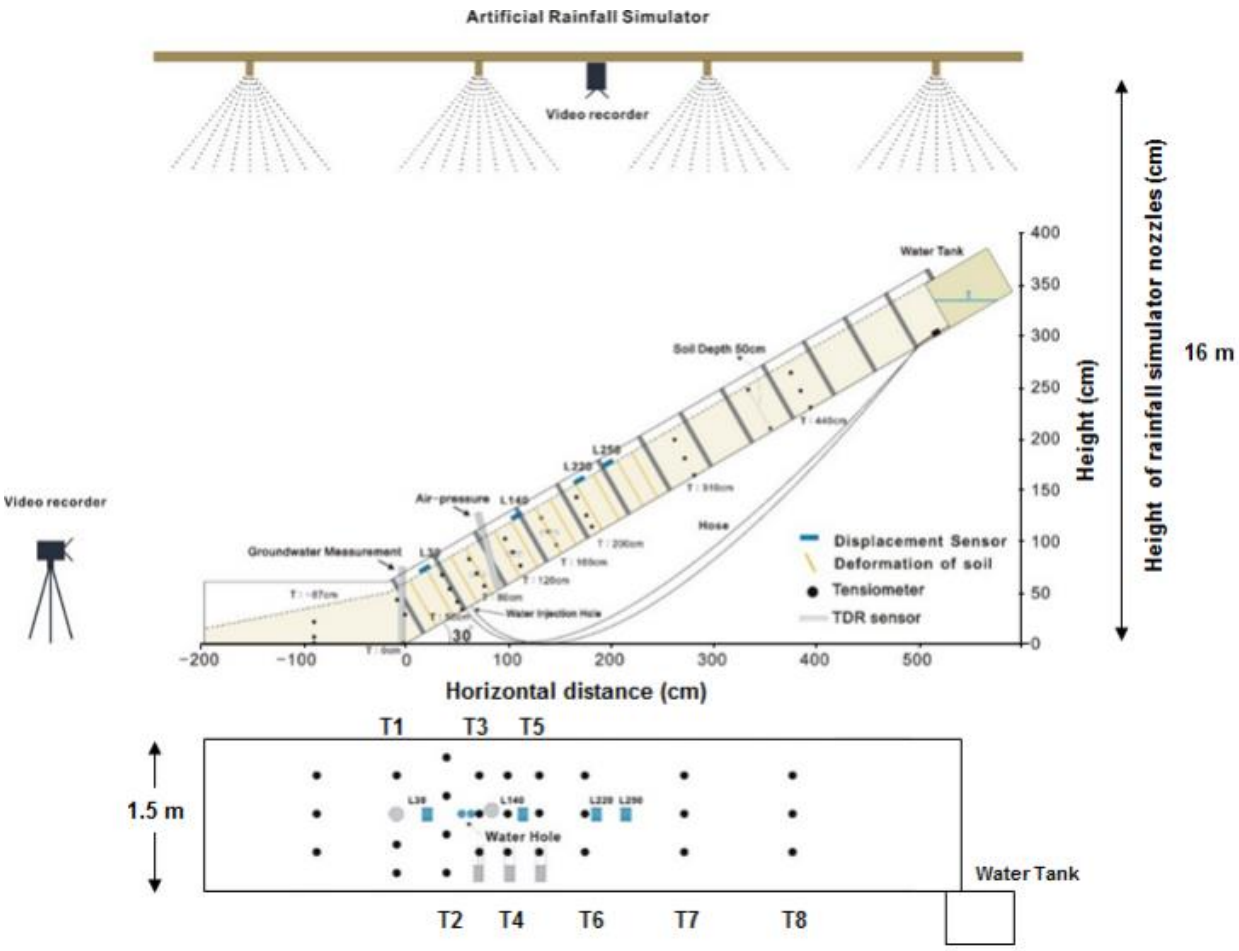

Fig. 4.3 Concept of artificial rainfall and a large flume experiment

A video camera (Sony, Tokyo, Japan) was used to monitor failure initiation time, location and subsequent retrogression of failures. This flume was filled with relatively homogeneous, isotropic granular sand with a soil thickness of 50 cm. Soil samples were collected from a depth of about 25 cm in the middle of the flume, and the physical properties of the soil were measured by triaxial compression test (Table 4.2). The density of the sand, dry density and wet density were 2.664, 1.478 and 1.638 g/cm^3, respectively. The saturated soil water content was 35.9%, and the saturated hydraulic conductivity, measured using the constant falling head method, was 2×10^{-2} cm/s. The median particle diameter (D_{50}) was 0.539 mm and the internal friction angle and soil cohesion were 35.2° and 0.8 kN/m^2, respectively.

Table 4.1 Artificial rainfall properties in NIED

Rainfall simulator	Properties	
Raindrop size	0.1 – 2.2 mm diameter	
Rainfall intensity	15 – 200 mm/hr	
Rainfall area	44 x 72 m (dividable into quarters)	
Nozzles ($0.7 – 5.0$ kg/cm^2)	System 1 : 15 – 40 mm/hr	544pcs.
	System 2 : 30 – 75 mm/hr	544pcs.
	System 3 : 60 – 130 mm/hr	544pcs.
	System 4 : 100 – 200 mm/hr	544pcs.
Nozzle height	16m above the ground	
Control	Remote control : flow rate/stress control	
Circulating pump	160 kW, 11 kg/cm^2, 5.5 kl/min, 2pumps	

Table 4.2 Soil properties in a large flume experiment

Analysis of soil	Material properties
Wetness density (g/㎤)	1.638
Dried bulk density (g/㎤)	1.478
Mean porosity (computed from bulk density)	0.45
Volumetric Water Contents (%)	35.9
Internal friction angle (°)	35.2
Soil cohesion（ kN/m^2)	0.8
Permeability (cm/s)	2.0×10^{-2} cm/s
Particle Density (g/㎤)	2.664

4.4.2 Monitoring sensors on the flume

Figure 4.2 shows the large flume and artificial rainfall simulator. To measure hydraulic response at several points of the flume, 21 tensiometers (diameter, 22 mm; range, 100 kPa; accuracy, 2%; Model P with glass filters attached to the tips; Irrometer Co., Inc., Riverside, CA) were installed vertically to the slope at 87, 0, 50, 80, 120, 160, 200, 310 and 440 cm along the flume surface, respectively; measuring depths ranged from 10 to 50 cm. The three Time Domain Reflect (TDR) sensors (CS series; Campbell Scientific Inc., Canada, Montreal, QC, Canada) for measuring the volume water contents (%) were installed at a depth of 25 cm on the slope (80, 120 and 160 cm). The sensors for surface water contents (%) were also installed at three points (30, 140 and 220 cm) on the slope part of the flume.

To monitor the failure position and location, four vertical displacement and four horizontal displacement sensors were installed at 30, 140, 220 and 250 cm on the sandy surface of the flume. The MEMS tilt sensor (Uchimura et al., 2009) was added on a small T-shaped peg, which was pushed into the slope surface to a depth of 3 cm to measure rotation. Moreover, white lines were embedded every 50 cm along the reinforced glass sidewall of the flume to determine the shapes of failures observed in the experiment (Fig. 4.3). The unit weight of the white markers, which corresponds to the saturated density of the soil (range: 1.47 – 1.638 g/cm^3), was used to detect the movement of any soil failures. I systematically investigated the hydrological responses within the sloping soil of the flume against water injection to the flume bed.

4.4.3 Experimental performance

I filled the flume with sand on 26 November 2009 after having already checked the temporal and spatial consistency of the artificial rainfall conditions. The specifications of the artificial rainfall simulator applied in this study are presented in Table 4.1. Artificial rainfall simulation was applied continuously, but I considered two phases, i.e., a first phase in which the main factor for landsliding was only rainfall, and a second phase in which the main factors were force and direction of seepage during rainfall simulation to evaluate the effects of seepage on landsliding potential.

Rainfall simulation ran continuously from 11:10 to 13:10 with a rainfall intensity of 80 mm/h. In the first phase, artificial rainfall was from 11:10 to 13:04, and the flow of subsurface water and seepage influenced only by rainfall simulation were monitored. In the second phase, artificial rainfall was from 13:04 to 13:10, and water injection into the sloping bed of the flume was applied forcibly from 13:04 to 13:06. Artificial water injection for piping was intended to observe the effects of seepage on landslide initiation. A landslide occurred during the 2 minutes of water injection and, water injection was stopped when the landslide slowed to a halt.

4.5. Results and Discussions

4.5.1 Hydraulic responses and seepage change during rainfall experiment

During the rainfall experiment, surface runoff was not observed and seepage outflow was only observed from the toe of the flume and I considered it to have been due to interflow along the soil–bedrock interface resulting from rising groundwater. Fig. 4.4 shows the failure mechanism processes of seepage erosion and washing out to the toe of the flume during the rainfall simulation. Fig. 4.4a shows that the sediment washed out to the toe of the flume by seepage erosion and seepage flow after 100 minutes from the onset of rainfall at 11:10. Over time, failure was caused by seepage flow and undercutting by seepage erosion. Fig. 4.4b shows that the failure was caused by undercutting of seepage erosion and sediment washout. In this experiment, subsurface flows and the surface motion of the failure were detected, and Fig. 4.5 shows the results of our subsurface monitoring and the surface motion of the failure due to subsurface processes during the experiment. The red dotted line in Fig. 4.5 indicates the time of water injection in the experiment for analysing the effect of subsurface flow by piping. T1 (a) to T8 (h) in Fig. 4.5 represent the pore water pressure (cm H_2O) data from the tensiometer nets. Fig. 4.4i shows the soil water contents (%) for monitoring the subsurface flow by applying TDR, and Fig. 4.5j illustrates the surface water content sensors (%) for monitoring the water content at the flume surface from wireless valve controller (WVC) sensors. Fig. 4.5k and 4.5l show horizontal motion and vertical motion sensors, respectively, used to monitor the surface motion of failure.

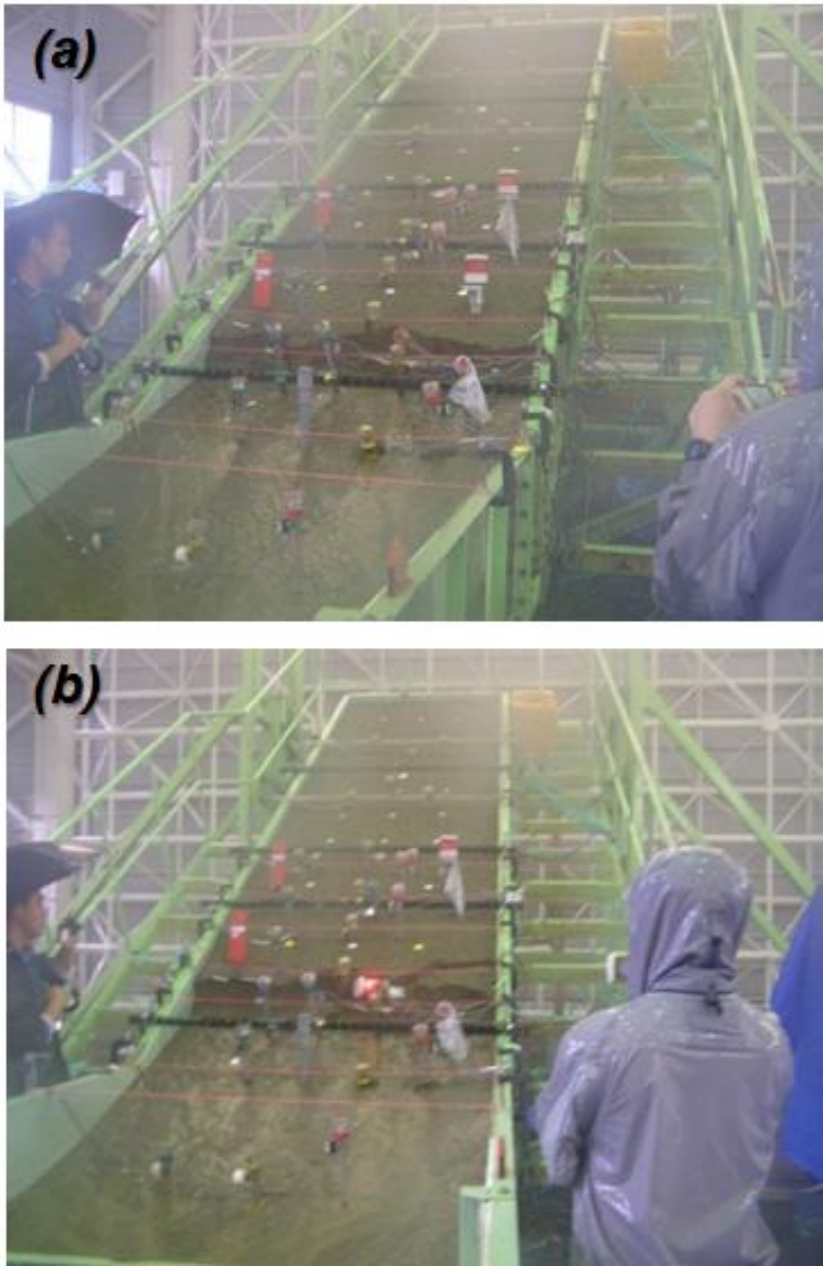

Fig. 4.4. Rainfall experiment for shallow landslide initiation. (a) is showing the sediment wash out to toe of flume by seepage and seepage erosion. (b) is showing the failure caused undercutting by seepage erosion and wash out to toe of flume.

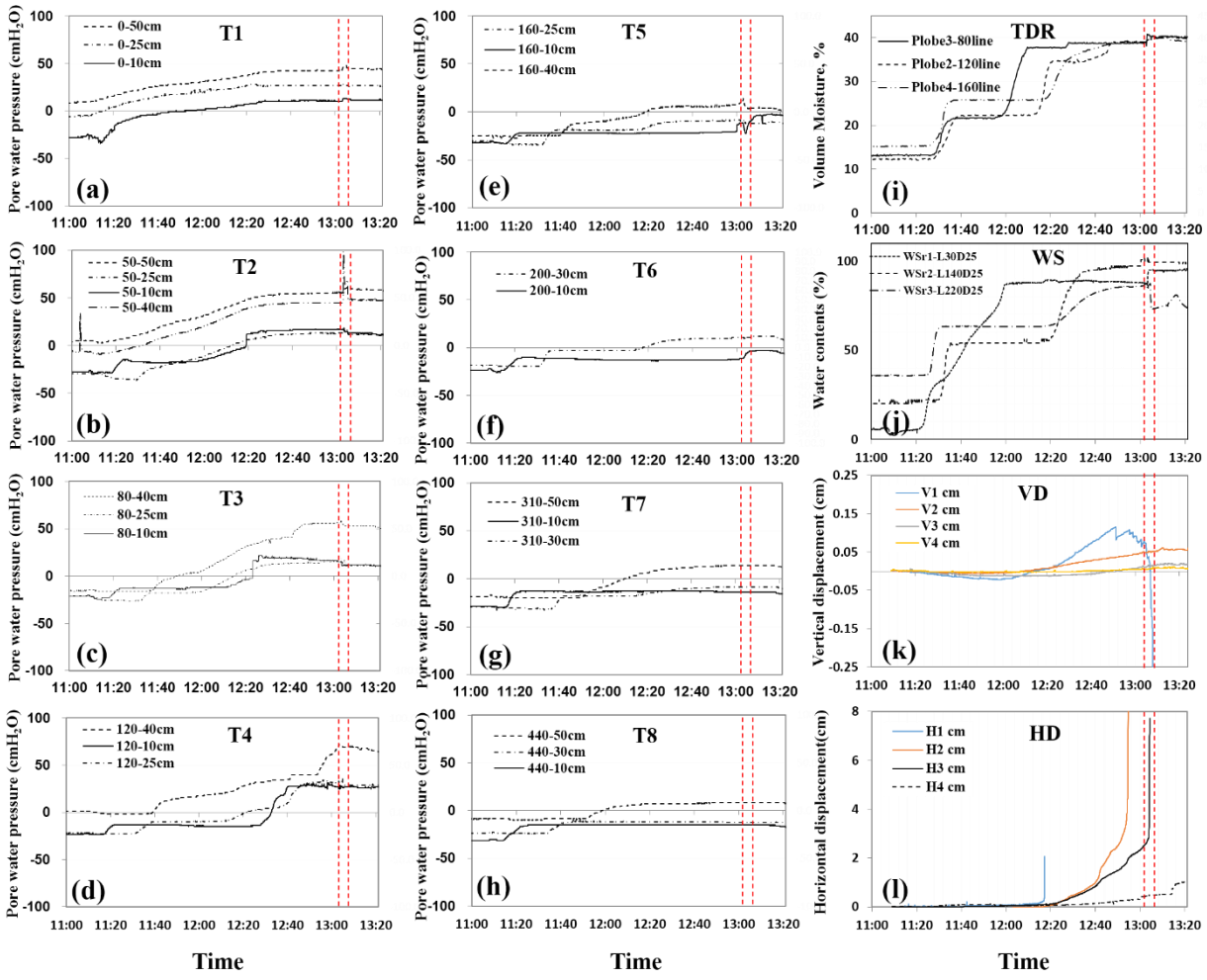

Fig. 4.5 Responses of various sensors for measuring the subsurface flow and surface failure motion during rainfall experiment (rainfall intensity, 80mm/h). Tensiometer-nets is from (a) to (h), (i) is TDR sensor, (j) is water contents, (k) is vertical movement sensors and (l) is horizontal movement sensors.

During the rainfall experiment (time from 11: 10 to 13: 00), the increase in pore water pressure was detected from T1, which was installed at the toe of the flume, and the pore water pressure increased over 0 cm H_2O at a depth of 50 cm, which indicated that the soil was saturated. For the onset of the rainfall experiment to around 80 minutes later, the pore water pressure values from T1 to T4 illustrated that measurements exceeded 0 cm H_2O, which indicated that the soil was completely saturated due to an increase in groundwater. According to Fig.

4.4a, undercutting due to seepage erosion and/or seepage flow occurred on the sandy surface at the same time as the above result. During seepage erosion and undercutting of the sandy surface, the pore water pressure increased abruptly (50 – 10 cm for T2, 80 – 10 cm for T3 and 120 – 10 cm for T4 as shown in Fig. 4.5). However, pore water pressure data obtained from T5 to T8 showed values less than 0 cm H_2O, indicating that the soils were unsaturated, except at depths of 40 and 50 cm)

Over time, undercutting from seeping water and seepage erosion occurred gradually toward the upward direction on the flume and sediment due to undercutting of the sand at a depth of 15 cm in the flume washed out at the toe of the flume (Fig. 4.4b). All nets of tensiometers initially measured negative pressures < 0 cm H_2O and then increased to over 0 cm H_2O until it reached the middle of the flume where T4 was located. All TDR probes in Fig. 4.5i show < 20% moisture by volume, indicating that the soil was unsaturated. However, after 90 minutes of rainfall, the volumetric moisture contents of all TDRs showed approximately 38% (close to porosity), indicating that the soil was completely saturated to a depth of at least 25 cm. In addition, as shown in Fig. 4.5j, water contents at WSr2 and WSr3 were over 90% as measured from the sandy surface, indicating that the soil was saturated.

H1 installed on the sandy surface at a distance of 30 cm, one of the horizontal displacement sensors for measuring motion of failure shown in Fig. 4.5l moved to the toe of the flume but failure did not occur until this time and after seepage erosion and washout occurred. During the experiment, H2 sensors installed at a distance of 140 cm on the flume surface moved in the downward direction when soil was saturated at approximately 12:20 at WSr2-140, as shown in Fig. 4.5j. However, this was because of undercutting and sediment washout caused by seepage erosion and seeping water. This means that sensors for failure motion did not clearly measure the relationship between pore water pressure and motion of failure because they had already been moved by washout to the toe of the flume due to seepage erosion.

When the pore water pressure and soil water contents increased after approximately 110 minutes from onset of rainfall at 11:10, retrogressive failure occurred by undercutting due to seepage erosion and sediment washout to the toe of the flume in response to the saturation process at the same time. Subsequently, the H2 sensor installed at 140 cm for measuring failure motion moved downward. In the video recordings in Fig. 4.4b and displacement sensors in Fig. 4.5l, retrogressive failure was observed and the movement of the soil was affected by the saturated state in Fig. 4.5i and 4.5j. At that time, small cracks occurred close to a distance of 200 cm on the flume surface but no movement was observed at H3 in Fig. 4.5l during the rainfall-induced landslide experiment.

This result was similar to at least two failure modes, i.e., seepage erosion as the driving failure mechanism and retrogressive sliding (e.g., Sassa et al., 2000; Lourenço et al., 2006; Huang et al., 2009). Howard and McLane (1988) conducted experiments on spring sapping using simulated slopes. The results showed that the hydraulic gradient and the direction of the saturated subsurface flow were related to the movement of soil particles. In our rainfall experiment, soil displacement began after the wetting front arrived at the deepest soil from the toe of the flume, which coincided with a directional change in subsurface flow. This suggested that directional changes in subsurface flow may be the main cause of soil displacement according to a rising groundwater table. As increasing groundwater can change the seepage direction, saturated soil can be changed due to cohesionless soil. Soil displacement, such as retrogressive failure, may occur.

Lourenço et al. (2006) conducted a flume experiment (3 m in length, 45 cm in height and 29.75 cm in width) and showed that seepage erosion occurred due to (1) drag induced by seepage in granular materials, and (2) macropore enlargement by shear stresses applied to their perimeters by water flowing through cohesive and unsaturated soils by Crosta and Prisco (1998). In addition, Huang et al. (2009) conducted flume (1.5 in m width, 1.7 m in height, 0.7 m

in depth and 3.94 m in length quasi-infinite sandy slope) and artificial rainfall experiments. They detected that the washout of sediment occurred before the retrogressive failure at the soil–bedrock interface due to increased soil moisture and pore water pressure. As some researchers mentioned above, the failure was related to seepage based on subsurface flow, such as the increase in groundwater, and then developed into retrogressive failure after seepage erosion.

Thus, I accomplished numerical modelling to evaluate the effects of seepage direction during a rainfall-induced experiment on how it affects seepage direction and topography for shallow landslide initiation. SEEP/W (GeoStudio 2004, Version 6.22) was used to evaluate the seepage direction and calibration of the model was achieved by slightly adjusting saturated hydraulic conductivity K_{sat}. The initial conditions of the models matched those of the constant hydraulic head imposed on the experiment. Cumulative mass flux at the inlet and outlet were taken from each (running) SEEP/W model and compared with observed data from the experiment. Hydraulic conductivity and van Genuchten (1980) parameters were calibrated to match the SEEP/W inflow and outflow to observe pore water pressure data and soil moisture data measured from the experiment.

Fig. 4.6 shows the relationship between seepage direction and topographic effect during the rainfall experiment (rainfall intensity, 80 mm/h). Fig. 4.6a presents the results of seepage direction, which increased gradually in the upward direction. When seepage erosion occurred on a sandy surface during the rainfall experiment, the seepage direction changed from slope-parallel to the upward direction at the toe of the flume and gradually moved towards the upward direction over time due to the rising groundwater table. The seepage erosion occurred from sand surface at the toe of the flume and sediment wash out to the toe of the flume at the same time (Fig. 4.6a). The topography of the sand surface on the flume changed due to seepage erosion from increased seepage during the rainfall experiment. I changed the topography of the sandy surface by using the motion of failure data obtained from a video camera in Fig. 4.6b and the

changed topography data were applied to our numerical modelling. In addition, Fig. 4.6b shows the result of seepage direction considering the topographic effect during the rainfall experiment. When changed topographic data were calculated by numerical modelling and compared with these results and video data, undercutting occurred near the sand surface and affected the groundwater (blue line). In addition, seepage erosion occurred from sand surface sediment washout to the toe of the flume at the same time (Fig. 4.6b).

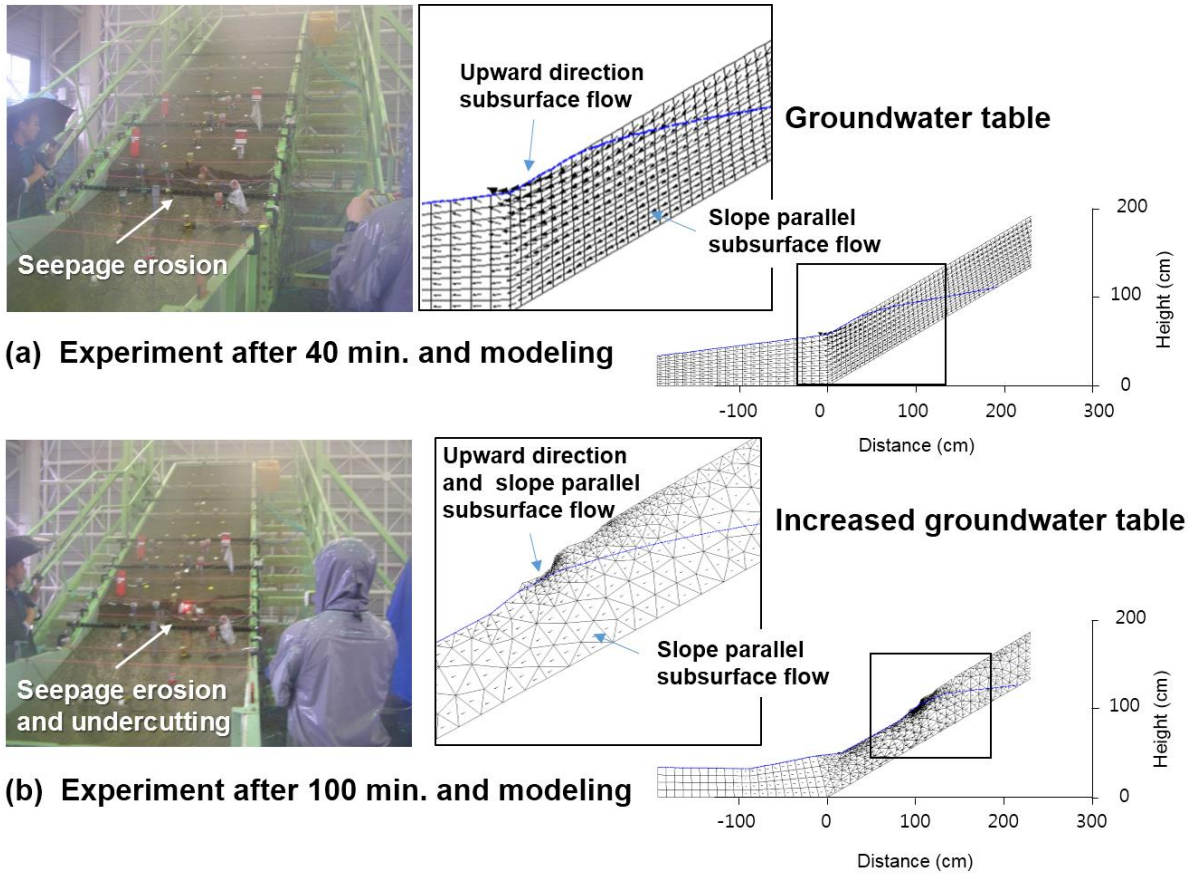

Fig. 4.6. Relation with Seepage direction and topography effect during rainfall experiment (Rainfall intensity, 80 mm/h) (a) is the result of seepage direction that gradually was increased to upward direction. (b) is the result of seepage direction considered the topography effect during rainfall experiment.

In our rainfall experiment, when the groundwater table approached the slope surface, especially near the middle part of the flume, slope failure was induced by undercutting due to the seepage effect; monitored data are shown in Fig. 4.5 and modelling results are presented in Fig. 4.6. Furthermore, no sudden sliding slope failure was observed even when the moisture content within a region such as that near the toe of the slope almost reached full saturation (e.g., Orense et al., 2004; Tohari et al., 2007). On the other hand, when the groundwater table in Figs. 4.5 and 4.6b was approached focusing on the soil surface (approximately 2 hours (13:00) after rainfall start at 11:10), the soil was completely saturated and failure by undercutting associated with the partially liquefied soil mass may be observed, instead of sudden sliding slope failure. The topography of the sand surface on the flume was changed due to seepage erosion by increasing seepage water and/or groundwater during the rainfall experiment. The beginning of soil displacement nearly coincided with the timing of the first directional change in subsurface flow.

4.5.2 Hydraulic responses and failure during the seepage induced landslide experiment

During the seepage-induced landslide experiment for the seepage force and direction of seepage with 80 mm/h continuous sprinkling rainfall at 13:04 – 13:06 pm in Fig. 4.7, the water was injected to a distance of nearly 50 cm at the bottom of the flume holes where seepage force and direction were directly made in an upward direction<unclear?>. In this experiment, failures on a large flume were detected and accelerated in the downward direction, and Fig. 4.7 shows failure and movement of failures during this experiment. Before water injection, failure did not occur but multiple failures did occur at point (a) and moved along slowly as water flowed into the flume (b). The failures moved abruptly in a downward direction after 1 minute during water injection (c). In this artificial seepage-induced landslide experiment with continuous sprinkling rainfall (rainfall intensity, 80 mm/h), I detected multiple failures from distances of 120 to 220 cm, the motion of the multiple failures was abruptly accelerated by piping, and the failures

moved in the downward direction as detected by video camera (Fig. 4.7).

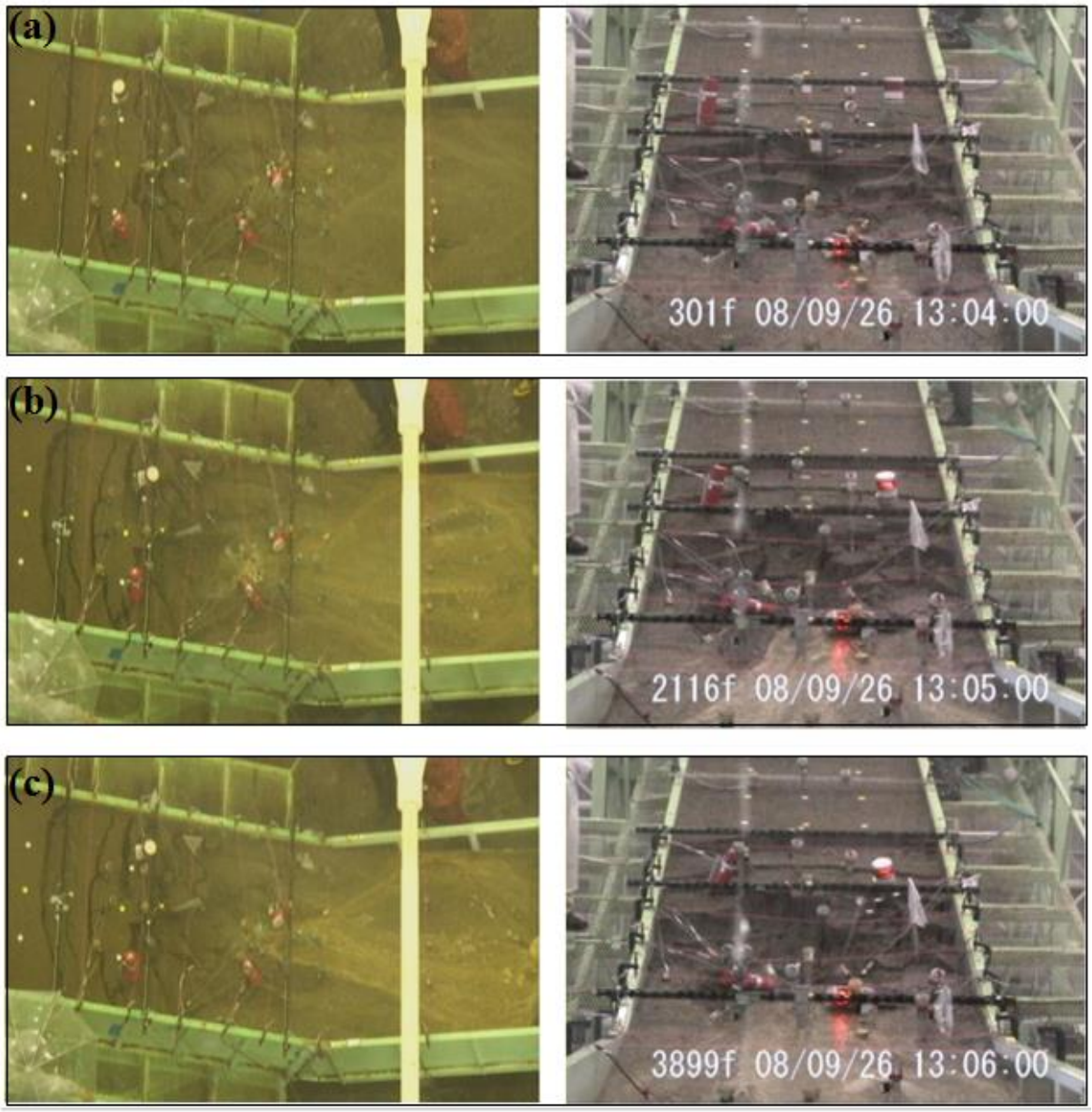

Fig. 4.7. Failure and movement during rainfall (rainfall intensity, 80mm/h) and water injection experiment from 13:04 to 13:06.

Fig. 4.8 shows the results of subsurface monitoring using various sensors installed inside the flume of the surface motion of the failure based on subsurface processes. From Fig.

4.8a to 8h, pore water pressure (cm H_2O) was measured using tensiometers. Fig. 8i shows soil water contents (%) measured from the TDR sensors to monitor the subsurface flow, and Fig. 4.6j illustrates surface water content (%) determined from WVC sensors for monitoring the water content at the flume surface. Fig. 4.8k and 4.8l show the horizontal and vertical motion sensors, respectively, for monitoring the surface motion of failure.

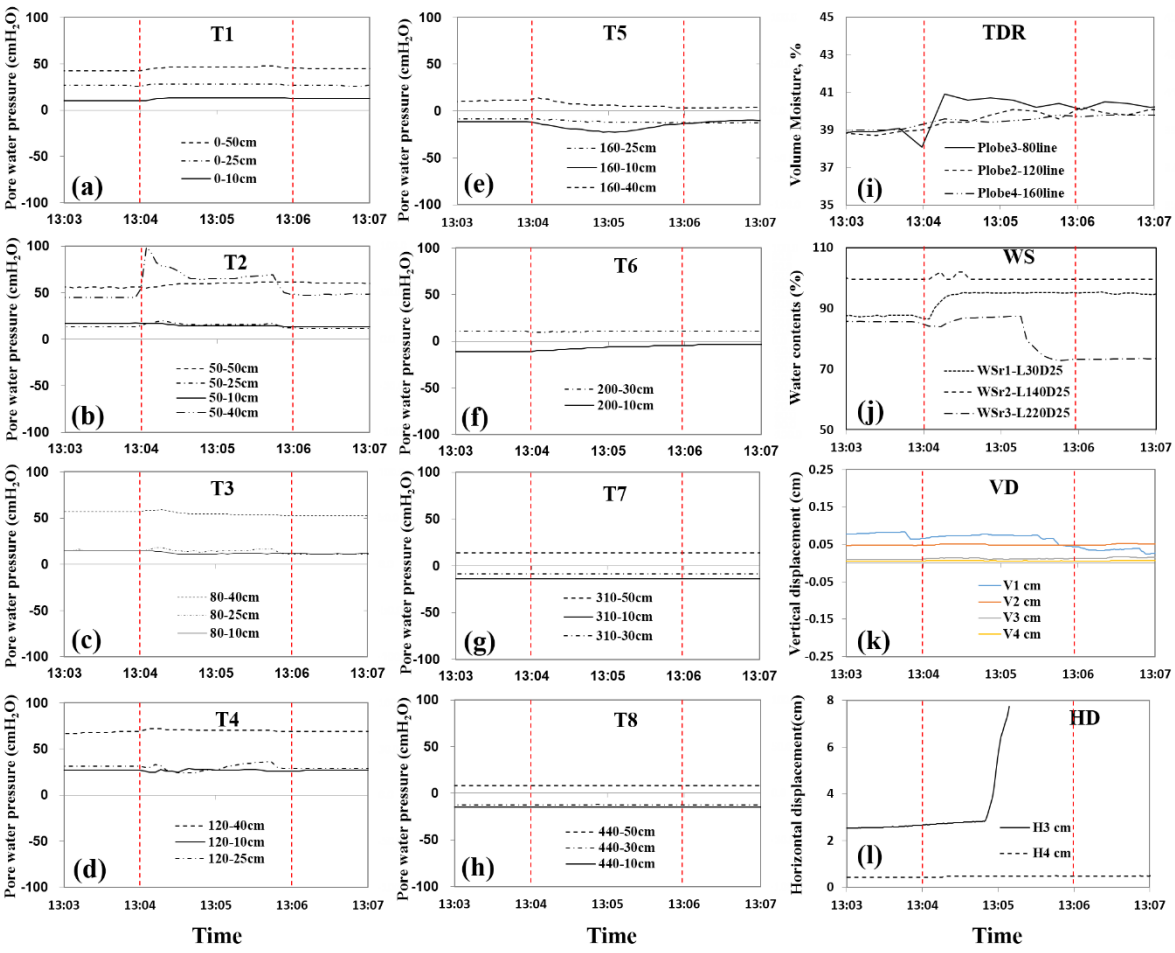

Fig. 4.8. Responses of various sensors for measuring the subsurface flow during rainfall experiment (rainfall intensity, 80mm/h) and water injection for bedrock flow by piping. Tensiometer-nets is from (a) to (h), (i) is TDR sensor, (j) is water contents, (k) is vertical movement sensors and (l) is horizontal movement sensors.

According to Fig. 4.8a – d, in the artificial seepage-induced landslide experiment during the two-minute period (13:04 – 13:06), pore water pressure data exceeded 0 cm H_2O, which indicated complete saturation. In particular, T2 in Fig. 4.8b shows a sudden increase in pore water pressure at a depth of 40 cm from 13:04 when water was injected into the flume, which decreased slowly over the following 10 seconds. However, the values of pore water pressure were over 50 cm H_2O because of the continuous water injection from the water tank and outflow of groundwater recharged the flume. At the same time, pore water pressure at a depth of 40 cm (Fig. 4.8c – e) showed some increase and decreased slowly. Other pore water pressures (i.e., depths of 10 and 25 cm) showed stable values in Fig. 4.8c and 4.8d, and under 0 cm H_2O in Fig. 4.8e because the tensiometers experienced failure (Fig. 4.7). However, pore water pressure in Fig. 4.8e – h showed a stable state and no response to subsurface flow during water injection, indicating no slope failure and no seepage effects as in Fig. 4.7.

During the seepage-induced landslide experiment, the volume moisture of sand from TDR increased in Fig. 4.8i and from all sensors increased to over 38%. These observations indicated that soil porosity increased or contributed to failures because moisture was detected over the limitation value of the TDR sensor (38%). In particular, for the Probe3-80 line located near the water injection holes, it showed a sudden increase of moisture (%) that may have been directly affected by upward seepage direction and high force. Water contents (%) in Fig. 4.8j showed values of 100% and over 95% for WSr1-L30 and WSr1-L140, respectively. These sensors had already moved to the toe of the flume due to seepage erosion and washout. H4 did not move, indicating that failure had not occurred at this position. However, the results for WSr1-L220 showed a decrease of water content (%) during the 30 seconds while water was being injected into the flume at 13:04. Subsequently, the water contents increased and stabilised. At the same time, the results for H3 at a distance of 220 cm, as shown in Fig. 4.8i, indicated abrupt movement in the downward direction after water was injected for about 1 minute. When the H3

sensor stopped, WSr3-L220 showed an abrupt decrease in water content (%). This may have been due to changes in seepage direction and groundwater level affected by the movement of the failing soil mass.

To evaluate the relationship between seepage direction and force for landslide initiation, I used monitored surface data (Fig 4.7) and the numerical model to estimate the topographic effect (failure motion was obtained using video cameras, and then transferred to the numerical model) and the seepage effect (direction was sustained upward and seepage force was also sustained at 5.6). Fig. 4.9 shows the relationships between seepage direction, seepage force, topographic effect during water injection, and the continuing sprinkling rainfall experiment (rainfall intensity, 80 mm/h). Fig. 9a presents the results of small tension cracks and numerical modelling before water injection. Furthermore, Fig. 4.9b illustrates the results of increased tension cracking and numerical modelling during water injection after 1 minute. Fig. 4.9c shows the results of the failure moving in the downward direction and of numerical modelling presenting the topography during water injection after 2 minutes.

When water moved in the upward direction and seepage force of 5.6 flowed into the flume (Fig. 4.9), the topography affected the seepage direction and force near the plane of failure and groundwater increased (Fig. 4.9a). After water was injected for 1 minute, the topography changed due to failure and I transferred the changed topographic data to numerical modelling. According to a comparison of monitoring and modelling data, the seepage direction particularly affected the initiation of failure and continued failure during its movement. After water was injected for around 2 minutes, the topography abruptly changed due to movement in the downward direction, and the changed data were applied to numerical modelling. According to the results of seepage direction and force (Fig. 4.9c), movement of the failure in the downward direction changed the topography and increased the pore water pressure near the failure plane of piping flow.

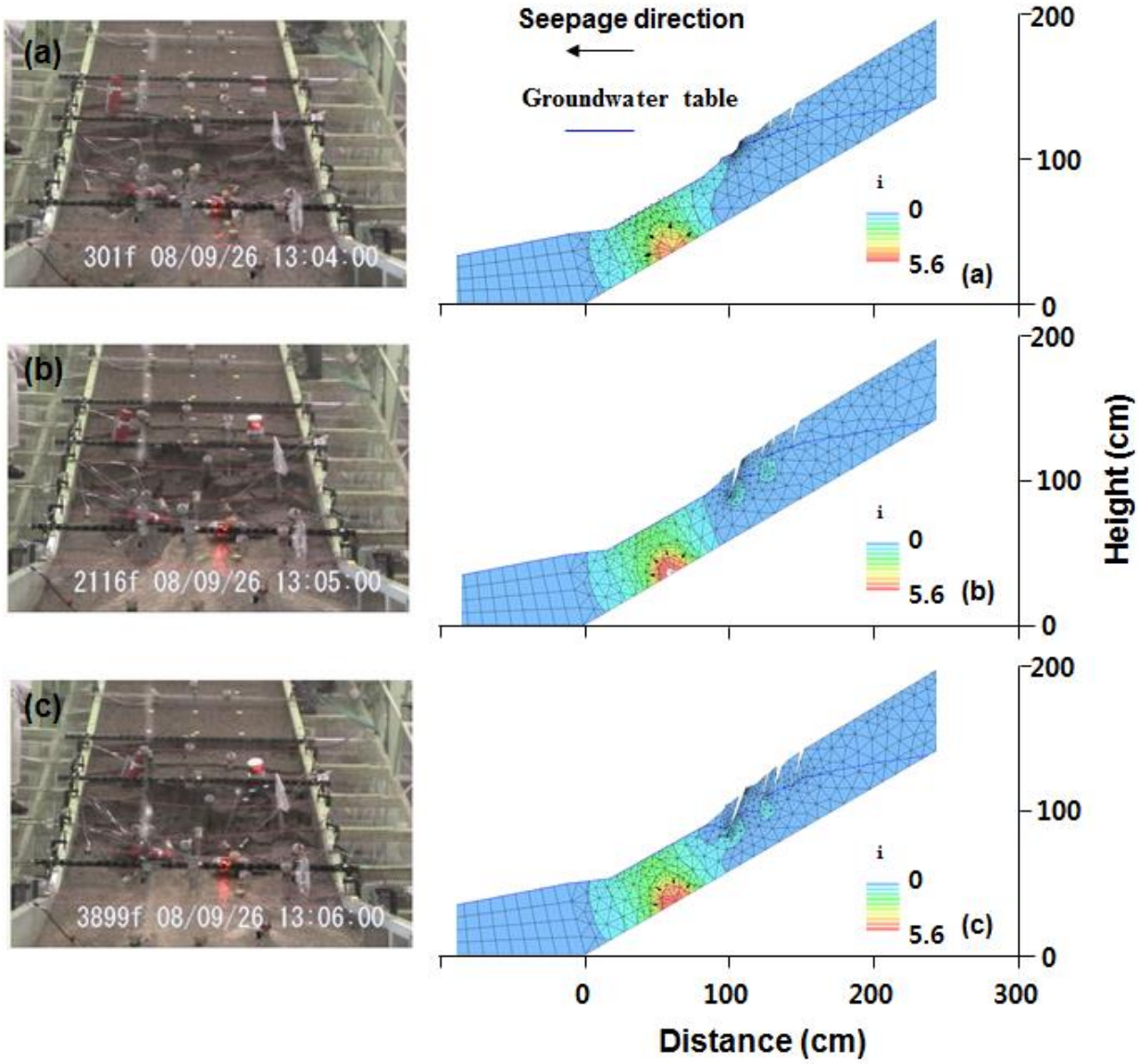

Fig. 4.9. Relation with seepage direction, seepage force and topography effect during rainfall experiment (Rainfall intensity, 80 mm/h) and water injection. (a) is the result of small tension crack before water injection, (b) is the result of increased tension crack during water injection after 1min. and (c) is the results of failure moved to downward direction during water injection after 2 min.

Fig. 4.10 presents the results obtained from sensors monitoring subsurface flow (T2 and TDR) and motion of failure during abrupt movement of the failure (H3). Fig. 4.11 shows the results of modelling during abrupt failure. These results indicate that seepage direction and force affect failure motion, and changed topography may also affect seepage direction and force. In addition, when the failure mass moved downward, I also detected the motion of failure until it reached the lower part of the flume after the experiment. Consistent with previous reports, this result suggests that liquefaction from rapid pore water pressure changes (e.g., Iverson and Major, 1986; Reid et al., 1992; Iverson et al., 2000; Teragima et al., 2014) contributed to landslide motion and the developed failures moved in the downward direction together with broken soil structure due to abruptly increased seepage direction and force.

Terajima et al. (2014) conducted an experiment using artificial rainfall to evaluate the initiation of instability due to hydrological factors. The results showed that directional changes in subsurface flow may be the main cause of soil displacement, and subsequently a shallow landslide. In addition, Zhang and Chang (2012) showed that when soils fail due to seepage forces, large deformation occurs and the soil failures emerged due to changing stress and reduction in shear strength due to the loss of fine particles. For slopes where the soil at the slope face is loaded asymmetrically, the hydraulic gradient causing failure will be much lower than the gradient obtained theoretically.

In this experiment, the soil loses strength and deforms by flowing rather than by frictional slipping (Iverson and Major, 1986; Skempton and Brogan, 1994; Tegragima et al., 2014). The loading of the landslide mass onto the lower slope caused fluidisation of the lower slope, which accounted for the excess pore water pressure (pore water pressure data are shown in Fig. 4.8b and TDR data in Fig. 4.8i) from the higher soil water content of the lower slope (Fig. 4.8j). In addition, the groundwater table defined by the pressure head of 0 cm H_2O, soil moisture from TDR data, which was over the threshold value, and simulated data using the numerical model, which showed upward seepage in Fig. 4.11, all support liquefaction.

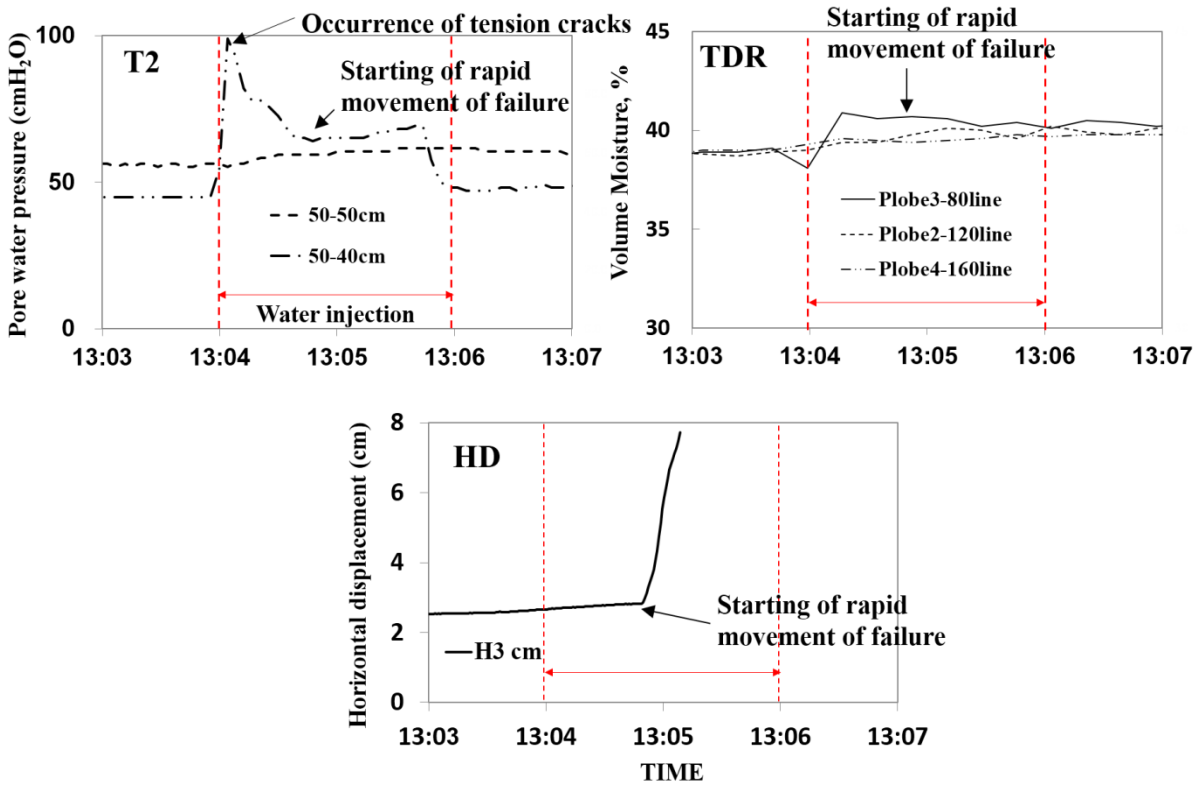

Fig. 4.10. Monitored sensors (T2, TDR and HD) for subsurface flow and motion of failure during rapid movement of failure near pipinn area positioned on 50cm along the large flume. In this data, T2 means tensiometer data installed on 50cm on flume and tensiometers, installed on 10cm and 25cm depth, respectively, washed out by seepage and undercutting during rainfall experiment. HD sensors were installed on four points (30cm, 120 cm, 220 cm and 240cm on flume) on large flume but H1 and H2 were also washed out by seepage and undercutting during rainfall experiment and H4 was not moved, indicating failure was not occurred at H4

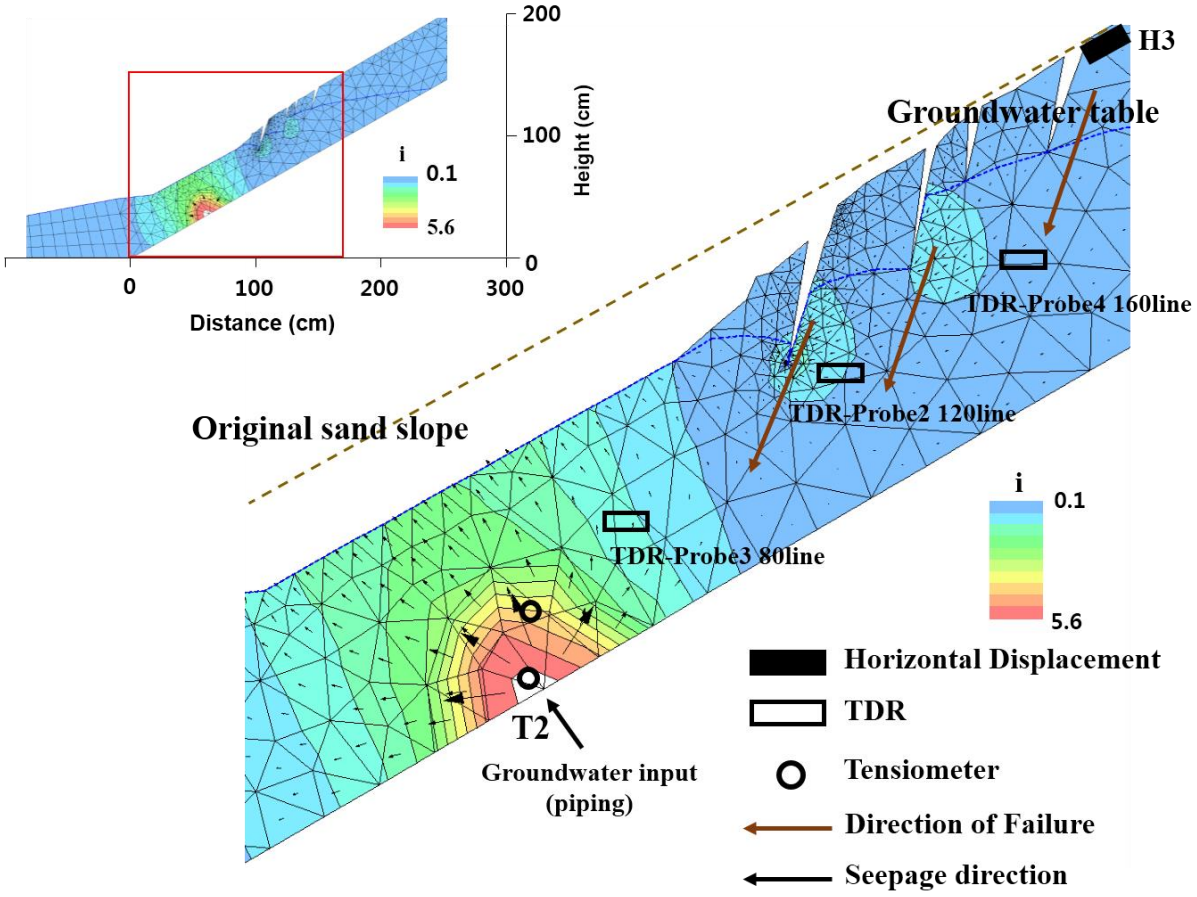

Fig. 4.11. Comparison with monitoring result and modeling result

Thus, I proposed that a saturated, non-cohesive soil mass may liquefy if it experiences a uniform seepage force with an upward vertical component and with a magnitude equal to the submerged unit weight of the soil (Iverson et al., 1997). These factors are related to changes in the direction and magnitude of the subsurface flow (e.g., seepage direction and force), and could be related to both soil displacement and the subsequent shallow landslide observed during the seepage-induced landslide experiment.

4.5.3 Analysis of stability by seepage effect and limitation

To evaluate the effects of seepage direction and seepage force, the FS (eq. 4.11) was applied to this experiment. In addition, a hydraulic gradient was used as the theoretical value (e.g., Iverson and Major, 1986; Budhu et al., 1996) and the experimental value using the water table of the water tank, respectively (eq. 4.12). The results of FS are presented in Table 4.3.

Table 4.3 Analysis of factor of safety for seepage direction and force

Description of seepage direction		During rainfall experiment	During artificial seepage experiment
		Distribution of FS	Distribution of FS1
$\lambda = 180^{\circ} - \alpha$	Vertically downward seepage flow	1.45 ~ 10	1.28 ~ 6.3
$180^{\circ} - \alpha > \lambda > 90^{\circ}$	Increasing to slope parallel seepage flow	1.02 ~1.37	1.1 ~ 0.25
$\lambda = 90^{\circ}$	Slope parallel seepage flow	1	0.2
$0 < \lambda < 90^{\circ} - \alpha$	Increasing upward seepage flow	0.87 ~ 0.97	0.32 ~ 0.05
$\lambda = 90^{\circ} - \alpha$	Horizontal seepage flow	0.85 ~ 0.02	< 0
$\lambda = 0^{\circ}$	Upward seepage flow	< 0	< 0

FS : Hydraulic gradient was used by $i = \sin\alpha / \sin\lambda$
FS1 : Hydraulic gradient was used by water level in water tank, $i = \Delta h / l$
* FS means factor of safety

During the rainfall-induced landslide experiment, for seepage direction (λ) 90° indicating that the slope parallels the seepage flow direction, F_S value < 1 indicates instability. The λ value was increased to 0° (0° is normally in an upward direction), and all calculated F_S values were < 1, indicating that high potential of landsliding. Groundwater increased (Fig. 4.5) and ret-

rogressive failure occurred from the toe of the flume then gradually increased upward; although modelling data shown in Fig. 4.6 support these results, I did not clearly monitor the seepage direction using only monitoring sensors.

In the artificial seepage-induced landslide experiment, when seepage direction reflecting a large hydraulic gradient (i.e., i = 5.6) changed from vertically downward seepage flow to slope-parallel seepage flow, calculated FS < 1 indicated instability. In addition, when the seepage direction λ was increased from horizontal to another seepage flow direction ($\lambda = 90° - \alpha$), the calculated F_S revealed serious instability. These results indicated that considering the seepage force may reduce the factor of safety, as seepage forces strongly influence the initiation of shallow landslides and possibly affect the beginning of soil displacement, which corresponds with a change in direction of the subsurface flow. Previous studies (e.g., Iverson et al., 1997; Reid et al., 1998; Lourenço et al., 2006; Huang et al., 2010; Teragima et al., 2014) considered only seepage direction and groundwater level. Therefore, in this study, I considered hydraulic gradient (seepage force) and directional data, which revealed that seepage can contribute to shallow landslide initiation, as shown by monitoring, numerical simulation data, and calculated Factor of Safety.

In nature, seepage direction and force are generally detected in various states according to the development of surface topography, subsurface geology, local properties, etc. However, this study analysed the initiation and development of landslides using artificial rainfall and artificial seepage flow by piping. I did not apply varying seepage sizes or forces as factors to landslide initiation. Therefore, further studies are needed to analyse various states of subsurface flow. Although our large flume experiment did not completely resolve the mechanisms of landslide initiation in natural hillslopes due to the various limitations, such as scale, rainfall and soil properties, our experiments may lead to an eventual explanation and verification of the various mechanisms of shallow landslide initiation.

6. Conclusion

The experiments of laboratory slope failure were conducted to evaluate the initiation process of rainfall-induced shallow landslide and seepage-induced slope failures by focusing on the topographic effect and bedrock flow from piping. In a rainfall-induced landslide experiment (rainfall intensity at 80 mm/h), failures were caused by undercutting, which occurred due to seepage erosion from increasing groundwater levels in both monitored and simulated data. In a seepage-induced landslide experiment with continued rainfall simulation, the failures were caused by seepage in the vertically upward direction with high seepage force. Both monitored and simulated data support this suggestion, and the safety factor results show that seepage direction and especially seepage force can strongly influence the initiation of shallow landslides. In this study, the results of monitoring and modelling experiments indicated that seepage can be one of the key factors in shallow landslide initiation and movement. Therefore, I suggest that seepage force and direction could be important to analyse landslide mechanisms, and these factors must be considered in landslide studies.

References

Anderson, S. A., and N. Sitar (1995), Analysis of rainfall-induced debris flows, J. Geotech. Eng.-ASCE, **121**(7), 544–552.

Brand, E. W., M. J. Dale, and J. M. Nash (1986), Soil pipes and slope stability in Hong Kong, Q. J. Eng. Geo., **19**, 301–303.

Budhu, M. and R. Gobin (1996) Slope stability from ground-water seepage, J. Hydraul. Eng.-ASCE, **122**(7), 415–417.

Campbell, A. P. (1966), Measurement of movement of an earth flow, Soil and Water, 2(3), 23–24.

Casadei, M., W. E. Dietrich, and N. L. Miller (2003), Testing a model for predicting the timing and location of shallow landslide initiation in soil mantled landscapes, Earth Surf. Processes Landforms, **28**, 925–950.

Crosta, G., and C. di Prisco (1998), On slope instability induced by seepage erosion, Can. Geotech. J., **36**, 1056– 1073.

Fredlund, D. G., and H. Rahardjo (1993), Soil Mechanics for Unsaturated Soils, John Wiley and Sons, New York.

Gabet, E.J., and S. M. Mudd (2006), The mobilization of debris flows from shallow landslides, Geomorphology, **74**, 207-218.

Ghiassian, H., and S. Ghareh (2008), Stability of sandy slopes under seepage conditions, Landslides, **5**, 397-407.

Hiramatsu, S., T. Mizuyama, and Y. Ishikawa (1990), Study of a method for predicting hillside landslides by analysis of transient flow of water in saturated and unsaturated soils, J. the Jpn Soc. of Eros. Con. Eng., **43**, 5–15 (in Japanese).

Howard, A.D., and C. F. McLane III (1988), Erosion of cohesionless sediment by groundwater

seepage, Water Resour. Res., **24** (10), 1659–1674.

Huang, C. C., Y. J. Ju, L. K. Hwu and J. L. Lee (2009), Internal soil moisture and piezometric responses to rainfall-induced shallow slope failures, J. Hydrol., **370**, 39-51.

Iverson, R. M., R. G. LaHusen (1989), Dynamic pore-pressure fluctuations in rapidly shearing granular materials, Science, **246**, 796–798.

Iverson, R. M., and J. J. Major (1986), Groundwater seepage vectors and the potential for hillslope failure and debris flow mobilization, Water Resour. Res., **22**, 1543–1548.

Iverson, R. M. (1997), The physics of debris flows, Rev. Geophys., **35**(3), 245–296.

Iverson, R. M., M. E. Reid, and R. G. LaHusen (1997), Debris-flow mobilization from landslides, Annu. Rev. Earth Pl. Sc., **25**, 85–138.

Iverson, R. M. (2000), Landslide triggering by rain infiltration, Water Resour. Res., 36, 1897–1910.

Iverson, R.M., M. E. Reid, N. R. Iverson, R. G. LaHusen, M. Logan, J. E. Mann, and D. L. Brien (2000), Acute sensitivity of landslide rates to initial soil porosity. Science, **290**, 513–516.

Jenkins, A., P. J. Ashworth, R.I. Ferguson, I. C. Grieve, P. Rowling, and T. A. Stott (1988), Slope failures in the Ochil hills, Scotland, November 1988, Earth Surf. Processes Landforms, **13**, 69–76.

Katsura, S., K. Kosugi, N. Yamamoto, and T. Mizuyama, (2006), Saturated and unsaturated hydraulic conductivities and water retention characteristics of weathered granitic bedrock, Vadose Zone J., **5**, 35 – 47, doi:10.2136/vzj2005.0040.

Kirkby, M. J. (1988), Hillslope runoff process and models, J. Hydrol., 100, 315–339.

Kochel, R. C., A. D. Howard, and C. F. Maclane, (1985), Channel networks developed by groundwater sapping in fine-grained sediments. Analogs to some Martin Valleys. In Models in Geomorphology, Woldenberg MJ (ed.). Allen and Unwin, Boston, 313–341.

Kohno, I., M. Nishigaki, and Y. Takeshita (1987), Levee failure caused by seepage and preven-

tive measures, Nat. Disaster Sci., **9**, 55–76.

Kosugi, K., and M. Katsuyama (2004), Controlled-suction period lysimeter for measuring vertical water flux and convective chemical fluxes, Soil Sci. Soc. Am. J., **68**, 371 – 382.

Kosugi, K., S. Katsura, M. Katsuyama, and T. Mizuyama (2006), Water flow processes in weathered granitic bedrock and their effects on runoff generation in a small headwater catchment, Water Resour. Res., **42**, W02414, doi:10.1029/2005WR004275.

Kosugi, K., S. Katsura, T. Mizuyama, S. Okunaka, and T. Mizutani (2008), Anomalous behavior of soil mantle groundwater demonstrates the major effects of bedrock groundwater on surface hydrological processes, Water Resour. Res., **44**, W01407, doi:10.1029/2006WR005859.

Krahn, J. (2004), Seepage modeling with SEEP/W: An engineering methodology, GEO-SLOPE International Ltd., Calgary, Alta., Canada.

Lambe, T. W., and R. V. Whitman (1969), Soil mechanics. Wiley, New York.

Lanni, C., J. McDonnell, L. Hopp, and R. Rigon (2013), Simulated effect of soil depth and bedrock topography on near-surface hydrologic response and slope stability. Earth Surf. Processes Landforms, **38**, 146–159.

Lourenço, S. D. N., K. Sassa, and H. Fukuoka (2006), Failure process and hydrologic response of a two layer physical model: implications for rainfall-induced landslides, Geomorphology, **73**, 115–130.

McDonnell, J. J. (1990), A rationale for old water discharge through macropores in a steep, humid catchment, Water Resour. Res., **26**, 2821– 2832.

Montgomery, D. R., and W. E. Dietrich (1994), A physically based model for the topographic control on shallow landsliding, Water Resour. Res., **30**(4), 1153–1171.

Mosely, M. P. (1982), Subsurface flow velocities through selected forest soils, South Island, New Zealand. J. Hydrol., **55**, 65–92.

O'Loughlin, C. L., and A. J. Pearce (1976), Influence of Cenozoic geology on mass movement and sediment yield response to forest removal, North Westland, New Zealand. B. Eng. Geol. Environ., **14**, 41–46.

Ohta, T., Y. Tsukamoto, and H. Noguchi (1981), An analysis of pipeflow and landslide, In Proceedings of Annual Meeting of Jpn Soc. Eros. Con. Eng., 92–93 (in Japanese).

Onda, Y., M. Tsujimura, and H. Tabuchi (2004), The role of subsurface water flow paths on hillslope hydrological processes, landslides and landform development in steep mountains of Japan, Hydrol, Process., **18**, 637-650. DOI: 10.1002/hyp.1362.

Okimura, T., R. Ichikawa, and I. Fujii (1985), Methods to Predict Failures on Granite Mountain Slopes by an Infiltrated Water Movement Model in a Surface Layer. J. Jpn Soc. of Eros. Con. Eng.,, 37, 44–49 (in Japanese).

Orense, R. P., S. Shimoma, K. Maeda and I. Towhata (2004), Instrumented model slope failure due to water seepage. J. Nat. Disaster Sci., **26**(1), 15−26.

Pack, R.T., D. G. Tarboton, and C. N. Goodwin (1998), The SINMAP Approach to Terrain Stability Mapping. 8th Congress of the Int. Assoc. Eng. Geol., Vancouver, British Columbia, Canada.

Pierson, T. C. (1983), Soil pipes and slope stability. Q. J. Eng. Geo., **16**, 1–11.

Reid, M. E., and R. M. Iverson (1992), Gravity-driven groundwater flow and slope potential 2. Effect of slope morphology, material properties, and hydraulic heterogeneity. Water Resour. Res., **28**, 939–950.

Richards, L. A. (1931), Capillary conduction of liquids in porous mediums, Physics 1, 318–333.

Rosso, R., M. C. Rulli and G. Vannucchi (2006), A physically based model for the hydrologic control on shallow landsliding, Water Resour. Res., **42**, W06410. http:// dx.doi.org / 10.1029/2005WR004369.

Sassa, K., H. Fukuoka, T. Kamai, and H. Shuzui (2000), Landslide risk at Inca's World Heritage

in Machu Picchu, Peru, Landslide Risk Mitigation and Protection of Cultural and Natural Heritage International Geological Correlation Programme, **1**, 1-14.

Selby, M. J. (1993), Hillslope materials and processes, 2nd ed., Oxford Univ. Press: Oxford; 451p.

Simon, A., A. Curini, S. E. Darby, and E. J. Langendoen (1999), Streambank mechanics and the role of bank and near-bank processes in incised channels. In: Darby, S.E., Simon, A. (Eds.), Incised River Channels. John Wiley and Sons, Chichester, UK, 193–217.

Simon, A., and A. J. C. Collison (2002), Quantifying the mechanical and hydrologic effects of riparian vegetation on stream-bank stability, Earth Surf. Processes Landforms, **27** (5), 527–546.

Sidle, R. C., Y. Tsuboyama, S. Noguchi, I. Hosoda, M. Fujieda, and T. Simizu (1995), Seasonal hydrologic response at various spatial scales in a small forested catchment, Hitachi Ohta. J. Hydrol., **168**, 227–250.

Skempton, A. W., and J. M. Brogan (1994), Experiments on piping in sandy gravels. Geotechnique, **44**, 449–460.

Starkel, L. (1976), The role of extreme (catastrophic) meteorological events in the contemporary evolution of slopes. In Geomorphology and Climate, Derbyshire E (ed.). John Wiley & Sons, New York, 203–246.

Talebi, A., P. A. Troch, and R. Uijlenhoet (2008), A steady-state analytical hillslope stability model for complex hillslopes. Hydrol, Process., **22**, 546–553.

Tanaka, T., M. Yasuhara, H. Sakai, and A. Marui (1988), The Hachioji Experimental Basin Study- Storm runoff processes and the mechanism of its generation, J. Hydrol., **102**, 139-164.

Terajima, T., and K. Moroto (1990), Stream flow generation in a small watershed in granitic mountain, Trans. Jpn. Geomorphol. Union, **11**, 75 – 96. (in Japanese with English abstract).

Terajima, T., and Y. Sakura (1993), Effect of subsurface flow on a topographic change at a valley

head of granitic mountains. Trans. Jpn. Geomorphol. Union, **14**, 365–38 (in Japanese with English abstract and captions).

Terajima. T., T. Sakamoto, Y. Nakai, and K. Kitamura (1997), Suspended sediment discharge in subsurface flow from the head hollow of a small forested watershed, northern Japan. Earth Surf. Processes Landforms, **22**, 987–1000.

Terajima, T., T. Sakamoto, and T. Shirai (2001), Bed load yield caused by subsurface water discharge in a forested 0-order basin in Hokkaido, Northern Japan. Transactions Jpn. Geomorphol. Union, **22**, 1–22. (in Japanese with English abstract and captions).

Teragima, T., E. Miyahira, H. Miyajima, H. Ochiai, and K. Hattori (2014), How hydrological factors initiate instability in a model sandy slope, Hydrological Process, **28**, 5711–5724.

Tsukamoto, Y, and T. Ohta (1988), Runoff processes on a steep forested slope. J. Hydrol., **102**, 165-178.

Tohari, A., M. Nishigaki, and M. Komatsu (2007), Laboratory rainfall-induced slope failure with moisture content measurement. J. Geotech. Geoenviron., **133**(5), 575−587.

Tsutsumi, D., R. C. Sidle, and K. Kosugi (2005), Development of a simple lateral preferential flow model with steady-state application in hillslope soils. Water Resour. Res., **41**, W12420，doi:10.1029/2004WR003877.

Uchida, T., K. Tamur, K. Akiyama (2011), The role of grid cell size, flow routing algorithm and spatial variability of soil depth on shallow landslide prediction. Ital. J. Engi. Geol. and Environ., 149–157. doi: 10.4408/IJEGE.2011-03.B-018.

Uchimura, T., I. Towhata, T. T. L. Anh, J. Fukuda, C. J. B. Bautista, L. Wang, I. Seko, T. Uchida, A. Matsoka, Y. Ito, Y. Onda, S. Iwagami, M. S. Kim, and N. Sakai (2009), Simple monitoring method for precaution of landslides watching tilting and water contents on slopes surface, Landslides, **7**, 351-357. doi: 10.1007/s10346-009-0178-z.

van Genuchten, M. (1980), A closed-form equation for predicting the hydraulic conductivity of unsaturated soils: Soil Sci. Soc. Am. J., **44**, 892–898.

Wang G., and K. Sassa (2003), Pore-pressure generation and movement of rainfall-induced landslides: effects of grain size and fine-particle content, Eng. Geol., **69**, 109-125.

Whitlow, R. (1983), Basic Soil Mechanics. Construction Press, New York.

Wilson, C. J., and W. E. Dietrich (1987), The contribution of bedrock groundwater flow to storm runoff and high pore pressure development in hollows, IAHS Publ., **165**, 49-59.

Wu, T.H., W. P. McKinnel, and D. N. Swanson (1979), Strength of tree roots and landslides on Prince of Wales Island, Alaska. Can. Geotech. J., **16**, 19–33.

Wu, W., and R. C. Sidle (1995), A distributed slope stability model for steep forested basins, Water Resour. Res., **31**, 2097–2110.

Zhang, L. M., and D. S. Chang (2012), Seepage Induced soil shear failure under complex stress states. In Third International Workshop on Modern Trends in Geomechanics (IW-MTG3), 93–95.

Zaslavsky, D., and G. Kassiff (1965), Theoretical formulation of piping mechanism in cohesive soils. Geotechnique, **15**, 305–316.

Chapter 5. General Discussion and Conclusion

5.1 Application of physically based models for topography effect and limitation

In Chapter 2, to evaluate the effect of topography for shallow landslide prediction, we applied physically based H-slider model to hillslope scale site by using diverse factors for shallow landslide prediction. In first simulation (Case I and Case II), two kinds of DEMs (GSTO and BSTO) were constructed and three soil thickness data, i.e. average soil thickness 1m, weathered soil thickness and bedrock soil thickness, respectively, were inputted to each DEMs for evaluation of H-slider model. In results of first simulation Case I and Case II, results of Case I had high accuracy of steady state critical rainfall prediction rather than Case II but the accuracy values using ROC analysis had a low value at both results due to various soil parameters, i.e. cohesion and internal friction angle. To evaluate these soil parameters, a stochastic hydro-geomorphologic model was applied and soil parameters, which represented the effect of three soil thickness distribution, were calculated to evaluate the effect of soil parameters. In second simulation Case III and Case IV using changed soil parameters, Case III had a high accuracy value and, especially Case III-c used GSTO, bedrock soil thickness and soil parameters, represented the effect of bedrock soil thickness, had a highest accuracy value using ROC analysis among the results of entire simulations

However, some researchers(e.g. Freere et al., 2002; Hopp and McDonnell, 2009; Lanni et al., 2012) mentioned that subsurface topography has a strong impact in controlling the connectivity of saturated patches at the bedrock interface but despite this evidence, most catchment-scale shallow landslide models fail to include a connectivity component. Therefore, considering the bedrock interface for shallow landslide prediction can be improved on simulation

results because the spatial distribution of soil depth is a strong control on local pore pressure dynamics.

On the other hands, Zhu and Lin (2009) also studied on the relation between subsurface interface DEM and land surface DEM using hydrologic model and, they mentioned that result of flow path in hydrologic modeling was almost same results with over 90%. And they interpreted on the distinction between results of ground surface interface and bedrock surface interface, respectively and they explained it. First, the topography of the interfaces was dominated by the variation in land surface elevation. Second, soil thickness points, which are measured at their research site, were lack and that affected to results of flow path simulation. In addition, Uchida et al., 2011 applied H-slider model to the Hiroshima areas in Japan which are similar with the our study site, and they also used surface interface DEM and bedrock interface DEM. In results of the critical rainfall prediction of Uchida et al., 2011, they mentioned that the precision of landslide susceptibility prediction had little effect between surface interface DEM and bedrock interface DEM.

Because researches on effect of the bedrock surface DEM for shallow landslide prediction are lacking, we are clearly unable to evaluate it. However, the effect of bedrock interface DEM in our research could not increase the accuracy on shallow landslide model such as the other study (e.g. Zhu and Lin, 2009 and Uchida et al., 2011). Consequently, for areas where subsurface interface topography is dominated by surface DEM, surface DEM can be sufficiently used to simulate the subsurface concentrated lateral flow paths. Otherwise, simulation based on subsurface interface DEM maybe more desirable (Zhu and Lin, 2009).

In Chapter 3, to improve the accuracy of shallow landslide prediction, we compared the results of shallow landslide predictions using a SHALSTAB model, varying the input soil data. Experimental soil data were used for the first simulation (Case I), whereas soil data represented the measured soil thickness (Case II) and represented average soil thickness (1 m, Case III)

data were used in the second and third simulations, respectively. The accuracy of shallow landslide prediction was evaluated by ROC analysis. The order of accuracy as determined by ROC analysis was Case II > Case III > Case I, indicating that Case II showed the highest predictive accuracy. Therefore, the use of soil properties reflecting soil thickness may improve the accuracy of shallow landslide prediction.

Thus, depth difference between soil properties maybe makes different soil's physical properties: cohesion and internal friction angle depending on soil depth. The prediction accuracy of critical rainfall intensity for shallow landsliding was better than when we consider the soil thickness by model input parameter in this study. That means that the accuracy of prediction for shallow landslide will be increased by using a soil thickness, after soil parameters were calculated by hydro-geomorphology model. Therefore, spatial variability in soil depth is likely to be important in determining shallow landslide susceptibility on other steep landscapes (keijsers et al., 2011).

Physically-based numerical models can be used successfully for examining the role of the conditions at the model boundaries (Lanni et al., 2012), but only under conditions of comprehensive data availability (Brontstert, 1999) where all relevant processes are accounted for and where there are sufficient knowledge of the real conditions (i.e. field) at the model boundaries (Cloke et al., 2003). Correct selection of boundary conditions is a critical step in model design (Anderson and Woessner, 1992) if a system is simulated based upon incorrect configuration decisions, then the numerical simulation is solving the wrong problem and, by definition, will provide the wrong solution (Franke and Reilly, 1987).

5.2 Shallow landslide mechanism by topography and piping flow

In Chapter 4, a large flume experiment using artificial rainfall in the National Research Institute for Earth Science and Disaster Prevention (NIED), Japan have been conducted to evaluate the initiation process of rainfall-induced shallow landslide and seepage-induced shallow landslide by topography effect and bedrock flow in model hillslope. In this study, shallow landslide initiation affected by seepage direction, force and effect of topography during rainfall experiment and water injection experiment for bedrock flow by piping, respectively. And changed topography accelerated shallow landslide initiation due to seepage direction and seepage force. We also found that when we changed cohesion value to evaluate effect of cohesion because value of cohesion was 0.08 in this experiment, values of FS increased and it had more value of safety even seepage force had large value.

Subsurface flow paths that link source areas to a generic point in the hillslope control the development of pore-water pressures at that point and the local value of the factor of safety, FS (i.e., the ratio of driving to resisting forces within the slope). These subsurface flow paths are spatially variable and temporally dynamic (Reid et al.,1997; Lanni et al., 2012). And Teragima et al., 2014 mentioned that seepage forces, controlled by changes in direction and magnitude of saturated and unsaturated subsurface flows, may be the main cause of shallow landslides. And they concluded the effect of apparent soil cohesion was the most important factor promoting slope stability, but seepage force became the most important factor promoting slope instability closer to the landslide occurrence. Results of our experiments were similar to those of Reid et al., (1997) and Teragima et al., (2014) but seepage force and direction were influenced by topography and pipeflow and, they became the most important factor promoting slope instability closer to the landslide occurrence. Thus, topography effect and subsurface such as pipe flow may contribute to shallow landslide initiation and developed to rapid movement of failure.

5.3 Future study issues

In this study, I used physically based model for prediction of shallow landslide induced by rainfall. Some issues, however, remain unsolved regarding steady state models. For examples, one is a time scale discrepancy in the supposed hydrological process. The concept of steady groundwater flow parallel to the slope above an impermeable bed can predict only the long-term distribution of groundwater pressure, which should be identified as a predisposition to landsliding. The second concern is that the model cannot apply to hill slopes underlain by highly permeable bedrocks, where the near surface lateral water movement becomes an unfeasible proposition. And these mostly physically based models have been used by factor of safety concept combined a simple hydrology model related with ground water increasing within soil layer by hydraulic conductivity and, they have expressed the output to stable or/and unstable using values of FS where the shallow landslide area is sensitive. So, to perform the shallow landslide prediction, weakness on steady state shallow landslide models have to be considered and the timing caused shallow landslide by rainfall also was needed to be considered.

And soil piping plays a significant role in a number of geomorphological processes and therefore more research should be devoted to explain and model observations from this research. Laboratory pipeflow experiments demonstrated that improved deterministic models are needed to better simulate soil piping and internal erosion processes. In many cases, soil pipes erode so quickly that transport-limited conditions can be created, which may potentially lead to pipe clogging and the buildup of pore water pressures that can cause geotechnical failure (Chu-Agor et al., 2008a).

Laboratory experiments are typically conducted on homogenous soils, manufactured to provide researchers with homogeneous and isotropic materials, although the manner in which the samples are reconstituted will affect the results. In nature, no soil slope is truly homogeneous, as

the gradation of the soil will differ from one sampling point to the next. Furthermore, the available numerical codes are not currently suitable for modeling seepage-induced instability in hillslopes. The development of new numerical methods to seepage-induced physically based model will provide practitioners with a means to better identify slopes susceptible to seepage induced mechanism, particularly in disasters areas encroaching on sloping topography. Further work is required to determine if in fact this solution is valid for natural slopes. Although a large flume experiment did not reflect on completely the mechanism of shallow landslide in real natural hillslope due to various limitations such as scale, rainfall and soil properties, these experiments maybe better method for explanation and proof on the various mechanism of shallow landslide.

5.4 Conclusion

This research tried to analysis of topography (i.e. ground surface interface and bedrock surface interface) effect, which is one of the important parameters for rainfall-induced shallow landslide prediction, by using physically based models. In results of application of physically based model, various factors (e.g. cohesion, internal friction angle and hydraulic conductivity) were influenced on topography but especially cohesion was very sensitive value to topography. However, these physically based models are based on steady groundwater flow parallel to the slope above an impermeable bed can predict the distribution of groundwater pressure, which should be identified as a predisposition to landsliding.

To evaluate topography effect and pipflow mechanism in shallow landslide, we conducted a large flume experiment using artificial rainfall and analyzed it. In results of experiment, shallow landslide initiation affected by seepage direction, force and effect of topography during

rainfall induced experiment and seepage induced experiment for bedrock flow by piping, respectively. And changed topography accelerated shallow landslide initiation due to seepage direction and seepage force. I also found that cohesion maybe can control seepage effect because seepage force and direction were influenced by especially cohesion by results of numerical modeling and analysis of factor of safety.

References

Anderson, M.P., Woessner, W.W., 1992. The role of the postaudit in model validation. Advances in Water Resources, **15** (3), 167-173.

Brontstert, A., 1999. Capabilities and limitations of detailed hillslope hydrological modelling. Hydrological Processes, **13** (1): 21–48.

Cloke, H.L, Renaud, J-P, Claxton, A.J., McDonnell, J.J., Andersona, M.G., Blake, J.R., Bates, P.D., 2003. The effect of model configuration on modelled hillslope–riparian interactions. Journal of Hydrology, **279**, 167–181.

Franke, O. K., Reilly, T. E., 1987. The effects of boundary conditions on the steady-state response of three hypothetical groundwater systems—results and implications of numerical experiments. US Geological Survey Water Supply Paper 2315, 19.

Freer, J., McDonnell, J. J., Beven, K. J., Peters N.E., Burns D.A., Hooper R.P., Aulenbach B., Ken-dall C., 2002. The role of bedrock topography on subsurface storm flow. Water Resource Research, **38**, doi: 10.1029/2001WR000872.

Hopp, L, McDonnell, JJ., 2009. Connectivity at the hillslope scale: Identifying interactions between storm size, bedrock permeability, slope angle and soil depth. Journal of Hydrology, **376** (3-4), 378-391.DOI: 10.1016/j.jhydrol.2009.07.047.

Lanni, C., McDonnell, J.J., Hopp, L., Rigon, R., 2012. Hydrological controls on shallow landslide triggering: the role of soil depth and bedrock topography. Preliminary accepted for publication in Earth Surface processes and landforms.

Reid, M.E., Iverson, R. M., 1992. Gravity-driven groundwater flow and slope potential 2. Effect of slope morphology, material properties, and hydraulic heterogeneity. Water Resources Research, **28**, 939–950.

Reid, M.E., LaHunsen R.G., Iverson, R. M., 1997. Debris flow initiation experiments using di-

verse hydrologic triggers. In Debris Flow Hazards Mitigation: Mechanics, Prediction and As-sessment, Chen CL (ed.). ASCE Proceedings. ASCE, 1–11.

Teragima. T., Miyahira, E., Miyajima. H., Ochiai. H., Hattori. K., 2014. How hydrological factors initiate instability in a model sandy slope. Hydrological Process, **28**, 5711-5724

Uchida, T., Tamur, K., Akiyama, K., 2011. The role of grid cell size, flow routing algorithm and variability of soil depth on shallow landslide prediction. Italian Journal of Engineering Geology and Environment - Book, doi: 10.4408/IJEGE.2011-03.B-018.

Zhu, Z. W., Liu, D. Y., Yuan, Q. Y., Dong, Q., 2009 Application of electro-optic technology in slope stability monitoring, Piezoelectrics & Acoustooptics, **31**, 112–114.

Acknowledgment

Above all, I wish to express deeply gratitude to my supervisor, Professor Yuichi Onda. He gave me the opportunity to study shallow landslide based on hydrology from two different and complementary perspectives, namely, modeling and experiment.

I am particularly grateful to Dr. Uchida, Erosion and Sediment Control Division, Research Center for Disaster Management, National Institute for Land and Infrastructure Management, for his comments and suggestions on shallow landslide modeling and field observations that helped me to create a solid framework for this Thesis.

I am also grateful to Professor Hiroaki KATO, Yoshitaka Komatsu, Dr. Yoshifumi Wakiyama, Dr. Sho Iwagami and for sharing some of their expert knowledge with me in Japan.

I would like to express deeply gratitude to Professor Jung Kwansoo and Professor Son Minwoo, Department of Civil engineering, Chungnam National University.

I would like to express deeply gratitude to Dr. Yi Sangheon, Korea Institute of Geoscience and Mineral Resources.

I would like to express deeply gratitude to Professor Kim Jinkwan, Chonnam National University, for his comments that helped me to create a solid framework for this Thesis.

I wish to thank Dr. Kang Jaewon and Dr. Kim Sukwoo for always being ready to help me when I was in need.

I am deeply and forever indebted to my wife's father and mother for their support throughout my life.

I am deeply and forever indebted to my parents for their support throughout my entire life.

Finally, my heartfelt thanks go to my wife Sachie, my son Taesung and my daughter Yoona for special support for our life.